

Lymphocyte-mediated drug nanoparticle delivery to disseminated lymphoma tumors *in vivo*

by
Bonnie Huang

Bachelor of Science, Bioengineering
University of California, Berkeley, 2005

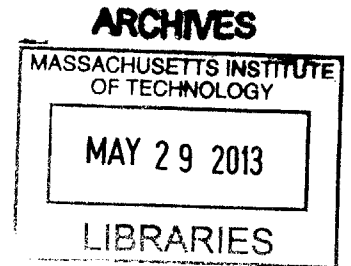
Submitted to the Department of Biological Engineering
in Partial Fulfillment of the Requirements for the Degree of

Doctor of Philosophy

at the
Massachusetts Institute of Technology

February 2013

© 2013 Massachusetts Institute of Technology
All rights reserved



Signature of Author: _____
Department of Biological Engineering
January 10, 2013

Certified by: _____
Darrell J. Irvine
Professor of Biological Engineering and Materials Science
Thesis Supervisor

Accepted by: _____
Forest M. White
Associate Professor of Biological Engineering
Chairman, Graduate Program Committee for Biological Engineering

Members of Thesis Committee

Darrell J. Irvine

Professor of Biological Engineering and Materials Science & Engineering
Thesis Supervisor

K. Dane Wittrup

Carbon P. Dubbs Professor of Chemical Engineering and Biological Engineering
Associate Director, Koch Institute for Integrative Cancer Research

Douglas A. Lauffenburger

Ford Professor of Biological Engineering, Chemical Engineering, and Biology
Head, Department of Biological Engineering
Thesis Committee Chair

Lymphocyte-mediated drug nanoparticle delivery to disseminated lymphoma tumors *in vivo*

by

Bonnie Huang

Submitted to the Department of Biological Engineering
On January 10, 2013 in Partial Fulfillment of the Requirements for the Degree of
Doctor of Philosophy in Biological Engineering at the
Massachusetts Institute of Technology

Abstract

The dissemination of lymphoma into anatomical compartments that are poorly accessible from circulation, such as lymph nodes, necessitates high doses of systemic chemotherapy. However, the potencies of many chemotherapeutic drugs are hampered by off-target toxicity and poor pharmacokinetics. To deliver drugs into disseminated lymphoma tumors *in vivo*, we took advantage of the fact that lymphoma distribution is mirrored by the homeostatic trafficking of healthy lymphocytes. We hypothesized that we could use T cells as live vectors to transport drug-loaded nanoparticles into lymphoid organs where lymphoma cells are enriched. To test this concept, we synthesized a controlled-release liposome system to encapsulate the topoisomerase II poison doxorubicin, and a lipid-based nanoparticle system loaded with the topoisomerase I poison SN-38. We then generated *in vitro*-activated primary murine T cell carriers using optimized culture conditions that induced robust proliferation and high expression levels of CD62L for lymph node homing. The dox liposomes and SN-38 nanoparticles were surface functionalized with maleimide groups to allow covalent conjugation of the particles to the plasma membrane thiol groups on T cells. In the orthotopic syngeneic murine Emu-myc Arf^{-/-} lymphoma model, drug nanoparticle-decorated T cells retained and delivered particles to multiple tumor sites *in vivo* as early as 15 h post-adoptive transfer. *In vitro* co-culture of Emu-myc Arf^{-/-} lymphoma cells and drug nanoparticle-functionalized T cells showed that lymphoma cells are much more sensitive to SN-38 nanoparticle-conjugated T cells than to dox liposome-conjugated T cells. Consistent with this, therapy studies in the Emu-myc Arf^{-/-} model indicated that dox liposome-carrying T cells have limited therapeutic efficacy, while SN-38 nanoparticle-functionalized T cells rapidly reduce tumor burden in all major tumor sites. Finally, we examined the post-treatment biodistribution of Emu-myc Arf^{-/-} lymphoma cells and discovered a therapeutic synergy between T cell-mediated drug particle delivery and blockade of lymphoma interactions with the bone marrow. These results suggest that autologous lymphocytes may be useful as chaperones for targeted delivery of chemotherapy-loaded nanoparticles to lymphoid tumors.

Thesis supervisor: Darrell J. Irvine

Title: Professor of Biological Engineering and Materials Science & Engineering

Table of Contents

1. Introduction.....	8
Efficacy and limitations of cancer chemotherapy.....	8
Chemotherapy for the treatment of lymphoma.....	8
Nanoparticle-mediated drug delivery	10
Tumor infiltrating cells as drug delivery vectors.....	11
Scope and aims of current thesis.....	13
2. Formulation and characterization of nanoparticle systems for doxorubicin and SN-38	15
Introduction.....	15
Methods	18
Results and Discussion	19
Summary and Conclusion.....	28
3. The Emu-myc Arf ^{-/-} lymphoma model and engineered T cell carriers.....	29
Introduction.....	29
Methods	31
Results and Discussion	32
Summary and Conclusion.....	38
4. Nanoparticle-cell conjugation and <i>in vitro</i> characterization.....	39
Introduction.....	39
Methods	39
Results and Discussion	40
Summary and Conclusion.....	51
5. <i>In vivo</i> characterization and therapeutic efficacy of drug nanoparticle-functionalized T cells	52
Introduction.....	52
Methods	52
Results and Discussion	53
Summary and Conclusion.....	70
6. Conclusion and Future Directions	71
I. Appendix: Dox nanoparticle formulations.....	73
II. Appendix: SN-38 particle formulations.....	75
III. Appendix: ICMV encapsulation of anti-CD40 antibody	78
IV. Appendix: Generation of the Emu-myc Arf ^{-/-} luciferase GFP line.....	79
References.....	80

List of Figures

Figure 1.1: Some single-agent drugs used in the treatment of non-Hodgkin lymphoma.	9
Figure 1.2: Some combination drugs used in the treatment of non-Hodgkin lymphoma.....	9
Figure 1.3: Lymphomas form disseminated tumors throughout the body.	10
Figure 1.4: Overview of cell-mediated drug nanoparticle delivery for lymphoma.....	13
Figure 2.1: Structures and mechanisms of dox and SN-38.	16
Figure 2.2: Mechanism of dox encapsulation in liposomes via gradient loading.	17
Figure 2.3: Effects of gradient loading and liposome composition on dox encapsulation and release.....	20
Figure 2.4: Lipid phase transition temperature is correlated with the half-time of dox release <i>in vivo</i>	21
Figure 2.5: Lipid T _m is correlated with dox retention time and inversely correlated to liposome stability.	21
Figure 2.6: Liposome modification schemes for surface maleimide functionalization.....	23
Figure 2.7: Comparing stability and conjugation efficiency of maleimide-PEG versus MPB dox liposomes.	24
Figure 2.8: SN-38 solubility in common solvents.....	25
Figure 2.9: Comparison of SN-38 particle formulations.....	26
Figure 2.10: Release kinetics of SN-38 from ICMVs.	27
Figure 3.1: The Emu-myc lymphoma model.	29
Figure 3.2: Emu-myc Arf ^{-/-} luciferase GFP line <i>in vivo</i> and <i>in vitro</i>	33
Figure 3.3: <i>In vitro</i> isolated resting B cells migrate to lymphoid organs <i>in vivo</i>	34
Figure 3.4: T cell proliferation and CD62L expression after culturing with cytokines.	35
Figure 3.5: Activated T cells can be generated in larger numbers and express higher levels of CD62L and free thiols in comparison to activated B cells.	35
Figure 3.6: Activated T cell are more robust and potent dox liposome cell carriers than activated B cells.	36
Figure 3.7: Emu-myc Arf ^{-/-} cells are killed at dox and SN-38 doses that do not affect T cell viability.	37
Figure 3.8: T cell responses to cytokine deprivation and SN-38 exposure.	38
Figure 4.1: SN-38 ICMVs conjugated to T cells.....	40
Figure 4.1: Non-covalent particle conjugation schemes.	41
Figure 4.2: Biotin-PEG-lipid containing unloaded liposomes are conjugated to maleimide-neutravidin (mal-NAv)-functionalized T cells.....	42
Figure 4.3: Antibodies against T cell antigens were screened as potential particle linkers.	44
Figure 4.4: Oligo-lipid conjugates rapidly insert into T cell membranes, but undergo endocytosis.....	45
Figure 4.5: Oligo-lipid containing dox liposomes are conjugated to complementary oligo-lipid-functionalized T cells.....	46
Figure 4.6: DTT and Traut's reagent do not increase the conjugation efficiency of maleimide-PEG dox liposomes on T cells.	48
Figure 4.7: Particles with smaller diameter are better retained on T cells <i>in vivo</i>	49
Figure 4.8: T cells carry sufficient doses of drug nanoparticles to kill Emu-myc Arf ^{-/-} cells in a co-culture.	51
Figure 5.1: Particle-conjugated T cells traffic into spleen, lymph nodes and bone marrow within 15 h.	55
Figure 5.2: T cells transport their conjugated particles into tumor sites.	57
Figure 5.3: T cell conjugation increases SN-38 ICMV accumulation in all tumor tissues.	58
Figure 5.4: Pharmacokinetics of free SN-38 are poor.....	59
Figure 5.5: Maleimide-PEG dox liposome-conjugated T cells are not therapeutically effective.	60
Figure 5.6: Multiple doses of maleimide-PEG dox liposome-conjugated T cells have modest therapeutic efficacy.....	61
Figure 5.7: MPB dox liposome-conjugated T cells are not therapeutically effective.	62
Figure 5.8: SN-38 ICMV have superior therapeutic effect when delivered via T cell conjugation.....	65

Figure 5.9: CXCR4 inhibition enhances the therapeutic efficacy of SN-38 ICMV-conjugated T cells.	66
Figure 5.10: Tumor burdens over the course of SN-38 therapy, as measured by IVIS bioluminescence...	67
Figure 5.11: CXCL12 and AMD3100 have no direct effect on Emu-myc Arf ^{-/-} cell proliferation or survival <i>in vitro</i>	68
Figure 5.12: AMD3100 increases Emu-myc Arf ^{-/-} redistribution into the blood, but does not significantly change Emu-myc Arf ^{-/-} tumor burden in lymph nodes, bone marrow or spleen.	69
Figure II.1: PLGA (Lakeshore 5050 4A) solubility, 10 mg in 1 ml solvent.	76
Figure II.2: Structures of PGPC and SN-38.	77
Figure III.1: FITC-labeled human IgG can be encapsulated into ICMVs.....	78

Acknowledgements

I would like to thank my advisor, Dr. Darrell Irvine, for his guidance throughout my PhD. He has consistently shepherded me towards a path of balance, by challenging me to pursue the rigorous experiments, to seek feedback at every stage of the project, and above all, to be cautious but optimistic. I am fortunate to have been part of his research group during its amazing growth.

Dr. Dane Wittrup has been a valuable collaborator on several of our group's cancer therapy projects. His engineering perspective and attention to detail have been very helpful in the analysis of our results and the design of new experiments to strengthen our data.

Dr. Doug Lauffenburger has been a supportive teacher as a committee member and as the department chair. His questions always remind us to consider our research in a broader scope. I appreciate the breadth of his scientific vision and his confidence in the abilities of every student.

I would like to thank the undergraduates who have worked with me, in particular Samantha Luo for her help with optimizing the SN-38 ICMVs. I would like to thank the lab staff, especially Sandra Bustamante López and Wuhbet Abraham, for making the large-scale animal experiments possible, and Erin Morehouse for making the lab a well-maintained working environment.

I want to thank current and former postdocs for greatly expanding the knowledge and ambition of the lab. Dr. Haipeng Liu generously synthesized reagents for this project and taught me to use the HPLC. Dr. James Moon was especially positive and provided helpful advice on ICMVs and *in vivo* experiments. Dr. Chris Jewell encouraged career development that was essential for the next step in my training. I want to thank my fellow students in the group for offering inspiration through their work ethic and successes: Junsang Doh, who was my first mentor in the lab, Sid Jain, Agi Stachowiak, Maria Foley, Yana Wang, Yuki Hori, Anna Bershteyn, Xingfang Su, Peter Demuth, Prabhani Atukorale, Melissa Hanson, Yiran Zheng, and especially Brandon Kwong and Adrienne Li for helping me to navigate the ups and downs of my PhD.

Dr. Michael Hemann and his lab members, in particular Luke Gilbert, generously shared and assisted with the Emu-myc Arf^{-/-} lymphoma cells and associated reagents and protocols, as well as provided their valuable points of view as cancer biologists.

Glenn Paradis, Michael Jennings and Michele Griffin of the flow cytometry facility, Scott Malstrom of the whole animal imaging facility, Michael Brown and Weijia Zhang of the histology facility, and Gladys Valeriano and Liz Horrigan of the Division of Comparative Medicine all provided superb technical instruction and assistance.

I would like to thank the friends that have accompanied me through graduate school: Abhinav Arneja, Nidhi Shrivastav, Alex Sheh, James Mutamba, Ta-Chun Hang and Adrienne Li.

Finally, I am grateful to my family, for their generosity, patience and love that made this PhD possible, from beginning to end. And I thank Brandon for being a source of unwavering support during these years of change and growth.

1. Introduction

Efficacy and limitations of cancer chemotherapy

Small molecule chemotherapy drugs are frontline therapies for a wide variety of cancers, due to their rapid and potent mechanisms of action. However, careful dosing of these drugs is required to achieve therapeutic efficacy while avoiding toxicity. This is often due to the mode of administration, in which patients are given bolus intravenous injections, causing drug accumulation in off-target tissues and severe side-effects. Pharmacological studies highlight many obstacles to tumor penetration by the drug, including metabolism and excretion (Undevia et al., 2005), as well as the physical barrier of the tumor vasculature and stroma (Minchinton and Tannock, 2006; Olive et al., 2009). Thus, very high systemic doses may be required to overcome these bottlenecks and achieve therapeutically relevant drug concentrations in the tumor.

Chemotherapy for the treatment of lymphoma

The Leukemia & Lymphoma Society reported “about 662,789 people were either living with, or in remission from, lymphoma” in the U.S. in 2011. Lymphomas are clinically classified into Hodgkin’s and non-Hodgkin’s lymphoma, the latter of which is comprised of diverse subtypes. The National Cancer Institute estimates that “70,130 [people] will be diagnosed with and 18,940 [people] will die of non-Hodgkin lymphoma in 2012.” The prevalence of these malignancies has motivated the development and application of a wide variety of single-agent (Figure 1.1) and combination (Figure 1.2) therapies.

DNA-Damaging Drugs

- bendamustine (Treanda®)
- carboplatin (Paraplatin®)
- carmustine (BCNU, BiCNU®)
- chlorambucil (Leukeran®)
- cisplatin (Platinol®)
- cyclophosphamide (Cytosan®)
- dacarbazine (DTIC, DTIC-Dome®)
- ifosfamide (Ifex®)
- melphalan (Alkeran®)
- procarbazine (Matulane®)

Antitumor Antibiotics

- doxorubicin (Adriamycin®)
- idarubicin (Idamycin®)
- mitoxantrone (Novantrone®)

Proteasome Inhibitor Drug

- bortezomib (Velcade®)

DNA Repair Enzyme Inhibitors

- etoposide (Etopophos®, VePesid®, VP-16)

Drugs That Prevent Cells From Dividing by Blocking Mitosis

- paclitaxel (Abraxane®, Onxol®, Taxol®)
- vinblastine (Velban®)
- vincristine (Oncovin®)

Hormones That Can Kill Lymphocytes

- dexamethasone (Decadron®)
- methylprednisolone (Medrol®)
- prednisone

Immunotherapy

- iodine131-tositumomab (Bexxar®)
- rituximab (Rituxan®)
- yttrium-90-ibritumomab tiuxetan (Zevalin®)

Histone Deacetylase Inhibitor

- vorinostat (Zolinza®)

<p>Antimetabolites</p> <ul style="list-style-type: none"> • cladribine (Leustatin®) • cytarabine (cytosine arabinoside, ara-C, Cytosar-U®) • fludarabine (Fludara®) • gemcitabine (Gemzar®) • nelarabine (Arranon(R)) • methotrexate (Rheumatrex®, Trexall®) • 6-thioguanine (Thioguanine Tabloid®) 	<p>Retinoid</p> <ul style="list-style-type: none"> • bexarotene (Targretin®)
---	--

Figure 1.1: Some single-agent drugs used in the treatment of non-Hodgkin lymphoma. Table 3 from the Leukemia & Lymphoma Society non-Hodgkin's lymphoma handbook.

<p>R-CHOP: Rituxan, cyclophosphamide, doxorubicin (hydroxydoxorubicin), Oncovin® (vincristine), prednisone</p> <p>R-FCM: Rituxan, fludarabine, cyclophosphamide, mitoxantrone</p>	<p>R- or F-CVP: Rituxan or fludarabine, plus cyclophosphamide, vincristine, prednisone</p> <p>R-HCVAD: Rituxan, cyclophosphamide, vincristine, Adriamycin® (doxorubicin), dexamethasone, alternating with R-MTX-ARAC: Rituxan, methotrexate-cytarabine</p>
---	--

Figure 1.2: Some combination drugs used in the treatment of non-Hodgkin lymphoma. Table 4 from the Leukemia & Lymphoma Society non-Hodgkin's lymphoma handbook.

Lymphomas were among the first cancers to be successfully treated with chemotherapy (Chabner and Roberts, 2005), and in general they are sensitive to a wide variety of cytotoxic drugs. However, their disseminated nature poses a challenge for anatomically-targeted therapy (Figure 1.3). Because lymphomas are able to traffic throughout the body and seed tumors in multiple organs (Pals et al., 2007), surgery and other local therapies cannot prevent or slow the spread of disease. One route by which lymphomas evade systemic treatment, e.g. drug in circulation, is to enter the lymph nodes by transmigration across the endothelial capsule. Selective drug delivery into lymph nodes could greatly benefit the potency of chemotherapy while reducing its systemic toxicity.

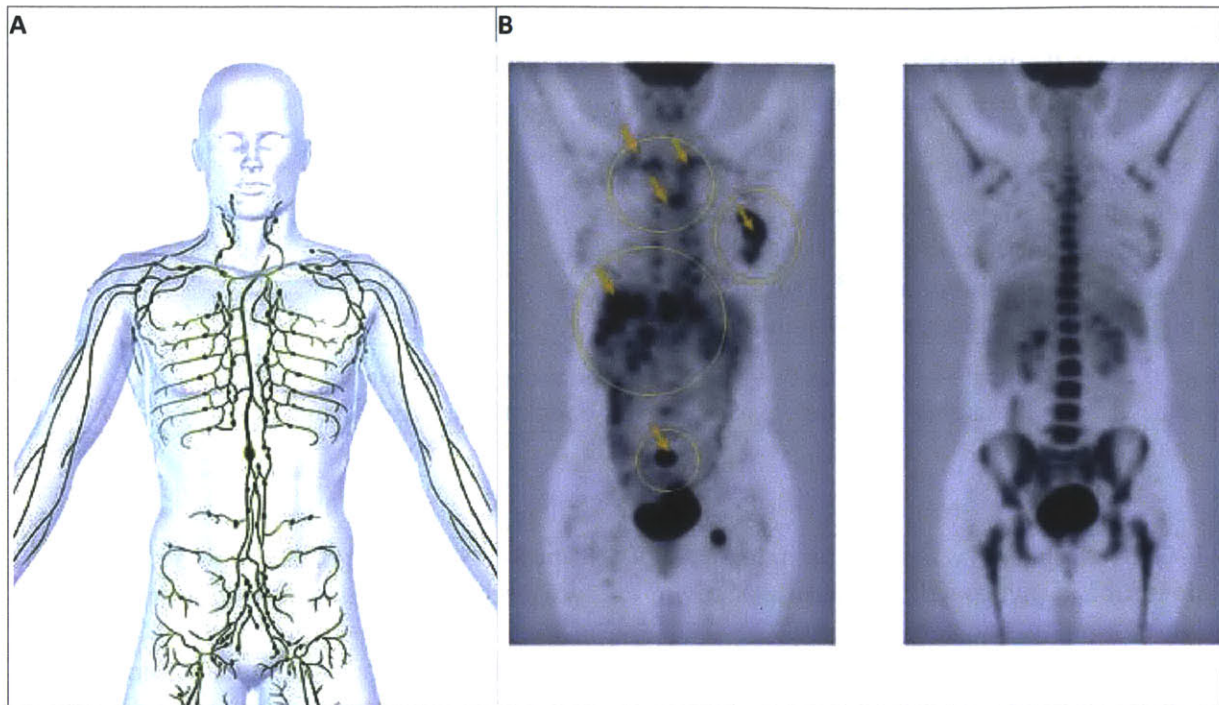


Figure 1.3: Lymphomas form disseminated tumors throughout the body. (A) Schematic of the human lymphatic system in green. Image from shutterstock.com. (B) PET scan of a patient with disseminated non-Hodgkin's lymphoma tumors (highlighted by yellow circles with arrows) before (left) and after (right) chemotherapy. Image from petforcancer.com.

Nanoparticle-mediated drug delivery

Nanoparticles are one class of controlled release platforms that are engineered to regulate the timescale of drug circulation *in vivo* and to improve targeting of drug payloads to tumors (Davis et al., 2008; Peer et al., 2007; Wang et al., 2012). Modification of particle material properties, surface chemistry and tumor microenvironment responsiveness can facilitate particle escape from scavenging by the reticuloendothelial system, as well as extend payload retention and thus the time between repeat doses (Moon et al., 2012). These nanoparticle systems have shown efficacy in some preclinical models of large solid tumors with leaky vasculature, where the enhanced permeation and retention (EPR) effect allows circulating nanoparticles to eventually drain into tumors. However, the extent of the EPR effect is highly dependent on the state of the vasculature, and in most cases particle penetration into the tumor is limited to perivascular regions (Jain and Stylianopoulos, 2010). These biological complexities have led to limited success of EPR-reliant drug delivery systems in clinical trials (Taurin et al., 2012). In the case of lymphoma, vasculature density and endothelial phenotype have been reported to be abnormal for some subtypes (Koster and Raemaekers, 2005), however, this area remains mostly unexplored, and more characterization is required to determine whether EPR is also of importance for lymphoma tumors (Ruan et al., 2009). Current research on nanoparticle targeting of lymph nodes focuses primarily on imaging and drug delivery to prevent metastasis (Ravizzini et al., 2009), or vaccination (Reddy et al., 2007). In both cases, particles are injected subcutaneously and drain into local lymph nodes. Since lymphoma cells can traffic throughout the entire lymphatic

network, an ideal drug delivery system would simultaneously target all lymph nodes. However, to date, no nanoparticle systems have been engineered to mimic the trafficking behavior of lymphocytes and their ability to actively migrate into lymph nodes.

Tumor infiltrating cells as drug delivery vectors

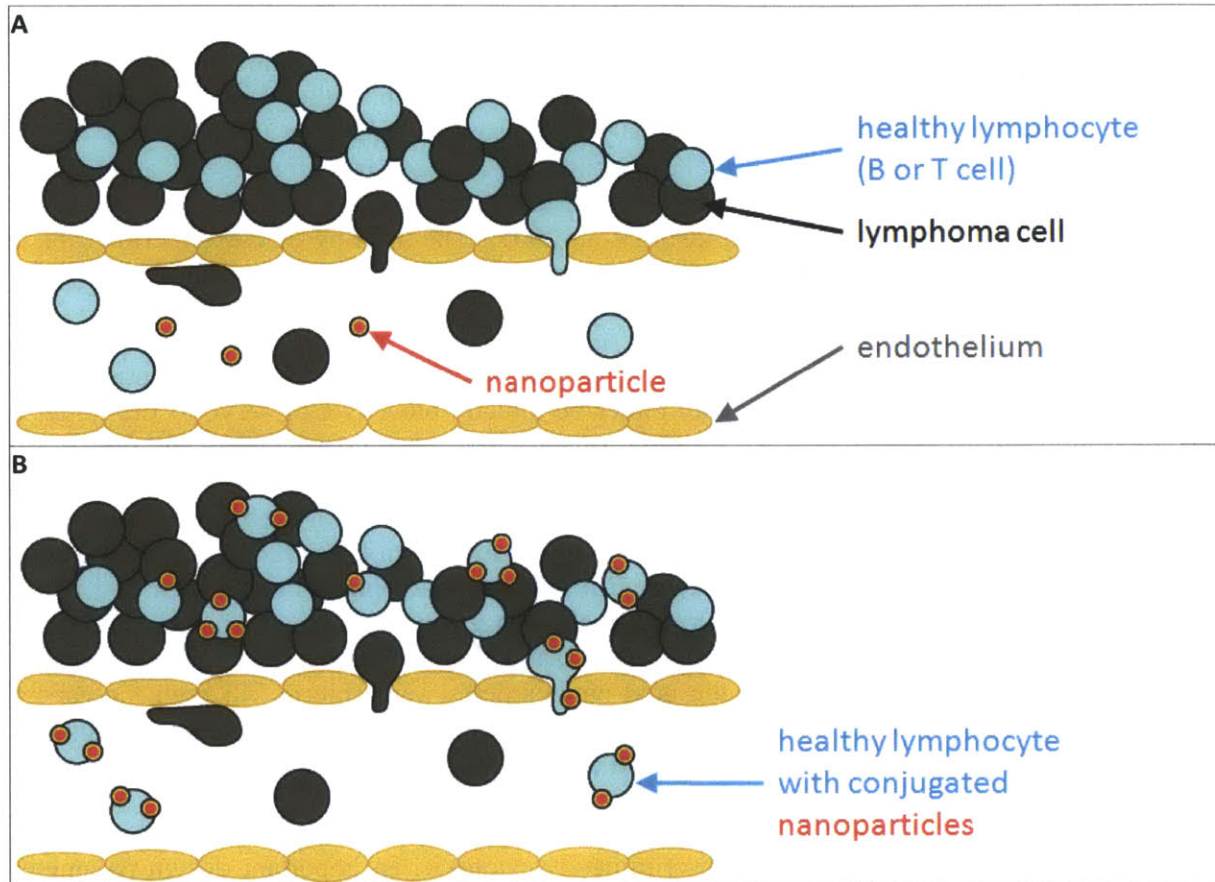
A burgeoning area of interest in cancer biology is the role of the tumor microenvironment in tumor progression (Hanahan and Weinberg, 2011). In both animal models and patients, it is clear that inflammatory signals in the tumor microenvironment often attract hematopoietic cells, including macrophages (Qian and Pollard, 2010), mesenchymal stem cells (MSCs), and T cells (Gooden et al., 2011; Yu and Fu, 2006). These infiltrating cells can be immunogenic and counter tumor progression, or conversely, they can promote tumor growth, angiogenesis and metastasis (Joyce and Pollard, 2009; Ogino et al., 2011; Zou, 2005). The motility of these recruited cells and the ability to manipulate them *ex vivo* has inspired their use as carriers for drug delivery into tumors.

Previous studies have used cells as drug delivery vehicles for a variety of therapeutic agents (Roth et al., 2008). The therapy cargo can either be directly bioactive, or serve to pre-target a second component to the tumor. One example of the latter are gold nanoparticles, which are normally biocompatible but are able to kill surrounding cells by converting local long-wavelength radiation to heat (Huang et al., 2008; Jain et al., 2012). Macrophages are highly phagocytic, which allows simple cargo loading by incubation with the cargo particles or drugs. Proof-of-concept studies have shown that *in vitro* cultured macrophages can ingest and retain gold nanoparticles, and that particle-carrying macrophages maintain their ability to migrate towards and infiltrate breast tumor (Choi et al., 2007) and glioma (Madsen et al., 2012) spheroids *in vitro*. When radiation was applied, the gold nanoparticles were able to kill both the carrier macrophages and portions of the surrounding tumor spheroid. Gold nanoparticles could also be loaded into human T cells by internalization and carried into subcutaneous lymphoma tumors in mice (Kennedy et al., 2011).

When the drug cargo is directly and indiscriminately cytotoxic, an important design parameter becomes the viability of the carrier cells while they are en route to the tumor(s). For a potent chemotherapeutic drug such as dox, toxicity can often be ameliorated by encapsulation into controlled-release particle systems. In one study, dox-loaded silica “nano-rattles” were conjugated with antibodies for attachment to MSCs. Nano-rattle-functionalized MSCs chemotaxed towards glioma cells *in vitro*, and were able to kill surrounding cells when they were locally injected into subcutaneous xenograft glioma tumors (Li et al., 2011). In a similar study, dox-loaded liposomes were engulfed by a macrophage-like leukemia cell line. After adoptive transfer by intravenous injection, these liposome-loaded cells trafficked to a subcutaneous lung cancer tumor, leading to a detectable intratumoral concentration of dox (Choi et al., 2012b). The same authors later loaded dox liposomes into primary macrophages and demonstrated reduced tumor growth in the same subcutaneous lung tumor model (Choi et al., 2012a).

While the aforementioned studies demonstrated feasibility of the concept, none of them, with the exception of (Choi et al., 2012a), showed therapeutic benefits resulting from cell-delivered drug nanoparticles. Furthermore, these studies were conducted using human tumors xenografted onto immunodeficient mice, a system which does not recapitulate the complexities of the tumor and

stroma of a syngeneic immunocompetent tumor model. Based on this previous body of work, we hypothesized that the efficacy of chemotherapy could be enhanced while greatly reducing off-target toxicity if healthy lymphocytes were used as carriers to target drug nanoparticles to the lymphoid tissue sites where lymphomas home. Furthermore, we investigated the efficacy of this approach in a well-studied syngeneic orthotopic model of B cell lymphoma.



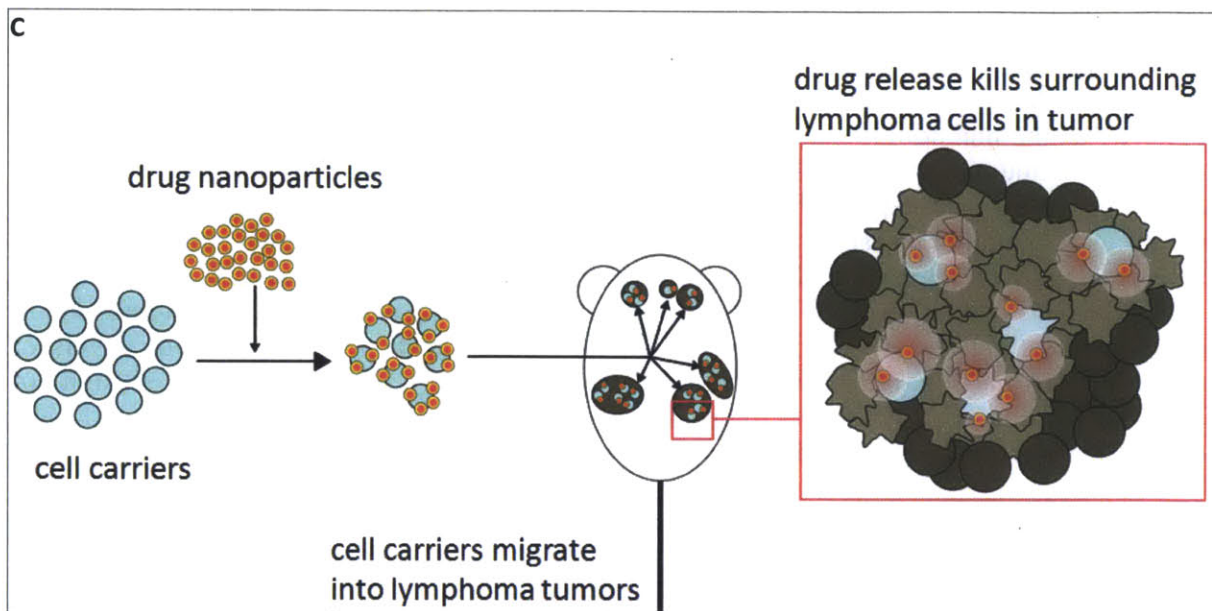


Figure 1.4: Overview of cell-mediated drug nanoparticle delivery for lymphoma.

(A) Lymphoma cells and healthy lymphocytes can transmigrate across the endothelium to enter lymph nodes, while nanoparticles cannot. (B) Healthy lymphocytes may serve as a vector to carry conjugated nanoparticle cargo into lymph nodes. (C) Cell carriers may be conjugated with drug nanoparticles *in vitro*, then adoptively transferred into lymphoma tumor-bearing mice. The cell carriers may home to lymphoma tumors and allow nanoparticle infiltration into the tumor bulk. Drug released from the nanoparticles may kill the surrounding lymphoma cells and reduce tumor burden.

Scope and aims of current thesis

In this thesis, we designed a cell-based drug delivery strategy that enables selective anatomical targeting of drug nanoparticles *in vivo*. Implementation of this strategy required optimization of the drug nanoparticle system, the cell carriers, and particle-cell conjugation method, concluded by evaluation of this strategy in a mouse model of lymphoma.

To begin, in Chapter 2, we designed and synthesized nanoparticle delivery systems for two small molecule chemotherapeutic drugs: doxorubicin (dox) and SN-38. While these drugs have similar mechanisms of action, their contrasting chemical and pharmacological characteristics required different types of controlled release nanoparticle systems for their *in vivo* application. In both cases, we sought to develop particle systems that have high drug encapsulation, colloidal stability, ability to conjugate to cells, and prolonged drug release. For dox, we modified gradient-loaded liposomes, an extensively-characterized formulation (Gabizon et al., 1994), with surface functional groups for cell conjugation. We tested different methods of substituting the chemically-inert lipids in the original liposomal formulation with lipids that are either directly reactive or could be further functionalized to bind cell surfaces. For SN-38, we explored a wide variety of particle systems: liposomes, lipid-coated poly(lactic-co-glycolic acid) (PLGA) nanoparticles, dehydration-rehydration vesicles, and interbilayer-crosslinked multilamellar vesicles (ICMVs) (Moon et al., 2011). We also attempted to slow SN-38 release by first conjugating it with a protein or lipid carrier, then incorporating the conjugate into ICMVs.

In Chapter 3, we generated the Emu-myc Arf^{-/-} luciferase GFP cell line, which allows tracking of tumor dissemination and growth via non-invasive whole animal bioluminescence imaging. We verified that the luciferase- and GFP-expressing line had the same *in vivo* dissemination and pathology as the unmodified parental lymphoma line. To produce cell carriers for nanoparticle delivery, we cultured primary splenocytes from healthy murine donors to generate activated T cells, which were then expanded with cytokines interleukin-2 (IL-2) or interleukin-15 (IL-15) and the mTOR inhibitor rapamycin. We also isolated B cells from donor splenocytes and expanded them with lipopolysaccharide (LPS), a Toll-like receptor (TLR) agonist. We compared the phenotype and function of the different cultured cell types, by measuring cell yield per donor, cell robustness, cell surface thiol density for particle conjugation, and expression levels of surface homing markers for lymph node migration *in vivo*. Lastly, we measured the sensitivity of T cells versus Emu-myc Arf^{-/-} cells to dox and SN-38 *in vitro*, as an estimate of whether T cells could carry tumoricidal doses of drug nanoparticles without apoptosis.

In Chapter 4, we compared direct maleimide-thiol conjugation of nanoparticles to cells to non-covalent conjugation strategies: biotin-neutravidin bridging, antibody binding, and DNA oligo hybridization. Since previous work showed excellent cell surface retention of particles using maleimide-thiol chemistry (Stephan et al., 2010), we examined similar characteristics for these alternative conjugation techniques. We quantified conjugation efficiency and the amount of drug that could be carried by T cells, by dissolving cells after conjugation and measuring the drug fluorescence. To estimate their lymphoma-killing function, nanoparticle-conjugated T cells were co-cultured with lymphoma cells and the viability of both cell types was measured.

Lastly, in Chapter 5, we tested drug nanoparticle-conjugated T cells in the transplanted Emu-myc Arf^{-/-} B cell lymphoma model. Nanoparticle-functionalized T cells trafficking was measured by whole animal imaging and by flow cytometry for all lymphoma compartments. Particle fluorescence by flow cytometry and whole tissue imaging was used to evaluate particle biodistribution. We then tested the ability of nanoparticle-conjugated T cells to suppress tumor growth in a therapeutic setting. Finally, we considered the role of the tumor microenvironment in the bone marrow and investigated the therapeutic efficacy of a small molecule inhibitor of lymphoma-stroma interaction in conjunction with nanoparticle-conjugated T cells.

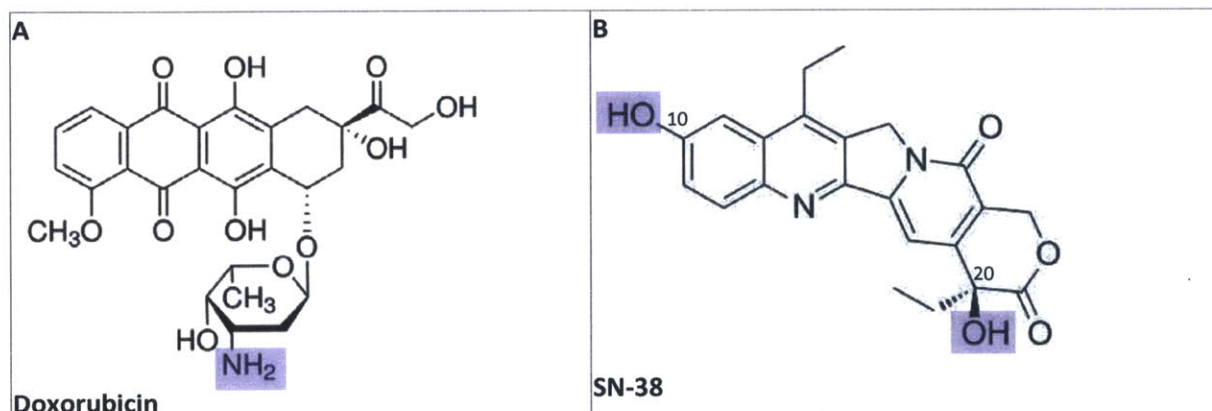
2. Formulation and characterization of nanoparticle systems for doxorubicin and SN-38

Introduction

In this chapter, we describe the synthesis and optimization of nanoparticle carriers for two small molecule chemotherapeutic drugs: doxorubicin and SN-38. Throughout the particle development process, we optimized for high drug encapsulation, particle stability, and ability to conjugate to cells. Doxorubicin (dox) has been in clinical use for decades, and its potency and toxicity have motivated the development of a wide variety of nanoparticle systems to improve its delivery. We modified one well-studied system, gradient-loaded dox liposomes, to present surface maleimide groups for cell conjugation, without compromising particle stability, encapsulation efficiency or release kinetics. In contrast to dox, SN-38 was discovered only twenty years ago as the potent active metabolite of irinotecan (Kaneda et al., 1990), but its clinical translation has been hampered by its poor solubility in multiple solvents. Given the limited literature on SN-38 controlled release systems, we began our design *de novo*, screened a number of nanoparticle formulations, and ultimately modified a vaccine particle system previously developed in our lab for encapsulation of SN-38.

Doxorubicin pharmacology

A member of the anthracycline antibiotics family, dox intercalates efficiently into genomic DNA and stalls the replication machinery containing Topoisomerase II, thus creating double-strand breaks and inhibiting DNA replication (Hurley, 2002) (Figure 2.1). Dox is water-soluble and is given as a slow intravenous infusion, to minimize tissue necrosis at the injection site. It is indicated for a number of cancers including ovarian cancer, and acute lymphoblastic and myeloblastic leukemias. It is also a component of post-resection adjuvant therapy for breast cancer, and as part of several combination therapies, including the standard-of-care combination CHOP for non-Hodgkin's lymphomas. Pharmacological studies revealed the dose-limiting toxicity of doxorubicin to be in the myocardial tissues. This motivated the development of controlled release carriers for dox that would change the drug biodistribution and prolong its retention in the body.



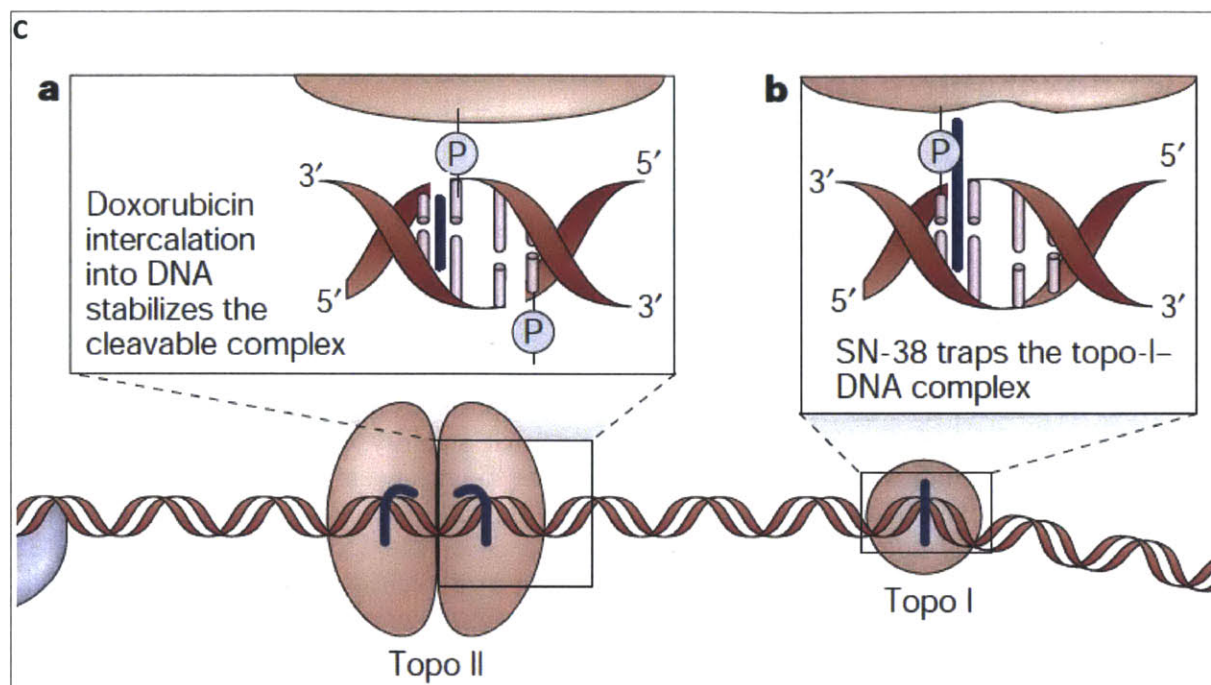


Figure 2.1: Structures and mechanisms of dox and SN-38.

(A) Structure of dox, with the reactive amine group highlighted in blue. (B) Structure of SN-38, with the reactive hydroxyl groups (on carbons 10 and 20) highlighted in blue. (C) Dox and SN-38 stall topoisomerase complexes and cause double-strand breaks. Schematic from (Hurley, 2002).

Gradient-loaded doxorubicin liposome systems

Gradient-loaded liposomes represent a major class of dox carrier systems, due to their ease and low cost of manufacturing, and their high drug encapsulation. Doxil is a dox liposome formulation approved by the FDA for platinum-resistant ovarian cancer, AIDS-related Kaposi's sarcoma, and as part of a combination therapy for multiple myeloma. Doxil is composed of unilamellar liposomes loaded with dox via an ammonium sulfate gradient. Developed in the 1990's, gradient loading methods take advantage of the weakly basic nature of dox (amine pKa 8.15) and the dependence of membrane permeability on charge. Dox is membrane-permeable in its neutral form, but when protonated, its permeability is reduced by several orders of magnitude (Haran et al., 1993). When added to liposomes whose interior is acidic and whose exterior is neutral, dox freely diffuses across the membrane in its neutral state, becomes protonated on the interior and therefore diffuses out from the liposome at a much slower rate (Figure 2.2). This transmembrane pH gradient drives an influx of dox which is then entrapped in the liposome at very high concentrations, $\sim 250 \mu\text{g dox}/\mu\text{mol lipid}$ ($206.6 \mu\text{g dox}/\text{mg lipid}$) (Gabizon et al., 1994). The counter-ion of the interior phase also contributes to dox retention; sulfate, citrate, acetate and phosphate anions interact electrostatically with protonated dox, forming precipitates which can be seen in cryo-electron micrographs of loaded liposomes (Fritze et al., 2006).

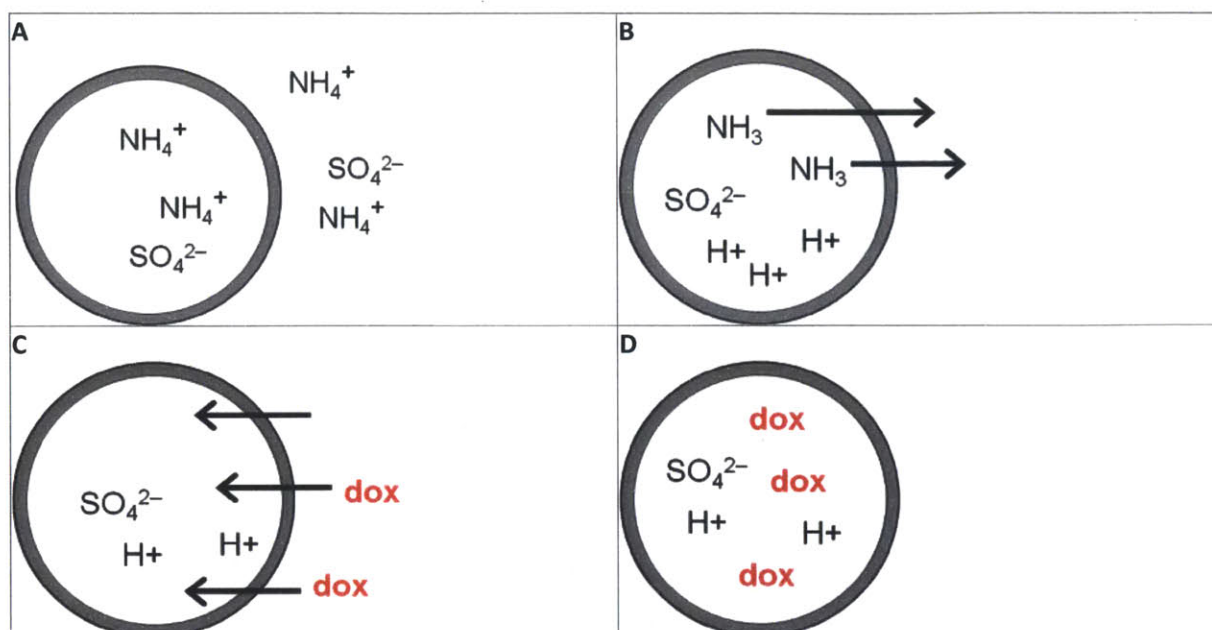


Figure 2.2: Mechanism of dox encapsulation in liposomes via gradient loading.

Dox is gradient-loaded into liposomes as follows. A) Liposomes are reconstituted in ammonium sulfate. B) Liposomes are buffer exchanged into NaCl to establish pH gradient by NH_3 efflux. C) Dox is added to the exterior phase and diffuses into the liposome. D) Dox is retained in the interior phase by protonation and interactions with sulfate ions, while the unencapsulated dox is removed by buffer exchange.

SN-38 pharmacology and controlled release systems

SN-38 belongs to the camptothecin family of Topoisomerase I poisons, with a mechanism of action analogous to that of doxorubicin (Figure 2.1). Its water-soluble pro-drug, irinotecan (also known as CPT-11), is metabolized by carboxylesterase into the active metabolite SN-38, which is then glucuronidated by UGT1A1 for excretion via bile. Once in the bowel, the glucuronidation is reversed by β -glucuronidase from commensal bacteria, restoring SN-38 to its active form and causing severe gastrointestinal toxicity. The polymorphism of UGT1A1 in humans produces unpredictable toxicity responses, in which patients with low UGT1A1 activity have higher SN-38 accumulation (Relling and Dervieux, 2001). While efforts have been made to sequence patient UGT1A1 prior to treatment, the heterogeneity of response remains an obstacle in the usage of irinotecan, which is only indicated for metastatic colorectal cancer following or alongside 5-fluorouracil. Interest in SN-38 as a stand-alone drug increased when it was shown to have much higher potency against tumor cells *in vitro*, as high as 1000-fold by measures of *in vitro* activity (Kawato et al., 1991). However, it is insoluble in saline and common pharmacological carriers, and therefore has not been successfully translated into clinical usage.

Unlike dox, SN-38 has not been widely explored as a drug cargo for controlled release carriers, due to its poor solubility and its relatively inert functional groups. Currently, two particle systems are in clinical trials. The first is a multilamellar liposomal formulation that passively entraps SN-38 (Zhang et al., 2004). The second is an SN-38-polymer conjugate that is linked via functionalization of the SN-38 (lactone-proximal) 20-hydroxyl, which self-assembles into micelles (Hamaguchi et al., 2010).

Methods

Reagents

With the exception of MPB-DOPE and SN-38-lipid conjugates, which were synthesized in house, all other lipids were purchased from Avanti Polar Lipids. Dox was purchased from Tocris and LC Labs. SN-38 was purchased from Tocris and AK Scientific.

Synthesis of gradient-loaded dox liposomes

1.28 umol total lipid (56.2 mol% HSPC, 38.3 mol% cholesterol, 5.3 mol% PEG2000-DSPE, 0.2 mol% α -tocopherol) in chloroform were mixed in a glass test tube and dried under a nitrogen stream into a film, then dried in vacuo overnight.

HSPC	Cholesterol	PEG2000-DSPE	Vitamin E
2 mg/ml	1 mg/ml	1 mg/ml	0.1 mg/ml
56.2 mol%	38.3 mol%	5.3 mol%	0.2 mol%
274 ul	190 ul	190 ul	11 ul

The lipid film was rehydrated in 500 ul 155 mM $(\text{NH}_4)_2\text{SO}_4$ and incubated in a 60C water bath with periodic vortexing until resuspended. The test tube was placed in a beaker of 60C water and sonicated in alternating power cycles of 6 W and 3 W in 30 s intervals using a Microson XL probe tip sonicator (Misonix) until the suspension was clear (1-5 min, depending on volume). If a narrow size distribution was required, the liposomes were then extruded at 60C through a 200 nm polycarbonate membrane (Whatman) 21x. A MiniTrap G25 column (GE Life Sciences) was primed with 150 mM NaCl and spun at 1000g for 2 min. Liposomes were loaded into the column bed and spun at 1000g for 2 min, then added to 150 μg dox and incubate at 60C for 30 min – 1 h. A new MiniTrap G25 column was primed with PBS and spun at 1000g for 2 min. The liposome-dox mixture was loaded into the column and spun at 1000g for 2 min. Dox encapsulation was measured by disrupting liposomes w/0.5% Triton X-100 and reading the fluorescence at 479 nm excitation/593 nm emission on an Infinite 200 Pro microplate reader (Tecan). Particle diameter was analyzed by dynamic light scattering on a 90 Plus Particle Size Analyzer (Brookhaven).

Dox liposome release kinetics

Dox liposomes were placed in Slide-A-Lyzer MINI Dialysis Devices 20,000 MWCO (Pierce) and incubated at 37C in 2.5 ml PBS + 10% FCS. Samples were diluted with PBS + 0.5% Triton X-100 and the fluorescence was read at 479 nm excitation/593 nm emission.

SN-38 ICMV synthesis and characterization

5.8 mol lipid (50 mol% MPB DOPE, 50 mol% DOPG) in chloroform and 150 μg SN-38 in tetrahydrofuran were mixed in a glass test tube and dried under a nitrogen stream into a film, then dried in vacuo overnight.

MPB-DOPE	DOPG	SN-38
25 mg/ml	25 mg/ml	0.5 mg/ml
50 mol%	50 mol%	150 μg
117 ul	92 ul	300 ul

The drug-lipid film was rehydrated in 1.84 ml of 10 mM bistrispropane buffer pH 7 and vortexed intermittently for 5 min. The suspension was sonicated on ice for 3 min in alternating power cycles of 6 W and 3 W in 30 s intervals using a Microson XL probe tip sonicator. The sonicated lipid mixture was pelleted at 21000g to separate out SN-38 precipitate. The SN-38 liposomes in the supernatant were fused with 4 mM CaCl₂ and crosslinked with 3 mM dithiothreitol at 37C for 1 h. ICMVs were pelleted at 21000g and washed in PBS three times. Particle diameter was analyzed by DLS on a 90 Plus Particle Size Analyzer. SN-38 encapsulation was measured by dissolving ICMVs in 0.1 M NaOH + 0.5% Triton X-100 and measuring the fluorescence at 380 nm excitation/560 nm emission.

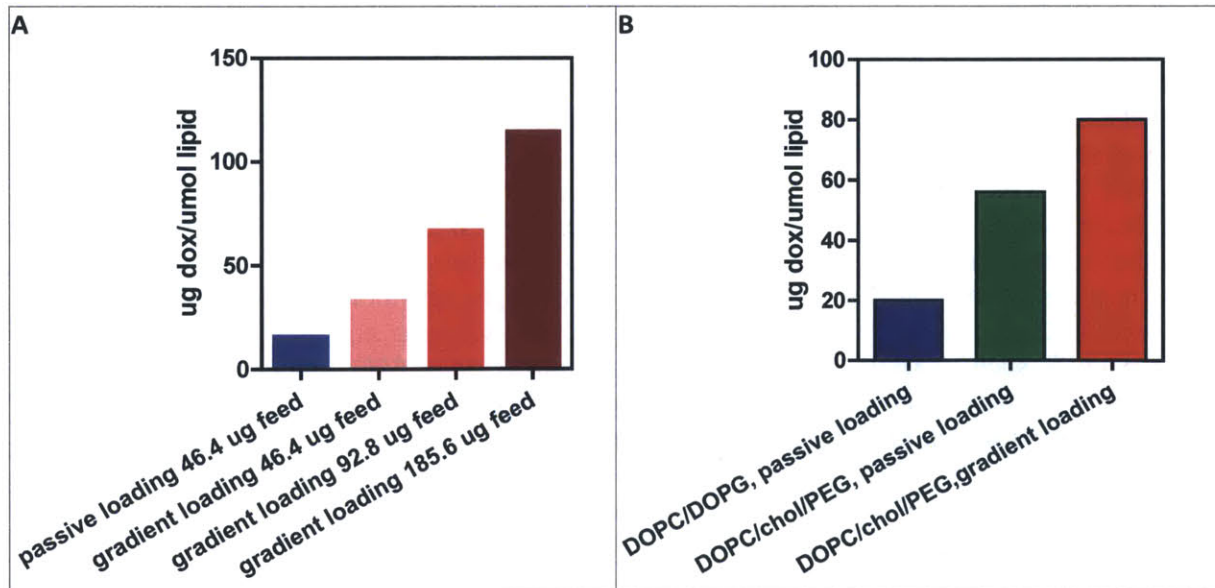
SN-38 ICMV release kinetics

SN-38 ICMVs were placed in 1 ml PBS + 10% FCS and incubated at 37C. Samples were pelleted at 21000g and the supernatant was diluted with 0.1 M NaOH + 0.5% Triton X-100 and the fluorescence was read at 380 nm excitation/560 nm emission.

Results and Discussion

Effects of gradient loading and high T_m lipids on dox retention and liposome stability

Based on its extensive characterization and clinical record, we used Doxil as a template for designing a liposome system that could be conjugated to cell carriers. First, we confirmed that dox loading via ammonium sulfate gradient yielded higher encapsulation efficiency and prolonged *in vitro* release compared to passive loading by mixing dox with lipids during the first step of liposome formation (Figure 2.3).



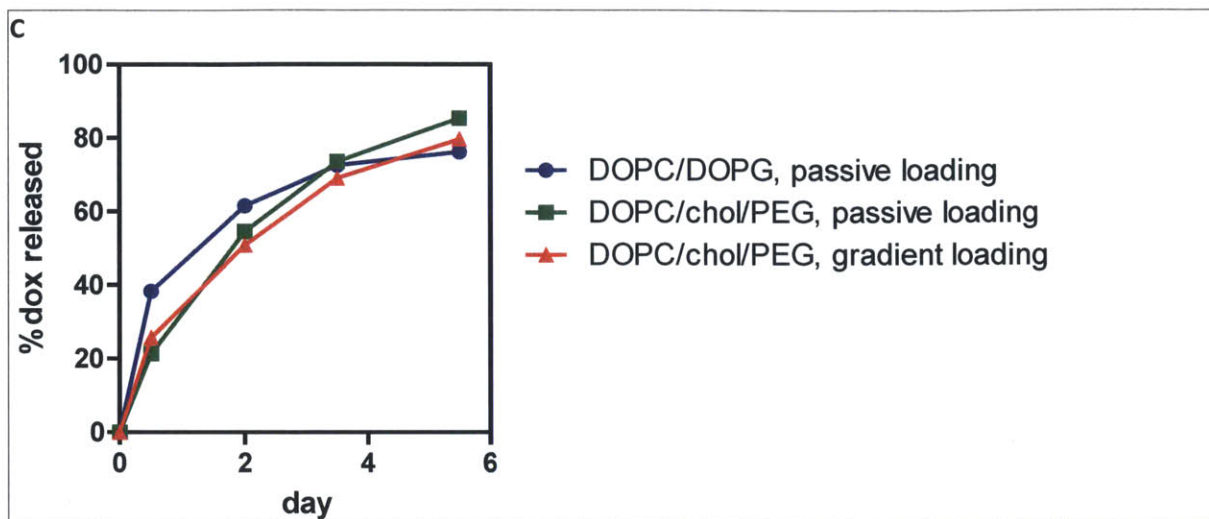


Figure 2.3: Effects of gradient loading and liposome composition on dox encapsulation and release (A) Gradient-loaded liposomes have higher dox encapsulation than passively-loaded liposomes. Liposomes composed of 80/20 mol% DOPC/DOPG (1 mg total lipids, freeze-thaw 21x, extruded through 400 nm membranes) were incubated with varying amounts of dox by either rehydrating the lipid film with dox solution or loading via an ammonium sulfate gradient. (B & C) Changing the lipid composition to resemble Doxil and gradient-loading both increase dox encapsulation and prolong release. Liposomes were made from 80/20 mol% DOPC/DOPG or 56.2/38.3/5.3 mol% DOPC/cholesterol/PEG2000-DOPE, and incubated with 185.6 μg dox by passive loading or gradient loading. Release kinetics of loaded liposomes was measured in PBS 10% FCS at 37C.

Prior kinetics studies of T cell homing *in vivo* showed significant accumulation of T cells in the lymph nodes 2-3 days post-adoptive transfer (Weninger et al., 2001), suggesting the need for slow drug release during this trafficking window, both to minimize T cell death and to increase the amount of remaining drug payload once T cells arrive in the tumors. While gradient-loaded DOPC/DOPG liposomes had slower dox release rates compared to passively-loaded liposomes of the same composition, the majority of dox was still released within the first 2 days (Figure 2.3). The lipid composition of Doxil has also been optimized for liposome stability *in vivo*. Cholesterol increases liposome stability and reduces the leakage of entrapped small molecules from the liposome lumen (Allen and Cleland, 1980). Multiple groups have reported the use of high T_m (phase transition temperature) lipids to increase the retention of dox in gradient-loaded liposomes (Allen et al., 2005; Charrois and Allen, 2004; Mayer et al., 1989)(Figure 2.4). While low T_m lipids such as DOPC are fluid at room temperature or 37C, higher T_m lipids such as HSPC are crystalline and much less permeable at those same temperatures, thereby providing an additional barrier to dox diffusion out of liposomes.

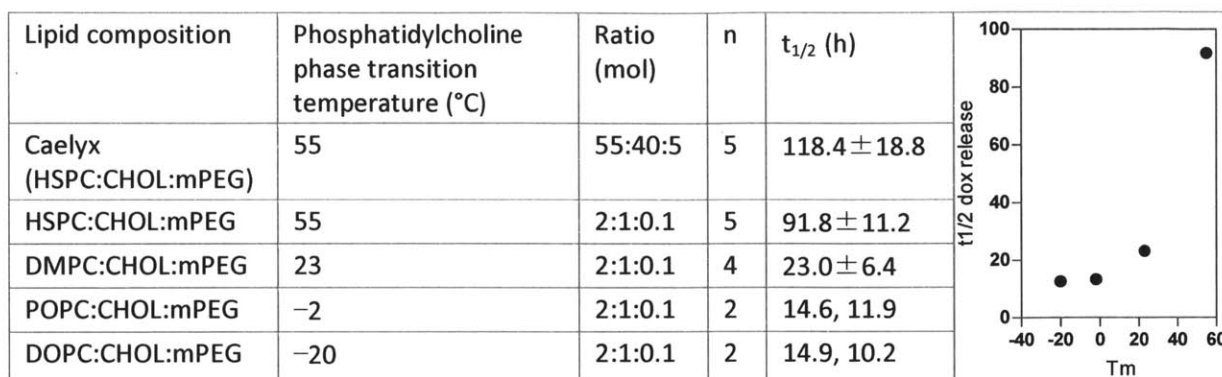


Figure 2.4: Lipid phase transition temperature is correlated with the half-time of dox release *in vivo*. Liposomes containing of high T_m lipids have increased release half-times of encapsulated dox release *in vivo*. Adapted from (Charrois and Allen, 2004).

We confirmed that the half-time ($t_{1/2}$) of dox release was correlated with lipid T_m . However, liposome instability and aggregation were also correlated with lipid T_m , resulting in low yields (Figure 2.5). PEG-grafted lipids were developed in the 1990's to increase the *in vivo* half-life of liposomes (Allen et al., 1991), and mechanistic studies have suggested their primary function is to prevent liposome aggregation (Dos Santos et al., 2007). Incorporation of PEG-lipids stabilized even the highest T_m liposomes, but also decreased cell conjugation, as discussed below.

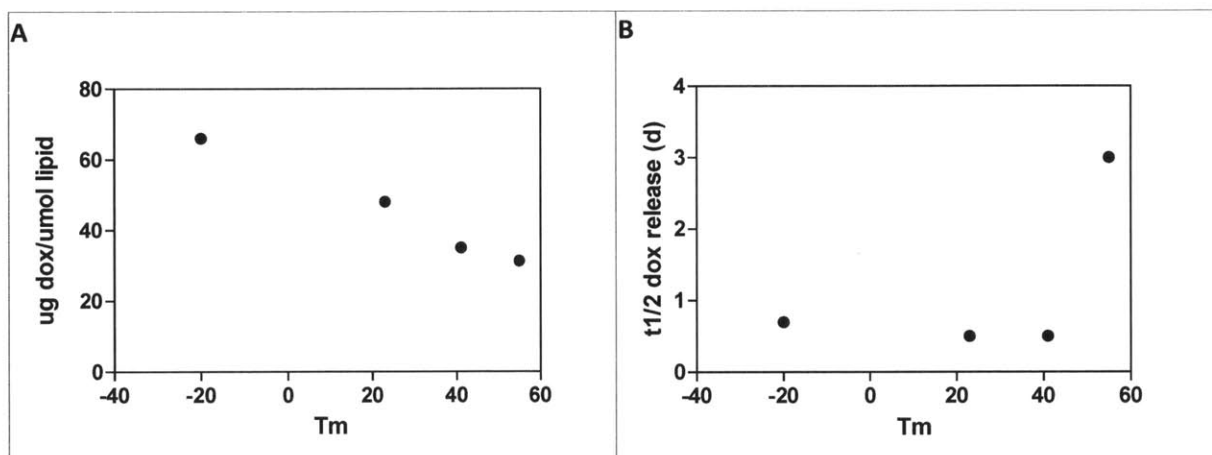


Figure 2.5: Lipid T_m is correlated with dox retention time and inversely correlated to liposome stability. Liposomes were synthesized from 38.3/0.2/3.4/61.5 mol% cholesterol/vitamin E/DiD/PC of increasing T_m (DOPC < DMPC < DPPC < HSPC) and gradient-loaded with dox. All samples except the one containing DOPC had significant aggregation and lipid loss during processing. (A) Liposome yield was estimated by DiD recovery and dox encapsulation was normalized accordingly. (B) Release kinetics of loaded liposomes was measured in PBS 10% FCS at 37C.

Modification of gradient-loaded doxorubicin liposomes for cell conjugation

Previous work in our group had successfully conjugated cells with liposomes and ICMVs composed of 50/40/10 mol% MPB-DOPE/DOPC/DOPG; therefore, our initial formulations of dox liposomes also used this composition. However, the resulting liposomes had a low

encapsulation rate of ~15 µg dox/mg lipid, compared to 200 µg/mg for Doxil. Increasing the feed amount of dox caused rapid aggregation and poor yield of liposomes, which was consistent with observations of as little as 1 mol% MPB-DOPE causing leakiness and precipitation of liposomes during dox loading (Hansen et al., 1995). We attempted to reduce liposome instability by using higher T_m lipids; however, substitution of MPB DOPE (T_m -16°C) with MPB DPPE (T_m 63°C) and/or substitution of DOPC (T_m -20°C) with HSPC (T_m 55°C) exacerbated liposome aggregation during synthesis, even without dox loading. Although the addition of lipids functionalized with PEG of differing lengths (MW 350-2000) could stabilize MPB-DOPE/HSPC/cholesterol and MPB-DPPE/HSPC/cholesterol liposomes prior to dox loading, it failed to rescue them from precipitation during dox loading. Therefore, we concluded it was not possible to directly include MPB-functionalized lipids from the beginning of the synthesis procedure.

One approach to surface functionalize liposomes is by post-inserting lipids into pre-formed vesicles. Allen et al. developed a protocol wherein PEG-lipid is incubated with dox-loaded liposomes at high temperatures, and the PEG-lipids redistribute from micelles to fluid liposome membranes via a dynamic equilibrium process (Iden and Allen, 2001; Ishida et al., 1999; Uster et al., 1996). Once the liposomes are cooled below the lipid T_m, the PEG-lipids are stably incorporated. In theory, this approach can be applied to all lipids, that spontaneously assemble into micelles in solution depending on their critical micelle concentration. We attempted to functionalize HSPC/cholesterol/DiD liposomes (not loaded with dox) by incubation with 1-20 mol% maleimide-PEG2000-DSPE. However, maleimide-PEG2000-DSPE post-insertion was very inefficient and the resulting liposomes did not conjugate to T cells to a detectable extent, as measured by cell lysate DiD fluorescence. In comparison, the same liposomes containing as little as 10 mol% MPB-DOPE but unloaded conjugated to T cells with 30% efficiency by the same measure. Attempts to post-insert MPB-DOPE into dox-loaded HSPC/cholesterol liposomes caused aggregation. Thus, post-insertion could not introduce maleimide-PEG-lipid at high enough density for cell conjugation, nor could it circumvent MPB-lipid mediated instability of dox liposomes.

The post-insertion method inspired us to pursue a two-step liposome synthesis strategy in order to separate the dox loading and maleimide functionalization steps. We assumed that the MPB head group of MPB-DOPE (or the analogous headgroup of the structurally similar MCC-DOPE) was responsible for precipitating dox during loading, so we sought to substitute this lipid with one that has an alternative functional group, which could be converted later to a maleimide via a bifunctional crosslinker.

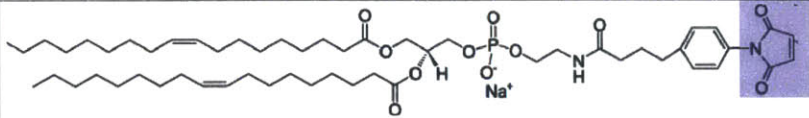
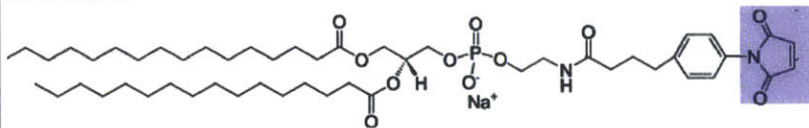
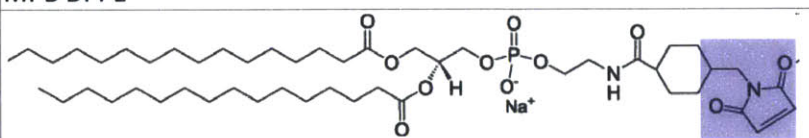
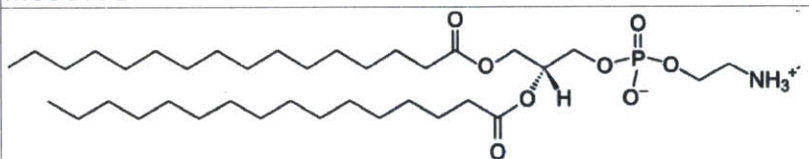
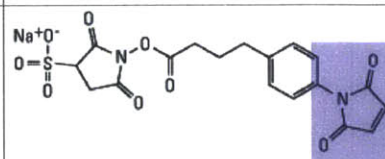
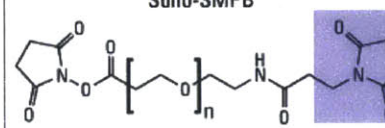
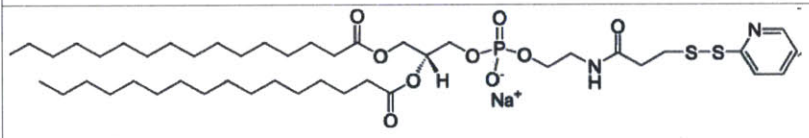
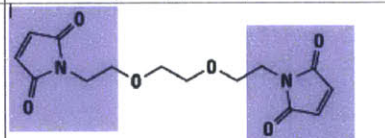
Functionalized lipid on liposome surface	Bifunctional crosslinker
 <p>MPB DOPE</p>	None
 <p>MPB DPPE</p>	None
 <p>MCC DPPE</p>	None
 <p>DPPE</p>	 <p>Sulfo-SMPB</p>  <p>SM(PEG)_n, n=4, 8 or 24</p>
 <p>PDP DPPE</p>	 <p>BM(PEG)₂</p>

Figure 2.6: Liposome modification schemes for surface maleimide functionalization.

Maleimide groups are highlighted in blue. DPPE (and other PE lipids) were reacted with NHS-maleimide crosslinkers at 1:10 molar ratio for 2 h at room temperature. PDP-DPPE was cleaved with 20 mM dithiothreitol for 1 h at room temperature, then reacted with bismaleimide crosslinkers at a 1:20 molar ratio for 1 h at room temperature.

Phosphatidylethanolamine (PE) has an amine headgroup that can react with a bifunctional NHS ester-maleimide crosslinker (Figure 2.6). Unfortunately, PE containing liposomes were extremely prone to aggregation, regardless of the PE tail length and T_m . Aggregation occurred even in the absence of dox loading and in a wide variety of buffers, consistent with earlier reports that PE liposome stability is very sensitive to osmolarity and pH (Allen et al., 1990). The minor fraction of non-aggregated PE liposomes isolated during synthesis was incubated with sulfo-SMPB or NHS-PEG-maleimide to convert the amine group of the PE lipids to maleimide. However, either the amount of PE incorporated was low, or the amine to maleimide conversion was inefficient, because even the resulting liposomes conjugated to cells with only 1-5% efficiency.

PDP-PE has a disulfide headgroup that can be cleaved by a reducing agent to activate a free thiol, which can then react with a bis-maleimide crosslinker (Figure 2.6). While PDP-PE liposomes were an improvement from PE liposomes, they still suffered from aggregation, modest dox yield, rapid dox release, and less than 5% conjugation efficiency.

Finally, we synthesized dox liposomes with all 5.3 mol% methoxy-PEG2000-DSPE substituted by maleimide-PEG2000-DSPE. Crucially, maleimide-PEG-lipid required sonication to incorporate successfully into liposomes. Liposomes with the same amount of maleimide-PEG-lipid made by extrusion did not conjugate to cells, whereas sonicated liposomes conjugated at 2-5% efficiency. These liposomes had comparable release rates as unmodified Doxil (Figure 2.7). Although maleimide-PEG liposomes conjugate at a lower level, the amount that is retained after 1 day *in vitro* is higher, compared to MPB dox liposomes.

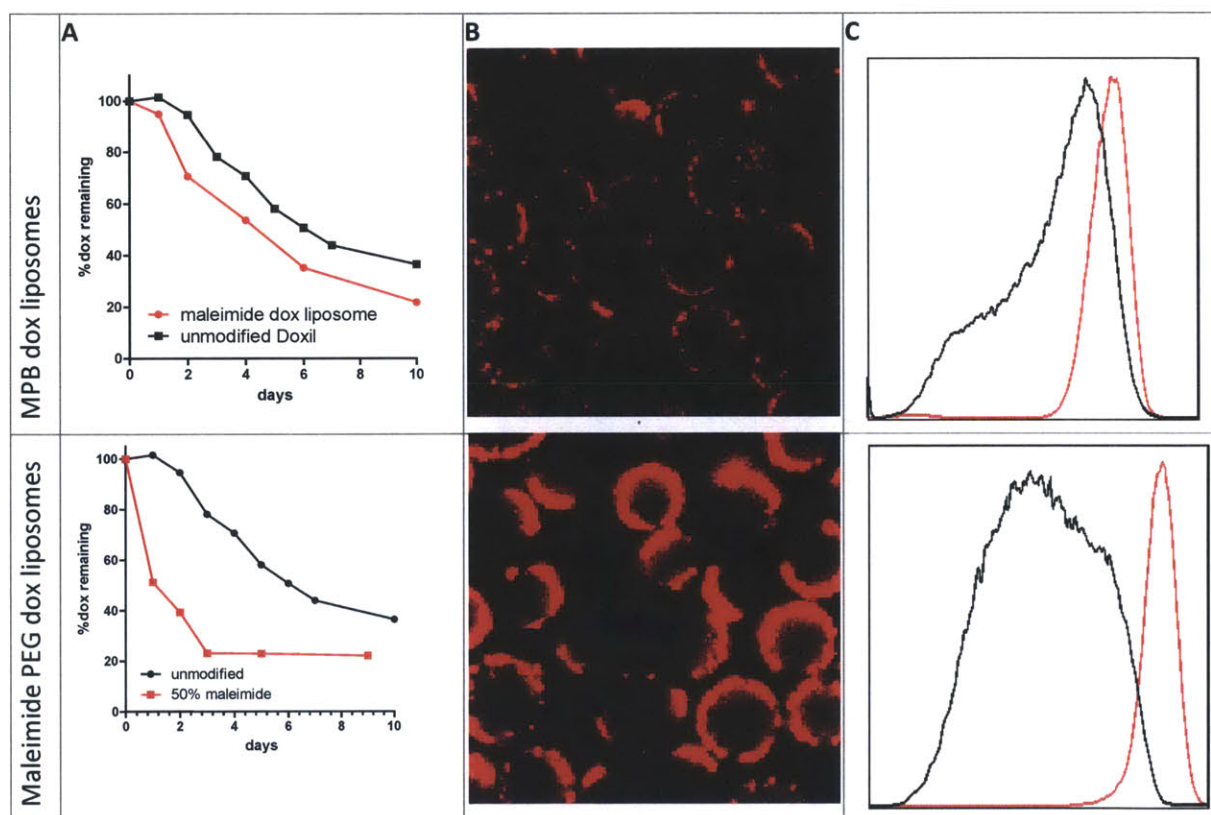


Figure 2.7: Comparing stability and conjugation efficiency of maleimide-PEG versus MPB dox liposomes. (A) Maleimide-PEG dox liposomes (red) have similar release kinetics to those of Doxil (black), while MPB dox liposomes (red) release much faster. (B) rhodamine-lipid labeled maleimide-PEG liposomes or MPB dox liposomes (red) were conjugated to the surface of T cells. (C) Rhodamine liposome fluorescence was measured by flow cytometry immediately after conjugation (red trace) and after 1 day of *in vitro* culture (black trace).

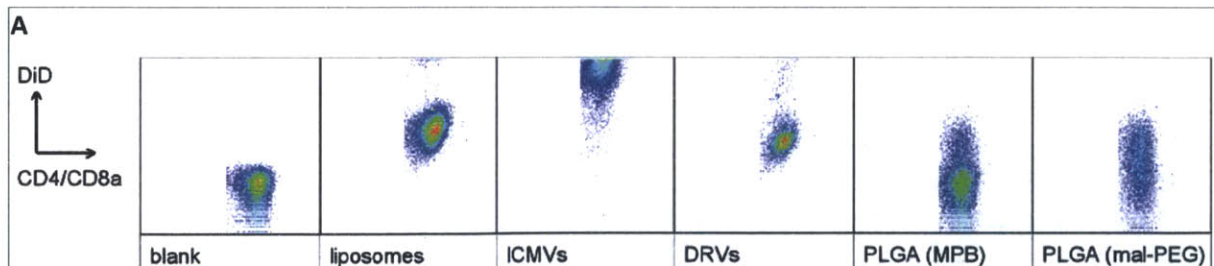
This final formulation preserved the high dox loading efficiency and particle stability of the original liposome system, and did not require additional processing steps during the synthesis.

Screening of SN-38 particle formulations

Based on the solubility of SN-38 in common solvents (Figure 2.8), we explored four compatible nanoparticle systems for its encapsulation: liposomes, dehydration-rehydration vesicles (DRVs), poly(lactic-co-glycolic acid) (PLGA) particles and lipid-based interbilayer-crosslinked multilamellar vesicles (ICMV). The characterization of the first three systems are detailed in Appendix II. ICMVs are structurally fortified multilamellar vesicles developed by Dr. James Moon (postdoc in the Irvine group) by fusing and crosslinking unilamellar liposomes (Moon et al., 2011). In pilot experiments, we synthesized all four particle systems from the same starting amount of lipid and SN-38, then added the same fraction of particles to Emu-myc Arf^{-/-} cells to measure toxicity. Although we did not quantify the exact encapsulation efficiency or particle yield, all four particle systems were very potent against Emu-myc Arf^{-/-} cells, suggesting successful encapsulation. However, only ICMVs reproducibly conjugated to T cells with high efficiency. Correspondingly, in a co-culture assay, only T cells conjugated with ICMVs were able to kill Emu-myc Arf^{-/-} cells efficiently (Figure 2.9). Therefore, we moved forward with the development of SN-38 ICMVs.

Solvent	Solubility
DMSO	>10 mg/ml
Aqueous buffers	~10 µg/ml
Aqueous buffer, pH ≥ 10 (0.1 M NaOH)	>1 mg/ml
Dimethylformamide	~0.5 mg/ml
Acetone	~125 µg/ml
Acetonitrile	Insoluble
Dioxane	~0.5 mg/ml
Tetrahydrofuran	~0.5 mg/ml
Ethanol	Insoluble
Methanol	Insoluble
Dichloromethane	Insoluble
Chloroform	Insoluble
4:1 DCM:methanol	10 mg/ml

Figure 2.8: SN-38 solubility in common solvents.
Compiled from empirical results and (Zhang et al., 2004).



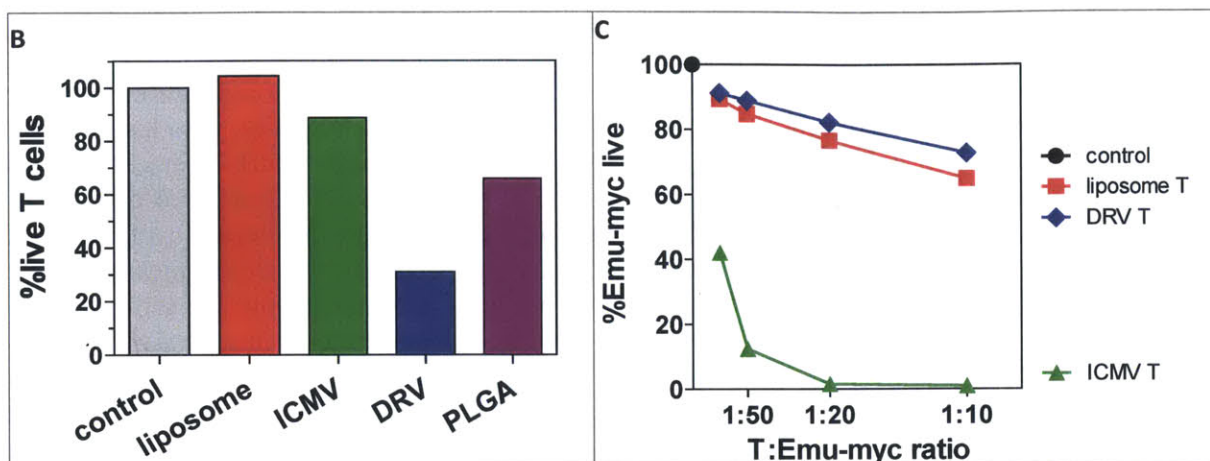


Figure 2.9: Comparison of SN-38 particle formulations.

(A) T cells were incubated with the same amount of particles, washed, and analyzed by flow cytometry for DiD particle conjugation. ICMVs conjugated to T cells with the highest efficiency. Each particle formulation had the same starting amount of SN-38, lipid, and DiD tracer. (B) Immediately after conjugation, T cell viability was measured by flow cytometry. In particular, DRVs seemed to be unstable and released SN-38 rapidly during conjugation, killing the majority of the T cells. (C) Particle-functionalized T cells were assessed for their ability to kill Emu-myc $Arf^{-/-}$ cells in a co-culture. ICMV-conjugated T cells were the most potent.

Optimization of SN-38 ICMVs

The primary source of SN-38 loss is in the first step of ICMV synthesis, where rehydration of the lipid and SN-38 film causes SN-38 aggregation and exclusion from liposomes. Starting from a composition of 50/50 mol% MPB-DOPE/DOPC, which has 10% SN-38 loss after sonication and final encapsulation efficiency of 44%, we tuned the lipid composition to decrease SN-38 loss and increase encapsulation. Complete substitution of DOPC with DOPG resulted in only 6.5% SN-38 loss after sonication, increased final ICMV yield and increased SN-38 encapsulation efficiency to 60%. This became our standard formulation of 50/50 mol% MPB-DOPE/DOPG, with 14 μ g SN-38 encapsulated per μ mol lipid. We speculate that, compared to zwitterionic DOPC, anionic DOPG can bridge apposing lipid bilayers more closely via electrostatic interactions with calcium ions during the stapling step, and thereby increase the efficiency of interbilayer covalent crosslinking, leading to more stabilized ICMVs. However, it is unclear how the charge of DOPG contributes to SN-38 solubilization, since the latter is neutral or negatively charged in solution.

Both MPB-DOPE/DOPC and MPB-DOPE/DOPG ICMVs released SN-38 over approximately 3 days *in vitro*, and we suspected this rapid release was due to the fluidity of DOPC (T_m -20C) and DOPG (T_m -18C) at 37C. We attempted to decrease the permeability of ICMVs by substituting in 10 mol% cholesterol, or up to 50% DMPC or DMPG (both T_m 23C). Unfortunately, none of these substitutions had any effect on SN-38 encapsulation or release. Although we capped the ICMVs with PEG2000-SH to quench the unreacted MPB groups on the surface, this also did not change the release kinetics. Similarly, post-insertion of PEG2000-DSPE or capping with beta-mercaptoethanol to reduce ICMV surface interactions with serum components also had no effect (Figure 2.10). SN-38 release rates were the same in PBS with or without 10% serum, but

increased with temperature, suggesting that it is purely limited by SN-38 dissociation from lipids and not affected by ICMV degradation.

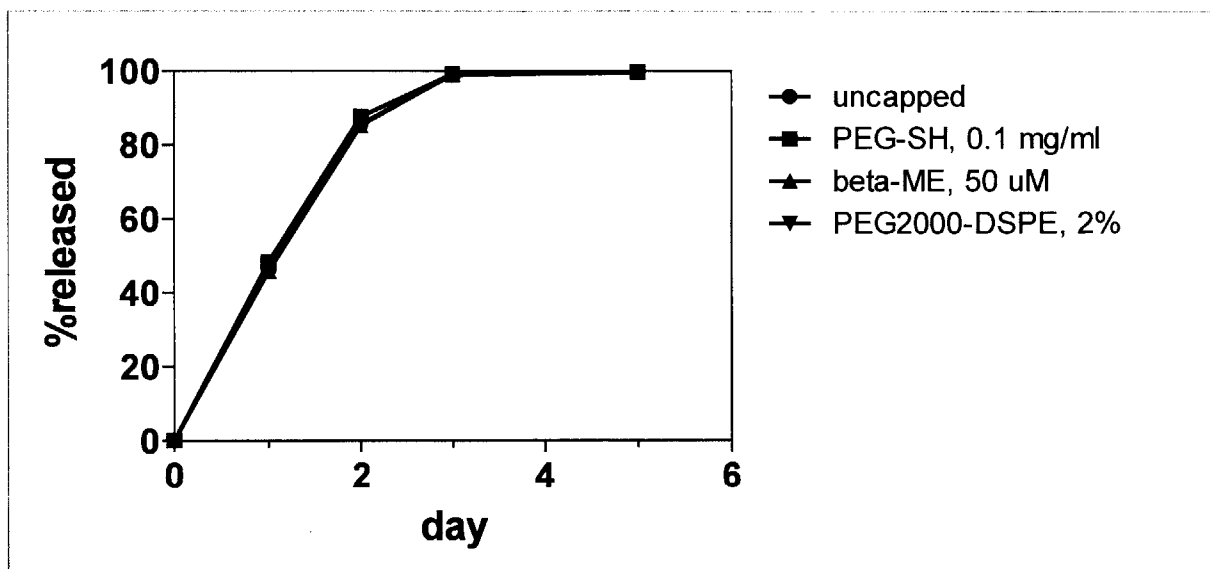


Figure 2.10: Release kinetics of SN-38 from ICMVs.

SN-38 ICMVs were synthesized from 50/50 mol% MPB-DOPE/DOPC and 50 μ g SN-38. ICMVs were either left uncapped, capped with 0.1 mg/ml PEG2000-SH, 50 μ M beta-mercaptoethanol, or post-inserted with 2 mol% PEG2000-DSPE. Particles were set up for release in PBS + 10% FCS at 37C.

SN-38 carriers for ICMV incorporation

Based on literature of irinotecan liposomes (Burke et al., 1993), we assume that SN-38 partitions to the lipid bilayers of ICMVs, but we have not performed studies on its exact localization. Due to the rapid precipitation of SN-38 after exposure to aqueous buffers, it is likely that the SN-38 incorporated in ICMVs is present in both lactone and carboxylate forms, probably in aggregates ranging from dimers to nanometer-sized precipitates. We attempted to control the drug distribution in ICMVs by two approaches: 1) non-covalent complexation with a carrier molecule, and 2) conjugation to a lipid. The goal was to prevent SN-38 self aggregation and to provide an additional dissociation/hydrolysis step that would slow SN-38 release from ICMVs.

SN-38 binds strongly to serum albumin, which transports a variety of hydrophobic molecules such as lipids (Burke and Mi, 1994; Combes et al., 2000). We pre-incubated bovine serum albumin (BSA) and SN-38, then used this mixture to rehydrate ICMV lipids in the first step of synthesis. However, BSA exacerbated SN-38 aggregation and increased drug loss to 63% prior to ICMV stapling. Therefore, BSA did not bind SN-38 with high enough affinity to stabilize it in solution, and did not improve its encapsulation or change its release kinetics.

We then sought to conjugate SN-38 to a lipid that could be used directly in ICMV synthesis. Given the lipophilic nature of SN-38, we hypothesized it would be optimal to conjugate it to the acyl tail, as opposed to the phosphate headgroup of a phospholipid, such that when the bilayers are formed, SN-38 would be embedded in the hydrophobic interior. Dr. Haipeng Liu (postdoc in the Irvine group) synthesized the conjugate of SN-38 and PGPC (detailed in Appendix II). The

resulting SN-38-lipid could be mixed in up to 10 mol% to form ICMVs with monodisperse size (~200 nm) and up to 86% SN-38 encapsulation efficiency. However, SN-38 release was complete in 1 day, which is even more rapid than from ICMVs encapsulating free SN-38. This is probably due to the rapid hydrolysis of the SN-38-PGPC bond. SN-38 conjugated to PEG-poly(glutamic acid) block copolymer via the 10-hydroxyl was ~60% hydrolyzed within 24 h of incubation in PBS at 37C (Koizumi et al., 2006). Previous reports of SN-38-antibody conjugates suggests that conjugation to the less reactive 20-hydroxyl improves conjugate stability;(Moon et al., 2008) however, this requires protection and de-protection steps to mask the 10-hydroxyl. If the chemistry could be modified to stabilize the SN-38-lipid bond, finer control over the release rate would be possible.

Summary and Conclusion

Doxil liposomes were developed to have minimal interaction with plasma components and resist clearance by the reticuloendothelial system, and therefore possess an inert surface chemistry. In our attempts to activate this surface chemistry for cell conjugation, we found that dox loading and retention were extremely sensitive to lipid composition. Unstable composition liposomes could be improved by the presence of a PEG corona, which can be tuned by both the mol% of PEG-lipids and the length of their PEG chain. However, as expected, the PEG corona also decreased cell conjugation efficiency, probably by sterically shielding liposome surface reactive groups from the cell membrane. Ultimately, the sole modification we made was substitution of the 5.3 mol% methoxy-PEG2000-DSPE with an equimolar amount of maleimide-PEG2000-DSPE. This change preserved the stability, high dox encapsulation and slow release of Doxil, but also allowed direct conjugation of loaded liposomes to T cells without additional modification of the liposomes or cells. However, the major disadvantage of this approach was low conjugation efficiency, limiting the total dose of dox that could be carried by each T-cell. The quantification and therapeutic consequences of which are discussed in latter chapters.

The primary challenge of encapsulating SN-38 was preventing drug precipitation upon exposure to aqueous buffers during particle synthesis. We addressed this by mixing SN-38 with lipids and allowing them to dry together prior to rehydration and ICMV formation. The resulting particles had high SN-38 encapsulation but particle size remained submicron and could be enriched for particles <500 nm by centrifugal fractionation. However, changes in the lipid particle composition did not significantly influence the drug release kinetics. One area of interest for future studies is the influence of drug release rate on therapeutic efficacy. We hypothesize that a too rapid release rate would kill the carrier T cells prior to their arrival in tumors, but a too slow release rate may not cause sufficient tumor clearance, and could allow the surviving tumor cells to acquire resistance.

In our studies, particle stability and particle surface group reactivity seemed to be mutually antagonist parameters, and much of the particle optimization was spent on finding the appropriate balance between these two factors. A more sophisticated particle design approach may be to first synthesize stable particles with relatively low surface reactivity that does not interfere with high drug loading, then amplify the number of surface reactive groups. Such a modular approach would allow the particle core to be optimized for the chemistry and desired release kinetics of each drug, while the conjugation chemistry can be separately optimized for the cell carrier type.

3. The Emu-myc Arf^{-/-} lymphoma model and engineered T cell carriers

Introduction

Emu-myc lymphoma as a model of disseminated cancer

The Emu-myc B cell lymphoma model was the first rationally-designed transgenic mouse model of spontaneous tumorigenesis (Hanahan et al., 2007). The transgene consists of the oncogene c-myc downstream of the immunoglobulin heavy chain enhancer E μ (Emu) (Adams et al., 1985). This genetically engineered molecular lesion models the c-myc translocation that defines human Burkitt's lymphoma, although the latter is frequently attributed to Epstein-Barr virus infection. During normal B cell development, VDJ rearrangement of the immunoglobulin genes causes Emu activity and subsequent c-myc expression. The c-myc transgene drives aggressive growth and proliferation in favor of differentiation, resulting in abnormally high percentages of pre-B cells in the bone marrow and spleen (Langdon et al., 1986). These pre-B cells can proceed to mature into B cells in a process requiring activation-induced (cytidine) deaminase (AID) (Kotani et al., 2007). During pre-neoplasia in Emu-myc mice, normal B cell function is preserved, with intact *in vitro* responses to LPS stimulation and *in vivo* responses to hapten immunization (Vaux et al., 1987). The transgene is completely penetrant and all mice develop lymphomas at ages ranging from a few weeks to six months.

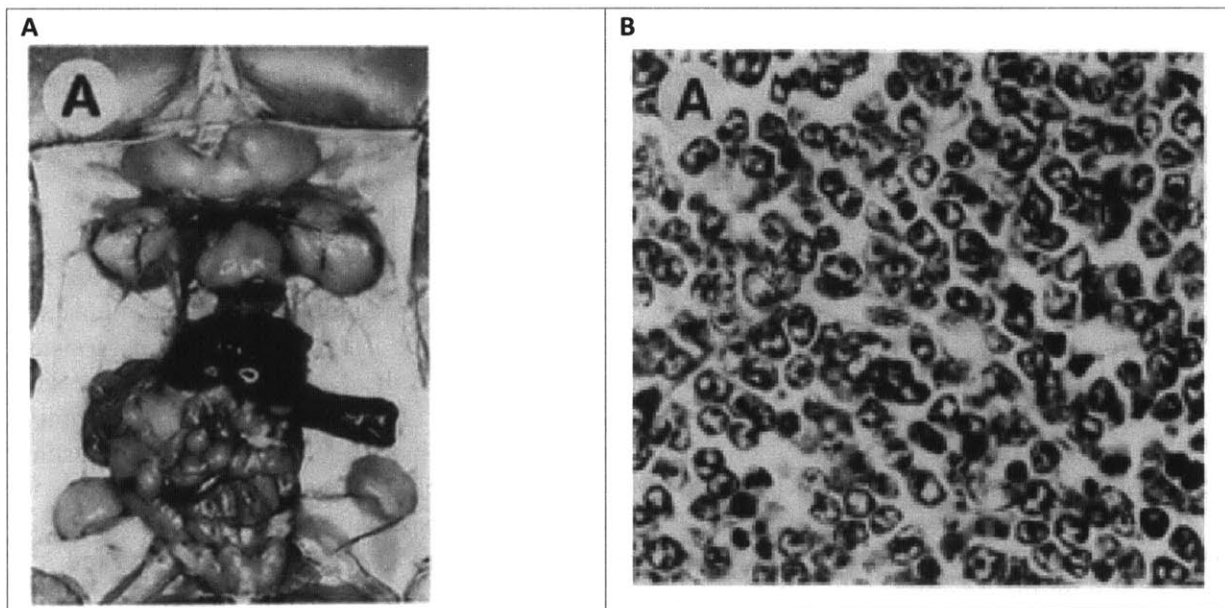


Figure 3.1: The Emu-myc lymphoma model.

(A) The Emu-myc transgenic model spontaneously develops lymphomas that infiltrate multiple organs, such as the enlarged spleen and lymph nodes shown in the photograph. (B) Emu-myc lymphoma-ridden lymph nodes have a "starry sky" histological pattern that is characteristic of Burkitt's lymphoma (Harris et al., 1988). Tumor cells isolated from primary tumors can be transplanted into wild-type recipients to recapitulate the disease.

Heterogeneity in tumor latency is partially due to the specific mutations acquired by the oncogenic cell(s) of origin. C-myc-fueled proliferation is opposed by p53-mediated apoptosis, and lymphoma progression is significantly accelerated when Emu-myc cells mutate or inactivate pro-apoptotic members of the p53 pathway, such as p19 Arf (Eischen et al., 1999; Jacobs et al., 1999; Schmitt et al., 1999). One approach to simplify the model has been to cross the Emu-myc mouse with other mouse models carrying tumor suppressor deletions, such that the p53 pathway is already inactivated and alleviates the pressure for the tumor cells to randomly inactivate a member of the pathway (Schmitt et al., 2002a). For example, the Emu-myc Arf^{-/-} strain has a much more synchronized lymphoma onset time than the parental Emu-myc strain.

The Emu-myc mouse can also be used to generate transplanted tumor models, either by bone marrow chimeras (Hemann et al., 2003) or by harvesting tumors to purify lymphoma cells (Schmitt et al., 2000). Primary tumor-derived lymphoma cells can be cultured *in vitro* for a short time without genetic instability, and are amenable to genetic manipulation via retroviral transduction with MSCV (mouse stem cell virus) based vectors (Schmitt et al., 2000). After adoptive transfer into healthy wild-type recipients, Emu-myc cells (both wild-type and with additional genetic modifications such as Arf knockout) recapitulate the same pathology as in the spontaneous tumor model, colonizing and expanding in the bone marrow, spleen, lymph nodes, and blood. Enlargement of spleen and lymph nodes proceeds very rapidly until morbidity. At late times, Emu-myc cells may also infiltrate the central nervous system via the spine, causing hind-limb paralysis, or the gut-associated lymphoid tissue, causing intussusception (Harris et al., 1988).

Based on the thorough characterization of this model, we chose the Emu-myc Arf^{-/-} transplanted lymphoma model for its experimental tractability, disseminated nature and well-defined sensitivity to chemotherapies, including dox and camptothecin, a SN-38 related drug. To facilitate monitoring of tumor burden kinetics in response to treatment regimens, we modified the Emu-myc Arf^{-/-} line to express luciferase and GFP reporters.

Adoptive T cell therapy of lymphoma

Trials of adoptive T cell therapy began in the 1980's as an experimental treatment for metastatic melanoma (Rosenberg et al., 2008). Tumor-specific T cells were isolated from tumor biopsies, expanded *ex vivo*, then re-infused into the patient. Once *in vivo*, the T cells home to tumor sites abundant with antigen and exert cytolytic activity. The remarkable clinical outcomes of adoptive T-cell therapy, especially in the case of an aggressive disseminated disease such as metastatic melanoma, is partially due to the ability of the T-cells to "seek and destroy" their targets with limited collateral damage of normal tissues. This targeting is especially crucial for disseminated tumors, where small metastatic populations may not be cleared by systemic therapy and can eventually initiate relapse.

Recent advancements in adoptive T cell therapy have focused on increasing the potency and duration of each T cell dose, as well as applications to a wider variety of malignancies. The *in vivo* persistence and activity of the T cells are dependent on the molecular state of the cells, both at the time of isolation (Hinrichs et al., 2009) and after *in vitro* culture (Klebanoff et al., 2004). The tumor microenvironment can cause T cells to become functionally inert or apoptose, and one strategy to counteract this immunosuppressive effect is to activate pro-survival and proliferative

T cell signaling pathways with cytokines, co-stimulatory receptors (Stephan et al., 2007), or anti-apoptotic molecules (Charo et al., 2005).

Although B cells are antigen presenting cells and can present self-antigens in the proper context with co-stimulatory receptors, the majority of B cell lymphomas fail to initiate anti-tumor immune responses, even if they have undergone mutations that generate neo-antigens. Early studies using the lymphoma idiotype as the tumor antigen showed promising results in mouse models (Biragyn et al., 1999), but failed to show a clear therapeutic effect in clinical trials (Brody et al., 2011). Recent studies have shown promising results for anti-CD40 antibody (Tutt et al., 2002), CpG (Goldstein et al., 2011), and α -galactosylceramide pulsed tumor cells (Chung et al., 2007; Mattarollo et al., 2012) as immunotherapies for lymphoma. However, the importance of various immune cell subsets and cytokines in lymphoma eradication varies depending on the model, and our understanding of how lymphomas interact with the normal components of the immune system remains incomplete (Brody et al., 2011; Schultze, 1999).

Alternative efforts have turned towards chimeric antigen receptor (CAR) technology to reprogram T cells against lymphoma antigens (June et al., 2009). Using viral vectors, syngeneic T cells are genetically modified with a transgene that encodes an extracellular antigen-binding receptor linked to an intracellular T cell receptor signaling domain. The CAR T cells are thus able to sense the antigen of interest without the need for it to be presented by an antigen presenting cell, bypassing the requirement for co-stimulatory signals that can be diminished by tumor immunosuppression (Liddy et al., 2012). Recently, CAR T cells engineered against the B cell surface receptor CD19 showed impressive clinical results (Kochenderfer et al., 2012; Porter et al., 2011). However, sophisticated protein engineering required for CAR development, and concerns regarding the safety of viral vectors remain challenges to widespread clinical translation. Our work focuses on synthetic approaches towards cell modification (such as the particle conjugation strategies to be discussed in Chapter 4) that may be complementary with CAR technology.

Here we explored a different strategy for employing T-cells in lymphoma therapy, and developed procedures to expand T-cell *ex vivo* for non-antigen-specific tumor chemotherapy targeting. We tested the ability of two well-studied cytokines, IL-2 and IL-15, to generate large numbers of T cells, and analyzed their proliferation, homing markers and resistance to chemotherapy. We compared the phenotypes of these T cells to both naïve and activated B cells, in order to determine the optimal cell type for nanoparticle delivery.

Methods

Emu-myc Arf^{-/-} cell culture

Emu-myc Arf^{-/-} cells were cultured as previously described (Gilbert and Hemann, 2010). Briefly, Emu-myc Arf^{-/-} cells were plated at 0.1×10^6 /ml in B cell medium (45% IMDM, 45% DMEM, 10% FCS, Penn/strep) on a sparse layer of irradiated 3T3 fibroblasts (40 Gy). Cells were passaged 1:3 every day and kept in culture for less than 1 month.

T cell culture

To expand T-cells, splenocytes were plated at 5×10^6 /ml with 2 μ g/ml concanavalin A (Sigma) and 2 ng/ml IL-7 (Peprotech) in RPMI-1640 (Gibco) supplemented with 10% FCS, Penn/strep, 2-mercaptoethanol, non-essential amino acids and sodium pyruvate. After 2 days, T cells were plated in fresh supplemented RPMI with 20 ng/ml murine IL-2 (Peprotech) and 20 nM rapamycin (EMD). After an additional 2-3 days, cultures were $>90\%$ CD3 ϵ^+ .

Resting B cell isolation

To purify resting B cells, splenocytes were processed using the CD43 Microbeads negative selection kit (Miltenyi Biotec) following manufacturer instructions and used immediately.

Dox and SN-38 titration on cells

Emu-myc Arf $^{-/-}$ cells were resuspended in fresh B cell medium. Live T cells were purified from cultures by Ficoll density centrifugation, following manufacturer instructions (GE Healthcare), and resuspended in supplemented cytokine-free RPMI medium. Cells were plated at 1×10^6 /ml. The dox stock was diluted in PBS, the SN-38 stock was diluted in DMSO, and the appropriate amount was added to each well. Twenty-four hours later, 250 μ l of each well was pelleted in a 96-well plate and resuspended in PBS + 0.1% BSA with DAPI. Samples were analyzed on the BD LSR HTS and total events were collected. The low forward scatter, low side scatter, and DAPI negative population was gated as live cells.

Results and Discussion

Generation and characterization of the Emu-myc Arf $^{-/-}$ luciferase GFP lymphoma line

To track the dissemination of Emu-myc Arf $^{-/-}$ cells *in vivo* and their response to therapeutic intervention, we transduced Emu-myc Arf $^{-/-}$ cells with a firefly luciferase-GFP reporter as described in Appendix IV. Luciferase expression allowed non-invasive longitudinal imaging of tumor-bearing mice and confirmed tumor dissemination and expansion in the appropriate compartments. At the termination of the experiment, necropsy revealed tumor burdens that were macroscopically identical to those arising from Emu-myc Arf $^{-/-}$ cells that are wild-type or transduced with only GFP, suggesting the reporter proteins are not immunogenic and do not alter tumor progression. Tumors could then be dissociation and analyzed by flow cytometry for Emu-myc Arf $^{-/-}$ cell phenotype or enumeration.

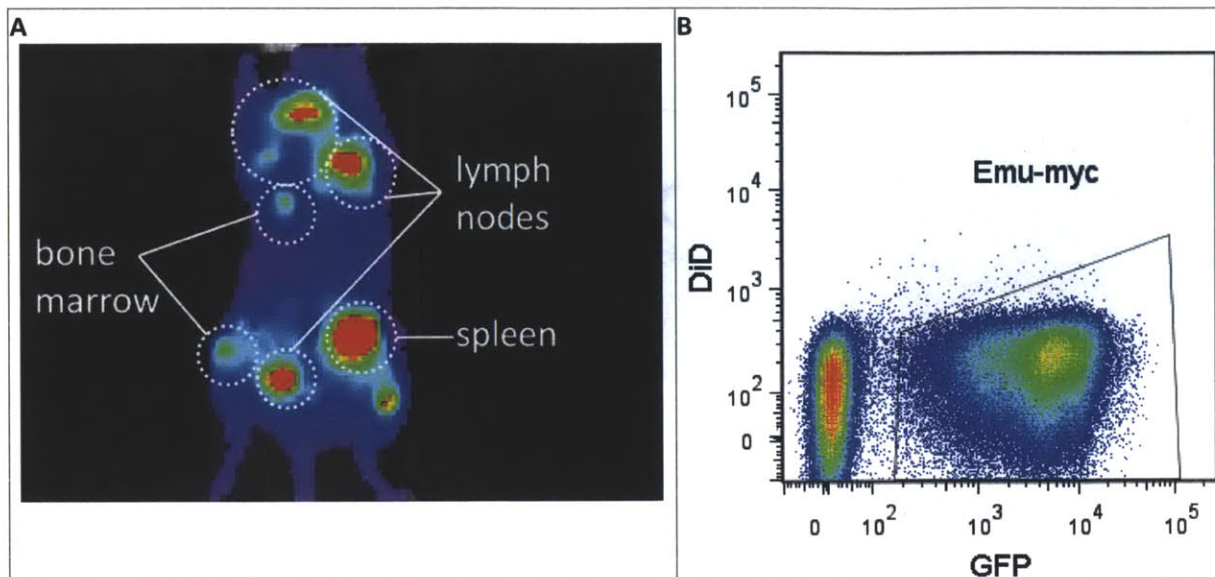


Figure 3.2: Emu-myc $Arf^{-/-}$ luciferase GFP line *in vivo* and *in vitro*.

(A) 1×10^6 Emu-myc $Arf^{-/-}$ luciferase GFP cells were transferred intravenously into a healthy albino C57BL6/J recipient. Fourteen days later, disseminated tumors were imaged IVIS. (B) Pooled lymph nodes of a tumor-bearing mouse, with a large population of GFP+ Emu-myc $Arf^{-/-}$ cells (gated).

Optimization of cells carriers to target lymphoid organs

Based on preliminary data, resting B cells ($CD43^-$) were shown to be promising cellular carriers for particle delivery, as they were easily conjugated with maleimide-functionalized nanoparticles *in vitro* and had very similar trafficking patterns as Emu-myc $Arf^{-/-}$ cells *in vivo* (Figure 3.3). However, flow cytometry analysis of tumor-bearing mice revealed that the transferred particle-carrying B cells were present at only a frequency of 0.1-1% of cells in the lymph nodes, spleen and liver. Assuming to first order that Emu-myc $Arf^{-/-}$ cells make up 50% of the lymphoid organs (estimate from Hemann lab histology analysis of H&E stained slides), this translates to fewer than two particle-functionalized B cell per 100 lymphoma cells, which we surmised would be too few for therapeutic effect. The number of B cells that could be transferred per mouse was limited by the initial cell isolation yield, which was $10-20 \times 10^6$ per donor mouse and required time-intensive cell preparation immediately prior to particle conjugation. These insufficient cell yields motivated the development of alternative primary cell carriers that could be expanded to larger numbers. Taking inspiration from the adoptive T cell therapy field, we aimed to generate large numbers of T cell carriers by *ex vivo* expansion with cytokines.

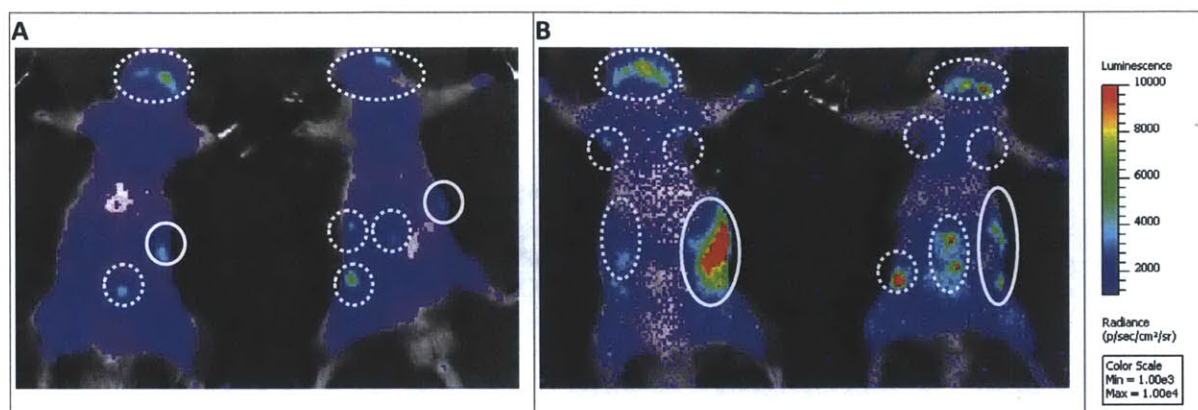


Figure 3.3: *In vitro* isolated resting B cells migrate to lymphoid organs *in vivo*.

Wild-type C57BL6/J mice were inoculated with 2×10^6 Emu-myc $Arf^{-/-}$ GFP cells. On day 12 post-inoculation, each mouse received 27×10^6 resting B cells (isolated from luciferase donor mice) and were imaged 1 day later. On day 15 post-inoculation, each mouse received 21×10^6 resting B cells conjugated with either empty liposomes (50:40:10 mol% MCC-DOPE:DOPC:DOPG, left mouse) or empty ICMVs (50:40:10 mol% MCC-DOPE:DOPC:DOPG, right mouse). Mice were imaged 1 day later. Lymph nodes are denoted by the dotted white outlines, spleens by the solid white outlines.

Activated T cells are robust cell carriers

IL-2 is a member of the common γ_c (common gamma chain) cytokines. As a potent T cell mitogen, it has been used to expand T cells *in vitro* for adoptive cell therapy, and is indicated for the treatment of metastatic renal cell carcinoma and metastatic melanoma. In physiological settings, it is produced by both antigen presenting cells during the priming of T cells, as well as the T cells themselves following activation. Its effects include increased metabolic activity, cellular proliferation, and down-regulation of naïve T cell homing receptors including CCR7 and CD62L. IL-15 is another cytokine member of the γ_c family, and has many overlapping effects as IL-2, but is thought to be crucial to the differentiation of memory T cells. We investigated the ability of these two cytokines to generate cell carriers for nanoparticles.

We activated splenocytes from wild-type donor mice with concanavalin A and IL-7 to enrich for polyclonal ($CD4^+$ and $CD8\alpha^+$) T cell blasts. After two days, we expanded the blasts with either IL-15 or IL-2, following existing protocols in literature (Weninger et al., 2001), then assessed cell number yield and CD62L expression levels. We also stained for CCR7, but saw very modest staining in all conditions. In all culture conditions, $CD4^+$ and $CD8\alpha^+$ T cells had comparable levels of CD62L and CCR7. While cultures with IL-15 produced T cell blasts with uniformly high CD62L expression, the cell yield was lower than those with IL-2 (Figure 3.4). Conversely, IL-2 gave robust T cell proliferation, but one effect of T cell exposure to IL-2 is the loss of CD62L via cleavage by TACE-ADAM proteases, and indeed, we observed a bimodal distribution of CD62L expression in IL-2 cultures. Consistent with the results of Cantrell et al with both transgenic and wild-type T cells (Sinclair et al., 2008), the PI3K inhibitor LY294002 induced CD62L and CCR7 upregulation in a dose-dependent manner in the micromolar range, but at the expense of cell proliferation and therefore cell yield. In contrast, nanomolar doses of the mTOR inhibitor rapamycin were sufficient to prevent the loss of CD62L expression without dampening the proliferative effects of IL-2. Therefore, using both IL-2 and rapamycin produced

large numbers of T cell carriers that had the appropriate surface receptors for lymph node homing.

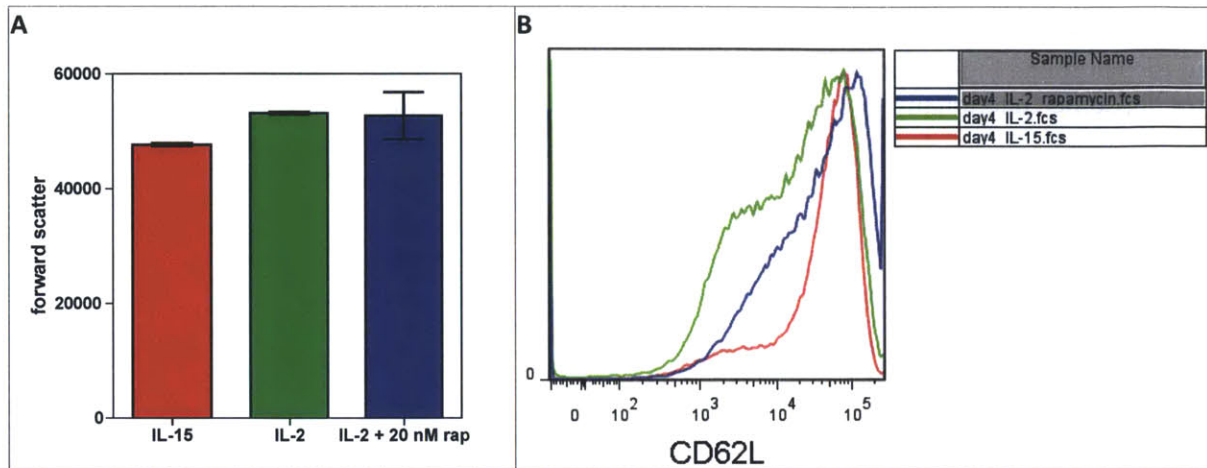


Figure 3.4: T cell proliferation and CD62L expression after culturing with cytokines. (A) BL6 T cells were activated with conA and IL-7 and cultured with IL-15, IL-2 alone or IL-2 + rapamycin. (B) CD62L expression levels were measured by flow cytometry.

To compare T cell blasts with other *in vitro* cultured leukocytes, we generated B cell blasts by culturing CD43⁻ splenocytes with 10 or 100 μ g/ml LPS for 2-4 days *in vitro*, which proliferated robustly but less than T cells blasts, yielding a two-fold lower number of cells per donor. Additionally, the expression levels of surface thiols and CD62L on B cell blasts were lower than that of T cell blasts (Figure 3.5).

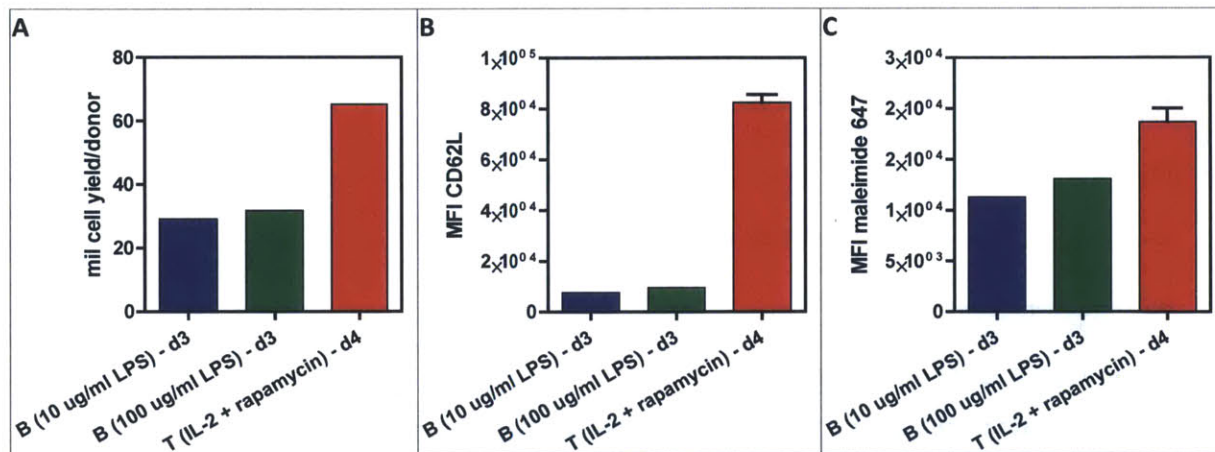


Figure 3.5: Activated T cells can be generated in larger numbers and express higher levels of CD62L and free thiols in comparison to activated B cells.

Splenocytes were sorted using a CD43-bead kit and the CD43⁻ fraction was cultured with 10 or 100 μ g/ml LPS to generate B cell blasts; the CD43⁺ fraction was cultured with concanavalin A + IL-7 for 2 days, then IL-2 + rapamycin for 2 days to generate T cell blasts. (A) The number of viable cells in culture was counted daily from days 2-5 to calculate the peak cell yield (day 3 for B cell blasts, day 4 for T cell

blasts). On the peak days, cells were stained with anti-CD62L PE (B) and maleimide Alexa 647 (C) and analyzed by flow cytometry.

B cell blasts were conjugated with maleimide-PEG dox liposomes to a similar extent as T cells, but the latter had higher rates of survival in culture. When co-cultured with Emu-myc *Arf*^{-/-} cells, dox liposome-functionalized T cells were more potent than functionalized B cells. (Figure 3.6)

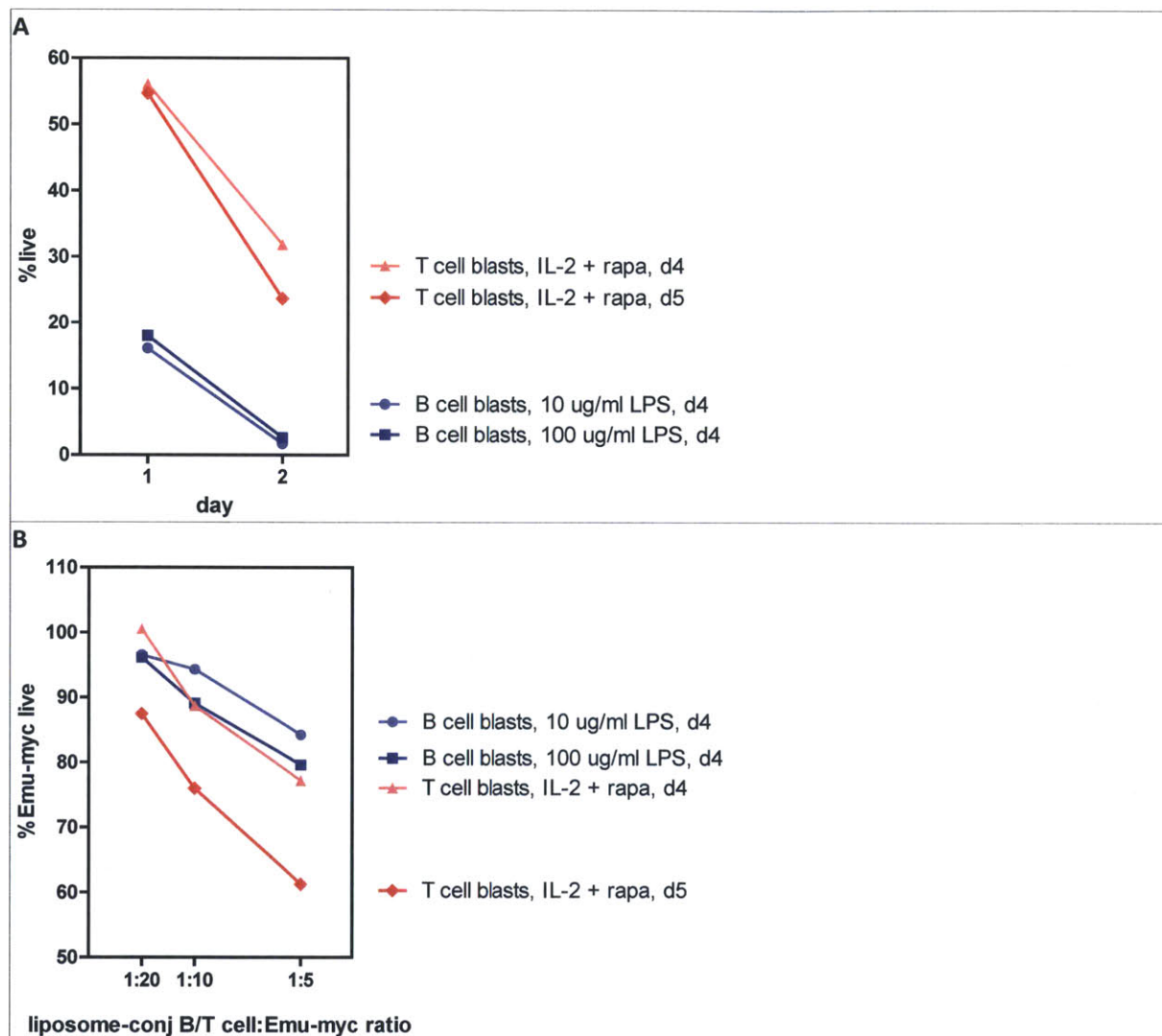


Figure 3.6: Activated T cells are more robust and potent dox liposome cell carriers than activated B cells. B and T cell blasts were conjugated with maleimide-PEG dox liposomes and cultured alone or co-cultured with Emu-myc *Arf*^{-/-} lymphoma cells. Cell viability was measured by flow cytometry for (A) B and T cells in monocultures and (B) lymphoma cells in co-cultures.

Emu-myc Arf^{-/-} cells and T cells show different sensitivities to chemotherapeutic drugs

Next, we assessed the sensitivities of Emu-myc Arf^{-/-} cells versus T cells to dox and SN-38. In order for T cells to shuttle nanoparticles to tumors, they must withstand the drug that is released *en route* during their trafficking. *In vitro*, Emu-myc Arf^{-/-} cells were very sensitive to low concentrations of dox or SN-38, while T cells were essentially unaffected at these doses (Figure 3.7). These data suggest that there is a concentration range within which T cells can carry therapeutic doses of drug, without suffering toxicity themselves.

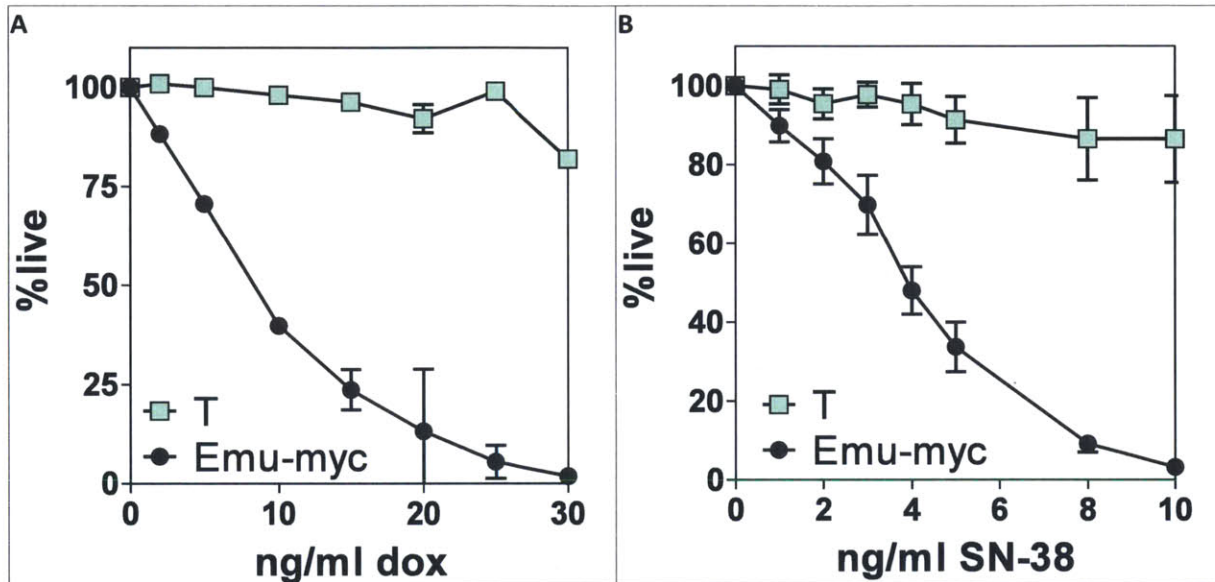


Figure 3.7: Emu-myc Arf^{-/-} cells are killed at dox and SN-38 doses that do not affect T cell viability. Emu-myc Arf^{-/-} cells and IL-2 + rapamycin cultured T cells were plated in cytokine-free media with (A) dox or (B) SN-38, and the %live cells was measured by flow cytometry after 1 day.

Although both Emu-myc Arf^{-/-} cells and T cells are highly proliferative *in vitro*, the latter appear to stop dividing upon cytokine withdrawal, as measured by CFSE dilution. Interestingly, sensitivity to SN-38 appears to be correlated with metabolic activity (glucose consumption and lactate production), as IL-2 T cells are more sensitive than IL-15 or IL-2 + rapamycin T cells (Figure 3.8).

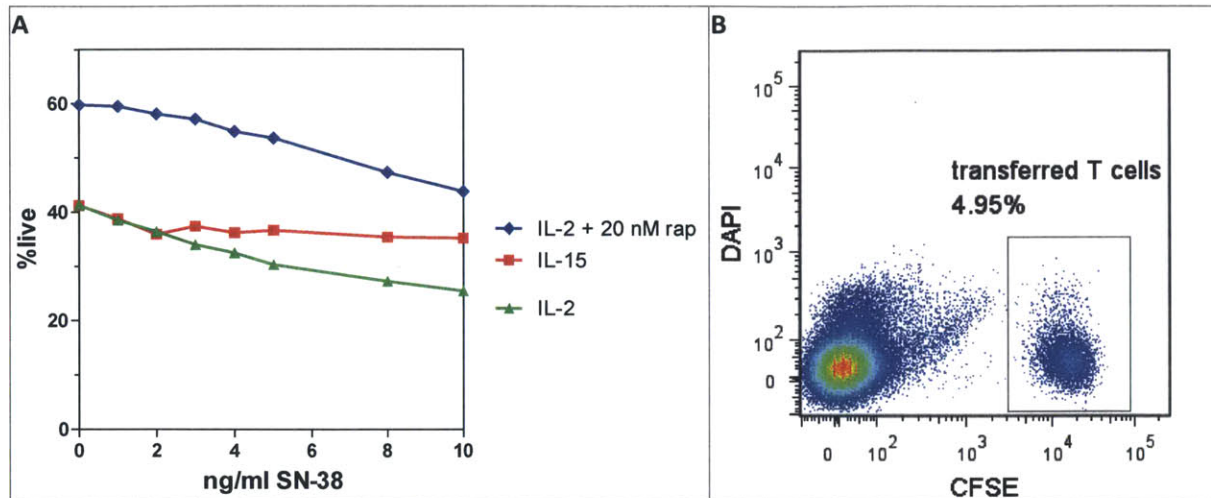


Figure 3.8: T cell responses to cytokine deprivation and SN-38 exposure. (A) T cells from different cytokine conditions were cultured with SN-38 *in vitro* for 1 day, then survival was measured by flow cytometry. (B) 36 ml IL-2 + rapamycin cultured T cells were CFSE stained and adoptively transferred into B6 mice, tissues were analyzed after 2 days.

Summary and Conclusion

The transplanted Emu-myc Arf^{-/-} lymphoma model is aggressive and disseminated, and provides a challenging setting in which to test our drug delivery strategy. *In vitro* titration studies indicated high sensitivity of Emu-myc Arf^{-/-} cells to both dox and SN-38, suggesting that targeted delivery of these chemotherapeutics has significant therapeutic potential.

In order to mirror the biodistribution of Emu-myc Arf^{-/-} cells, we generated cell carriers that had high levels of surface thiols for particle conjugation, expressed the appropriate homing receptors, and showed robustness to dox and SN-38. Through the cell culture optimization process, we learned that although multiple mitogens – IL-2, IL-15, LPS – could expand splenocytes to yield large numbers of lymphocytes, the phenotypes of the resulting cells were not always optimal, e.g. activated B cells were prone to apoptosis after LPS withdrawal. Judging by receptor expression and robustness, T cells were better-suited for nanoparticle delivery than B cells, but still were not optimal, since IL-15 gave high CD62L expression and lower yield and robustness, while IL-2 gave the reverse phenotype. To achieve all of the desired phenotypes, cells were supplemented with rapamycin to select for only the mitogenic but not the apoptotic and maturation effects of IL-2 alone. These studies highlight the importance of screening potential cell carriers for multiple phenotypes, not only the ability to migrate into tumor sites.

4. Nanoparticle-cell conjugation and *in vitro* characterization

Introduction

A wide variety of cell types, ranging from pancreatic beta-islet cells (Wilson et al., 2011) to mesenchymal stem cells (Cheng et al., 2010) to macrophages (Doshi et al., 2011), have been shown to be amenable to conjugation with particles, coatings, and other materials (Stephan and Irvine, 2011). Cells can be functionalized with materials containing molecules that act either on the carrier cells themselves, such as growth factors in a tissue-engineering scaffold (Cheng et al., 2010), or on surrounding cells in the tissue, such as drug delivery for tumors (Choi et al., 2012a). The chemotherapeutic drugs we wish to deliver act on both the carrier T cells and the target lymphoma cells, and to maximize the fraction that reaches the latter, we focused on conjugating drug nanoparticles on the cell surface, as opposed to entrapping them within the carrier cells. We assume that when the nanoparticle is phagocytosed, the released drug will reach the target cells more easily if it can diffuse out into the intercellular space directly and does not have to cross the organelle and plasma membranes of the carrier cell first. Cell surface conjugation of nanoparticles can be achieved via a number of chemical and biological methods, but the efficiency and stability of the cell-nanoparticle bond vary, depending on the method (Stephan and Irvine, 2011). An efficient conjugation reaction introduces a high density of particles onto the cell surface, and therefore a larger cargo. A stable conjugation increases the retention time on the cell surface, and therefore influences the dose and release kinetics of the drug to the surroundings.

It has been previously reported that leukocytes have thiols on their plasma membranes that are accessible for chemical modification (Sahaf et al., 2003). Maleimide-thiol reactions occur rapidly in mild conditions and form a stable thioether bond. We had previously successfully attached maleimide-functionalized particles to T cells, B cells and hematopoietic stem cells (Stephan et al., 2010). We applied this conjugation chemistry to liposomes and ICMVs, and measured the efficiency of conjugation, as well as the retention. We quantified the drug cargo that could be attached to T cells and approaches to increase the cargo per cell. We also explored a number of other particle conjugation strategies and compared them to maleimide-thiol conjugation.

Methods

Reagents

Crosslinkers, Traut's reagent, and dithiothreitol were purchased from Pierce. Lipid-oligo conjugates were synthesized in-house by Dr. Haipeng Liu.

T cell-nanoparticle conjugation

T-cells were prepared as described in Chapter 3. Live cells were purified from T cell cultures by Ficoll gradient (GE Healthcare), washed in PBS, and resuspended in serum-free unsupplemented RPMI-1640 at 50×10^6 /ml. Particles were added and incubated with gentle mixing at 4C for 30 min. Cells were washed in PBS, resuspended in serum-free RPMI with 1 mg/ml PEG2000-SH (Laysan Bio), and incubated with gentle mixing at 4C for 15 min. Cells were washed in PBS and used immediately.

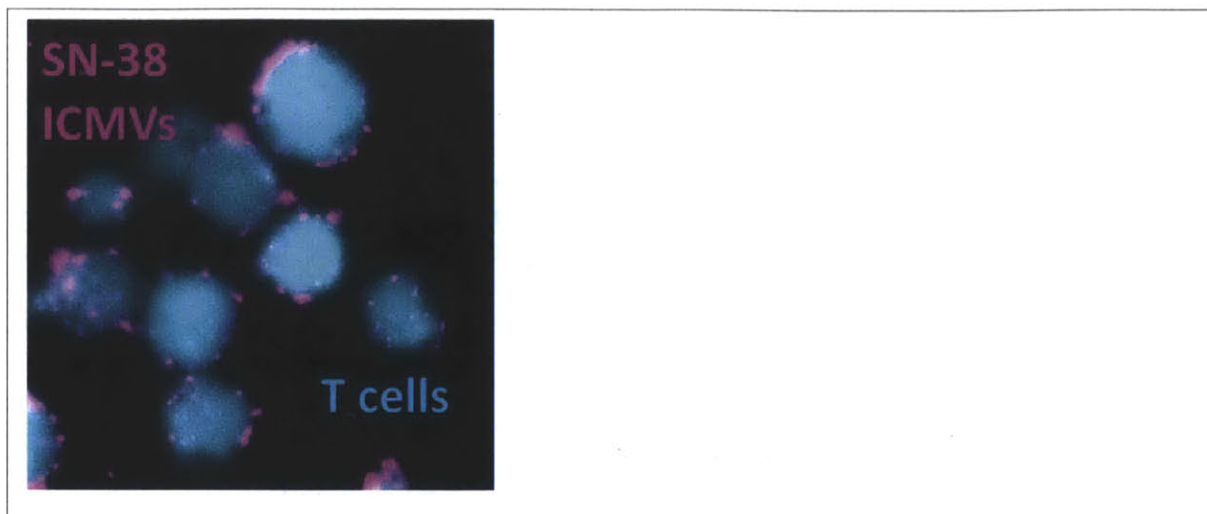


Figure 4.1: SN-38 ICMVs conjugated to T cells
SN-38-loaded ICMVs were synthesized and conjugated to T cells as described in the Methods.

Dox liposome conjugation efficiency quantitation

The amount of dox liposomes conjugated to T cells was quantified by a protocol from (Laginha et al., 2005). T cell pellets were resuspended in lysis buffer (0.25 M sucrose, 5 mM Tris-HCl, 1 mM MgSO₄, 1 mM CaCl₂, pH 7.6) and sonicated for 30 sec at power 5 on ice. 200 ul of the homogenate was mixed with 100 ul 10% Triton X-100, 1.5 ml acidified isopropanol (0.75 M HCl), and 200 ul water, vortexed and stored at -20C overnight. Samples were pelleted at 16000g and the dox fluorescence in the supernatant was read and compared to a standard curve.

SN-38 ICMV conjugation efficiency quantitation

The amount of SN-38 ICMVs conjugated to T cells was quantified by dissolving T cell pellets in 200 ul 0.1 M NaOH + 0.5% Triton X-100, vortexing to lyse cells, pelleting at 16000g, reading the SN-38 fluorescence in the supernatant and comparing to a standard curve.

Co-culture assay

In order to model the *in vivo* interactions between lymphoma cells and ICMV-conjugated t cells, we set up a simple *in vitro* co-culture system. Emu-myc Arf^{-/-} cells were plated at of 1×10^6 /ml, and T cells were added such that they were equal in number to 1-25% of Emu-myc Arf^{-/-} cells (10,000 – 250,000 T cells). After 24 h of incubation, we measured cell viability for both populations by flow cytometry. The high density of the culture was aimed towards mimicking the physical proximity between Emu-myc Arf^{-/-} cells and T cells *in vivo*, while supplying adequate medium for Emu-myc Arf^{-/-} proliferation during the assay period.

Results and Discussion

Previous work in our lab discovered that modification of T cells via maleimide-thiol chemistry resulted in stable cell surface retention of nanoparticles without endocytosis (Stephan et al.,

2010). However, conjugation efficiency was low for some particle systems, as detailed in Chapter 2. We attempted to increase the conjugation efficiency via other methods of particle attachment, which required modification of both the T cells and the particles.

Non-covalent cell conjugation methods

We examined a number of non-covalent strategies for particle conjugation to T cells. (Figure 4.2) These studies suggest cell conjugation with particles is a generalizable strategy that can be achieved via diverse chemical linkages. Some of these alternate approaches may be applied to non-hematopoietic cells that do not have accessible surface thiol groups, or to particles that are required to be endocytosed for optimal function.

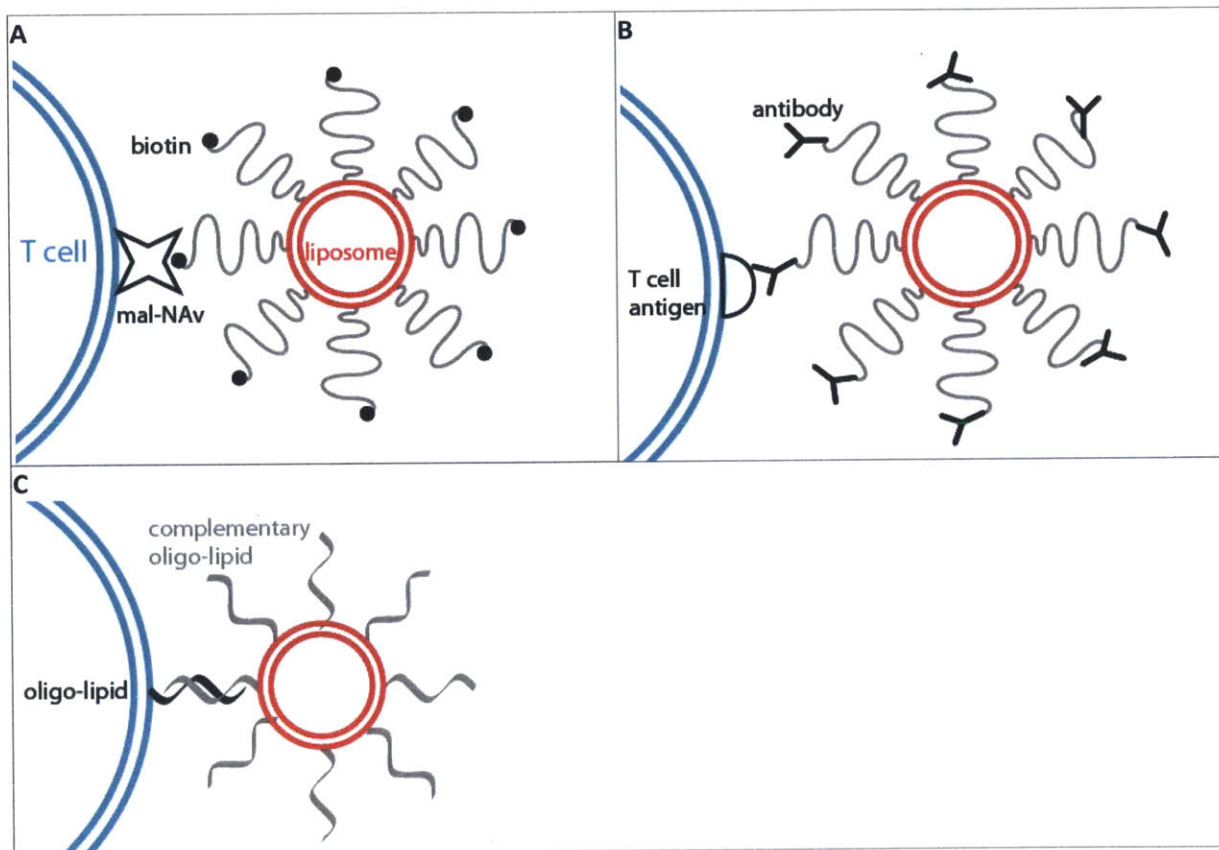


Figure 4.2: Non-covalent particle conjugation schemes.

(A) Biotin-avidin mediated particle conjugation: T cells are functionalized with maleimide-neutravidin, then conjugated with liposomes that contain biotin-PEG lipids. (B) Antibody-mediated particle conjugation: liposomes are functionalized with antibodies against T cell surface antigens. (C) Oligo-lipid mediated particle conjugation: T cells are functionalized with one oligo-lipid, and the liposomes contain the complementary oligo-lipid.

One of the best-studied non-covalent conjugation systems is the extremely high affinity binding between biotin and streptavidin. A previous study showed successful surface binding of particles to mesenchymal stem cells and endothelial cells using a biotin-streptavidin bridge (Cheng et al., 2010). We modified liposomes with a low percentage of biotin-PEG lipid, and chemically

functionalized T cells with maleimide-neutravidin. While conjugation was observed even with liposomes containing 1 mol% biotin-PEG lipid, it was optimal when liposomes were maximally functionalized with 5.3 mol% biotin-PEG lipid. T cell modification was saturated at 0.1 mg/ml maleimide-neutravidin (Figure 4.3). However, biotin-PEG liposomes were shed from T cells very rapidly; the fluorescent liposome signal on cells fell 90% after 1 day of *in vitro* culture. Given the multiple steps required for T cell functionalization and poor liposome retention, we decided that biotin-avidin conjugation was not suitable for our application.

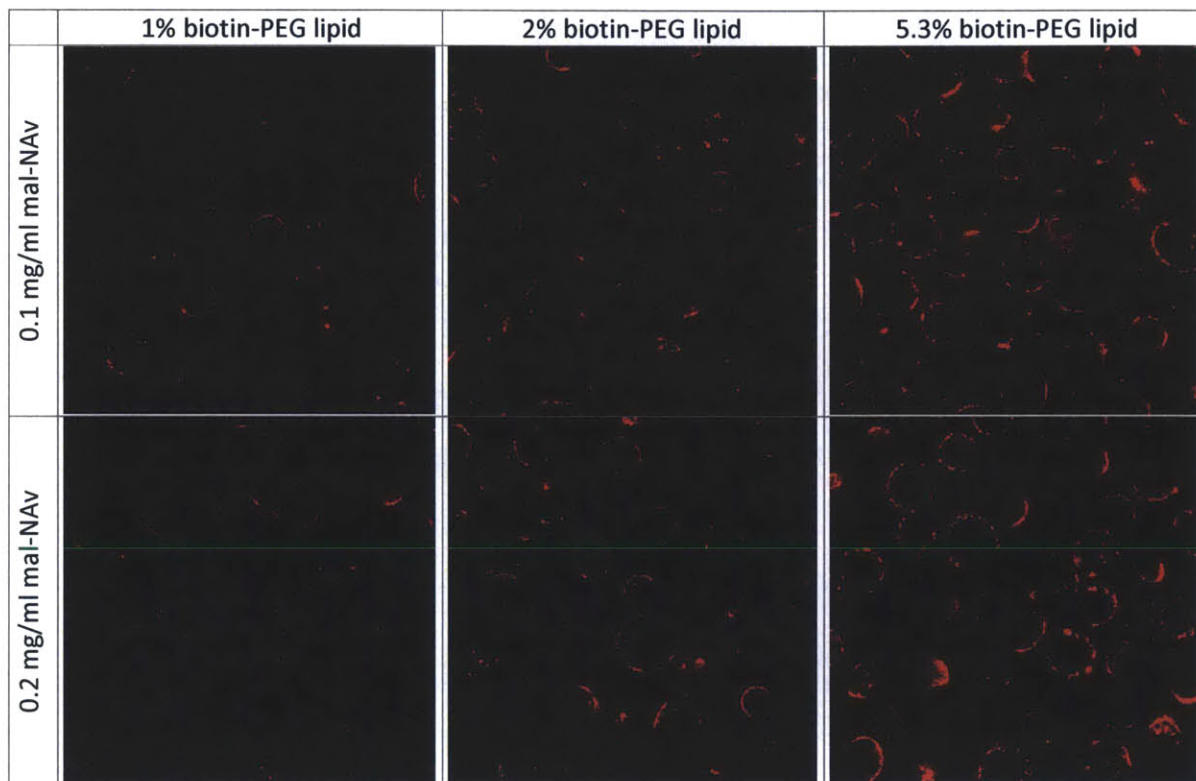


Figure 4.3: Biotin-PEG-lipid containing unloaded liposomes are conjugated to maleimide-neutravidin (mal-NAv)-functionalized T cells.

Liposomes had Doxil composition, except for an additional 1 mol% rhodamine-DPPE, and 1, 2, or 5.3 mol% of methoxy-PEG2000-DSPE was substituted with biotin-PEG2000-DSPE. Lipids were rehydrated in PBS and sonicated at 60C for 1 min. T cells were modified with 0.1 or 0.2 mg/ml mal-NAv for 25 min at 4C, washed, then incubated with biotin dox liposomes for 40 min at 4C. T cells were imaged for liposome conjugation.

To target tumor cells *in vivo*, particles are often surface functionalized with antibodies specific for tumor surface proteins. Analogously, particles can be functionalized with antibodies that bind T cell surface antigens. We screened a panel of antibodies against highly expressed T cell surface markers: CD3ε, CD4, CD8α, CD11a, and CD44, as well as an antibody against Thy1.1, the Thy1 isoform expressed by the luciferase donor mice (anti-Thy1.2 can be used for wild-type donors). Ideally, to stably anchor particles onto T cell surfaces for *in vivo* delivery, the antibody would bind its target with high affinity and long half-life, and the target protein would not be endocytosed, to prevent the drug payload from being internalized by the T cell. We stained T

cells with antibodies to the aforementioned markers and observed antibody localization by imaging, and staining intensity by flow cytometry. Unfortunately, none of the candidate antibodies were suitable for particle targeting (Figure 4.4). As expected from literature, anti-CD3 ϵ was rapidly internalized (Dinauer et al., 2005) and the signal was almost background 1 day after staining. Anti-CD4 and anti-CD8 α intensities also dropped rapidly, though it is not clear from imaging whether the antibodies were shed from the cell surface or internalized and degraded. Anti-CD11a and anti-CD44 did not seem to be internalized, but a large fraction of surface staining was lost after 1 day. Similarly, anti-CD43 and anti-CD45 staining levels were initially bright but decayed significantly after 1 day. While anti-Thy1.1 signal was well maintained after 2 days, large portions of the antibody could be seen within the cell starting on day 1, indicating endocytosis. Therefore, none of the antibodies we tested were suitable for surface retention of particles. However, current efforts in our lab are underway to use some of these antibodies to target drugs to act on T cells intracellularly, for the enhancement of adoptive T cell therapy.

Recently, Dr. Haipeng Liu in our group developed lipid-conjugates which dynamically and reversibly insert into cell membranes (Liu et al., 2011), similar to PEG-lipid post-insertion into liposomes (Chapter 2). One class of these lipid conjugates is functionalized with short DNA oligos on the headgroup. We hypothesized that dox liposomes could contain one oligo-lipid, and the T cells could be inserted with the complementary sequence oligo-lipid, such that when the liposomes and cells are mixed together, oligo hybridization will allow tethering of the liposomes to the cell surface. Dr. Liu's previous work showed that oligo-lipids present at 5 μ M in solution insert into the membranes of B16F10 melanoma cells within minutes and are endocytosed within 1 h. Following his protocol, we tested the ability of two constructs, 20R-TMR and 18R-(PEG)₂₄-TMR, to insert into T cell membranes at 2 μ M. As expected, oligo-lipid insertion was rapid, reaching saturation by 30 min (Figure 4.5). Oligo-lipids did not appear to preferentially insert into lipid rafts or other domains, since as little as 1 μ M oligo-lipid was sufficient to uniformly cover the cell surface. 20R-TMR inserted with much higher efficiency than 18R-(PEG)₂₄-TMR, probably because the PEG linker in the latter increases its water solubility and increases the stability of the micellar form in solution. We then synthesized rhodamine-labeled liposomes containing 20R conjugate, and hybridized the liposomes to T cells that had been functionalized with the complementary oligo-conjugate. Interestingly, liposome attachment was higher when T cells were functionalized with a higher amount of oligo-lipid, and did not depend on the amount of oligo-lipid in the liposomes (Figure 4.6). Since we observed oligo-lipid endocytosis and cell death even at 2 μ M, we did not pursue this conjugation strategy further.

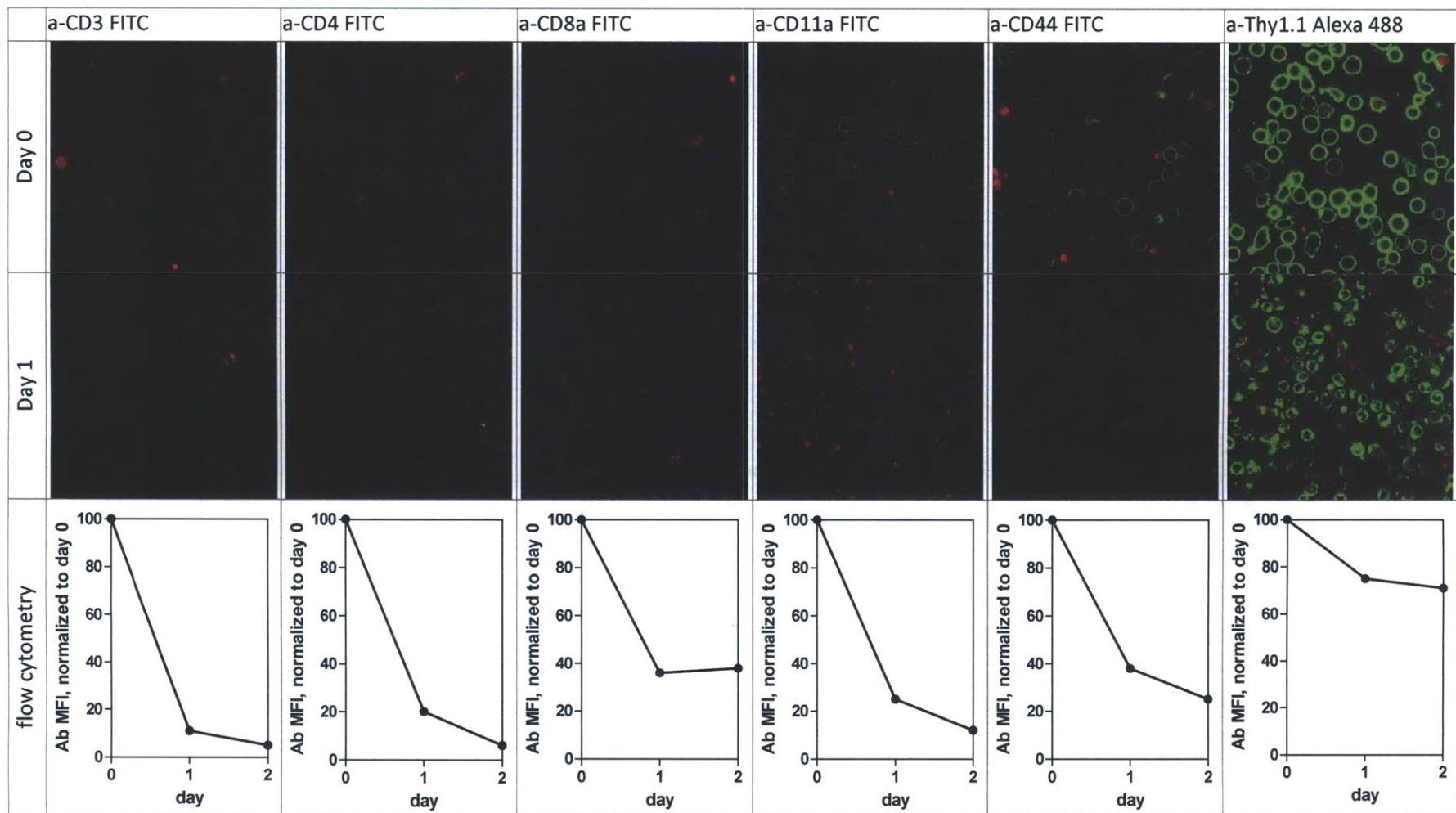


Figure 4.4: Antibodies against T cell antigens were screened as potential particle linkers.

All antibodies were shed or internalized by T cells, and therefore not good candidates for particle conjugation to T cell surfaces. T cells were stained with FITC/Alexa488 antibodies, washed, and kept in culture for imaging and analysis by flow cytometry on days 0 (immediately after staining), 1 and 2. Antibody staining is shown in green and propidium iodide viability stain is in red. For each antibody, the median fluorescence intensity is plotted as a % of the initial day 0 staining MFI. Anti-CD43 staining (data not shown) was weak and decayed to 35% by day 1.

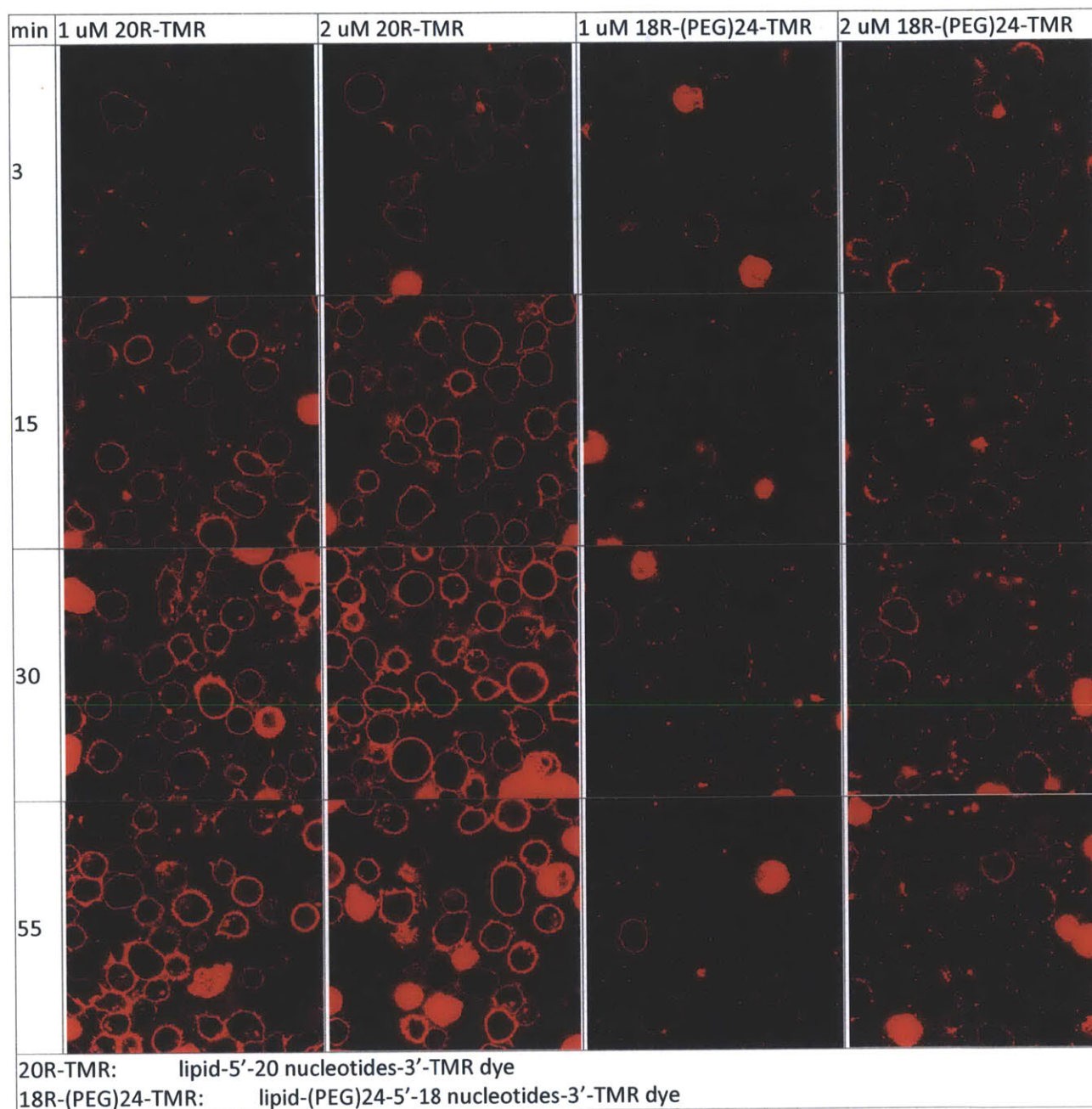


Figure 4.5: Oligo-lipid conjugates rapidly insert into T cell membranes, but undergo endocytosis. Oligo-lipid constructs 20R-TMR and 18R-PEG24-TMR were incubated at 1 or 2 uM with 500,000 T cells in 200 ul HBSS at room temperature. Cells were imaged during incubation to track kinetics of oligo-lipids localization.

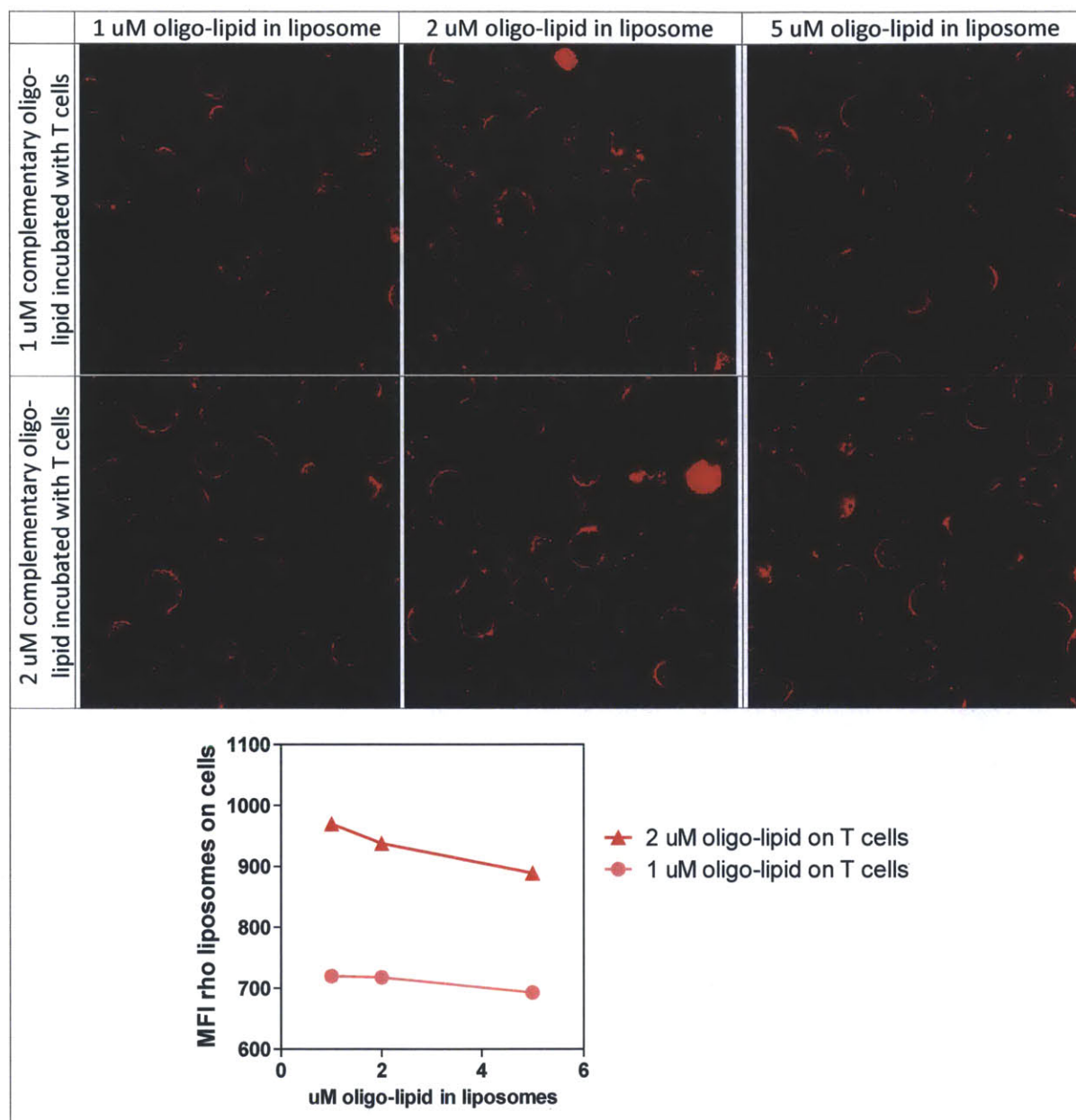
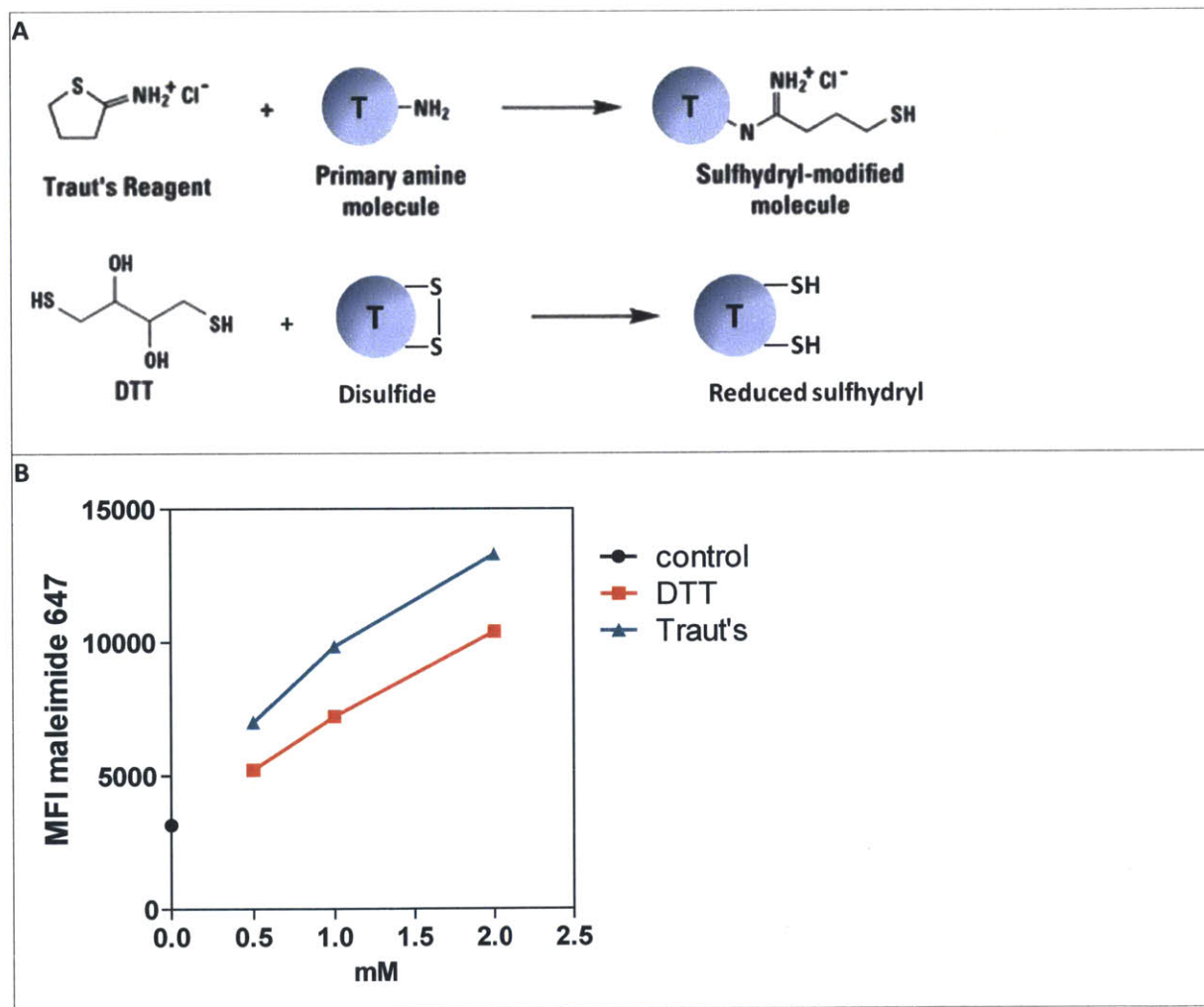


Figure 4.6: Oligo-lipid containing dox liposomes are conjugated to complementary oligo-lipid-functionalized T cells.

Liposomes had Doxil composition, except for an additional 1 mol% rhodamine-DPPE. Lipids were rehydrated with 1, 2 or 5 uM 20R oligo-lipid in PBS and sonicated at 60C for 1 min. T cells were modified with 1 or 2 uM of the complementary oligo-lipid for 20 min at 4C, washed, then incubated with 20R liposomes for 30 min at 4C. T cells were imaged and analyzed by flow cytometry for liposome conjugation.

Direct covalent conjugation of particles to T cells and drug cargo quantification

Since none of the non-covalent conjugation methods improved upon our original approach of thiol-maleimide crosslinking of particles to cells, we focused on enhancing thiol-maleimide conjugation by modifying the T cell surface, rather than the particle. The free thiols on the T cell surface are naturally exposed by large receptors (Stephan et al., 2012). We artificially increased the number of free thiols by treating T cells with low concentrations of reducing agents, as measured by a small molecule maleimide dye (Figure 4.7). However, the increased cell thiol density did not result in enhanced maleimide particle conjugation, suggesting that the binding of particles is saturated at native T cell thiol levels, and may be sterically inhibiting further binding.



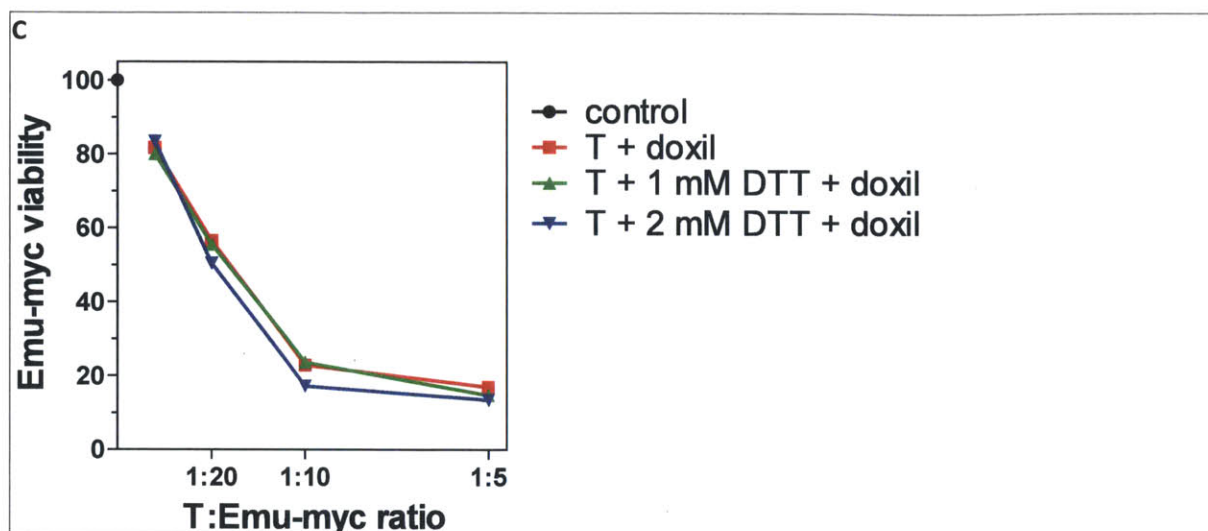


Figure 4.7: DTT and Traut's reagent do not increase the conjugation efficiency of maleimide-PEG doxil liposomes on T cells.

(A) Traut's reagent converts cell surface amines into thiols, and DTT breaks disulfide bonds into two free thiols. (B) Incubating T cells with Traut's reagent or DTT increases the number of thiol groups on the cell surface, as measured by maleimide-Alexa 647 staining. (C) However, T cells conjugated with doxil liposomes with or without additional thiolation were the same potency in killing Emu-myc Arf^{-/-} cells in a co-culture.

Physical parameters of nanoparticle-cell conjugation

In addition to the conjugation chemistry, which affects conjugation efficiency and rates of endocytosis, particle retention on cells is also dependent on the physical properties of the cell membrane-particle interaction. Previous work in our lab found liposomes and ICMVs were retained better than PLGA nanoparticles after conjugation to cells. When nanoparticle-conjugated T cells were imaged in a 3D collagen matrix, particles were shown to be localized to the uropod of the polarized T cell (Stephan et al., 2012). When T cells squeezed through small pores in the collagen matrix, ICMVs remained bound to the cell, whereas a portion of PLGA particles were stripped off. Consistent with the imaging data, in a transmigration assay through a confluent endothelial layer, T cells retained a greater fraction of their ICMVs compared to PLGA nanoparticles (Stephan et al., 2010). We speculate that this may be because ICMVs are softer and more able to deform in response to shear or compression, compared to PLGA particles that are stiffer and would extract a portion of the cell membrane instead.

Particle size is also a crucial parameter for conjugation stability of particles to T cells. *In vitro*, ICMVs of varying sizes conjugate to T cells to comparable extents. However, *in vivo* retention is only achieved with smaller ICMVs on the order of 400 nm, as shown by flow cytometry of T cells after adoptive transfer. Larger ICMVs may be more vulnerable to being stripped off of the T cell membrane by the shear forces it encounters in circulation or the small pores in the fenestrated vasculature of the liver and spleen.

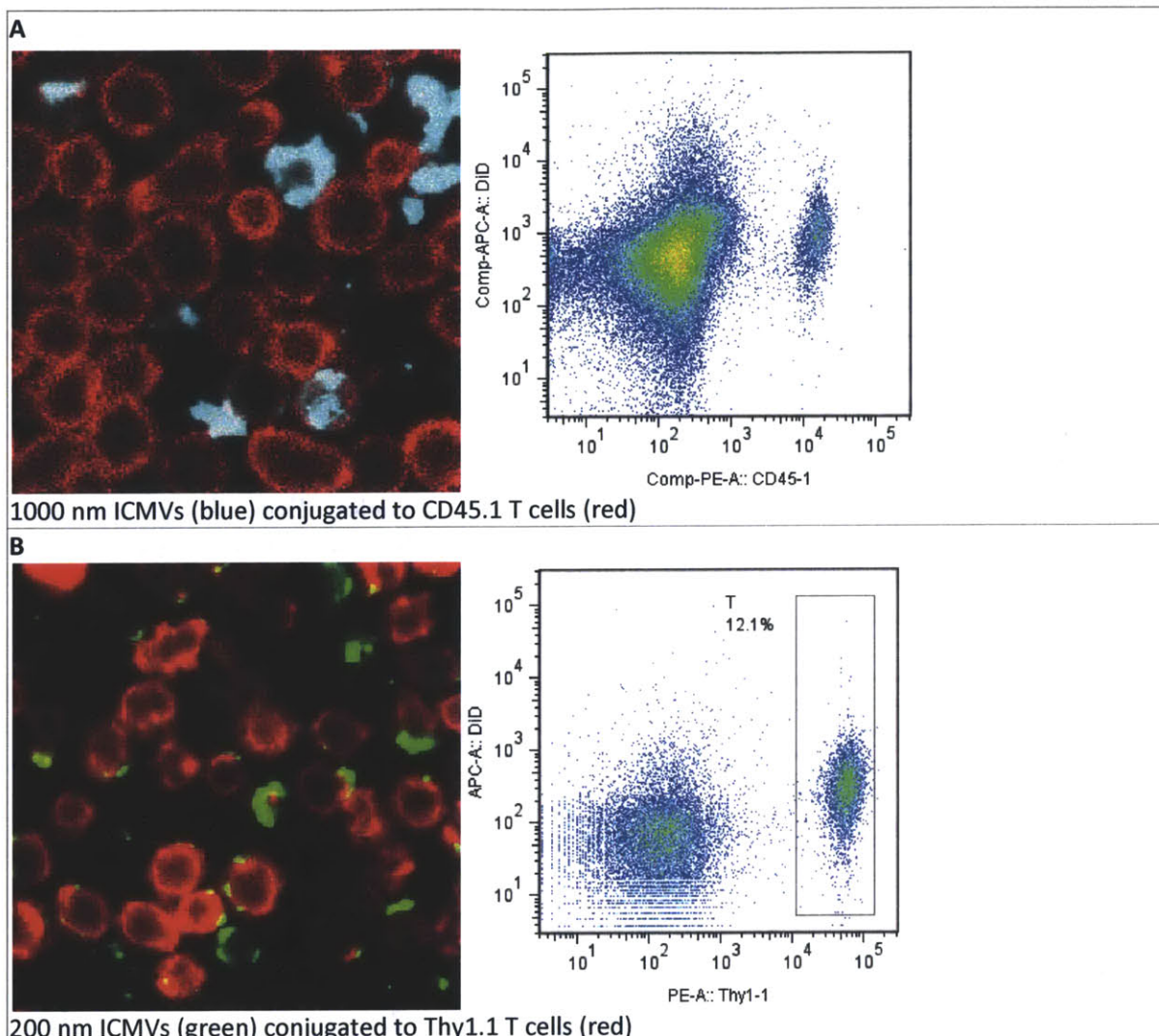
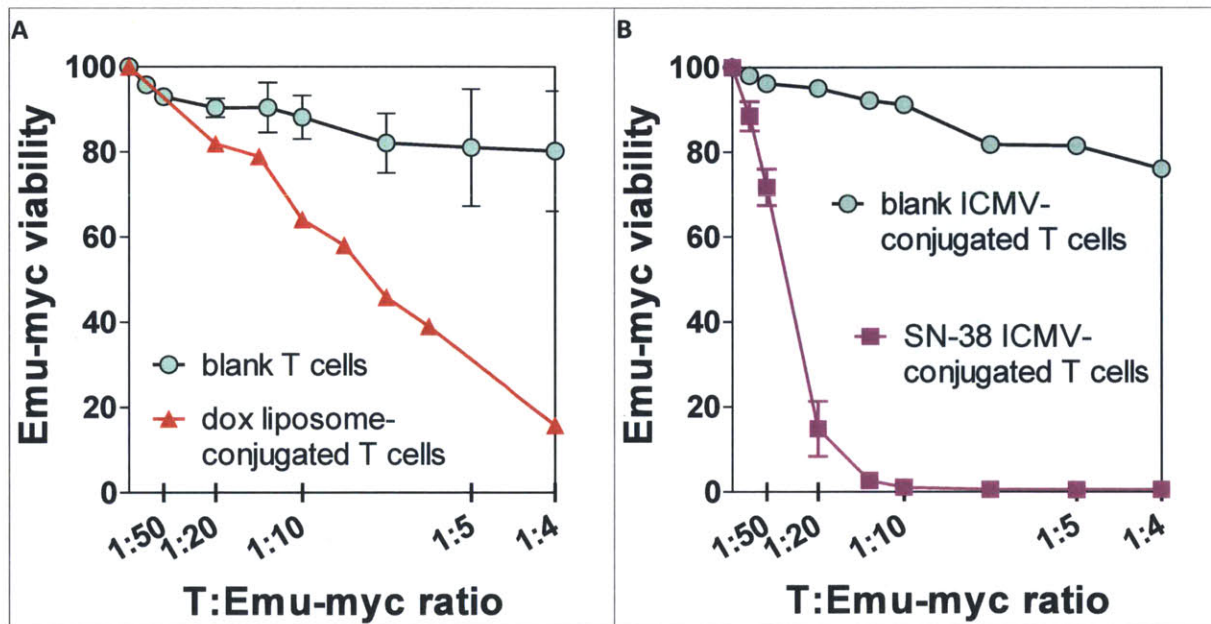


Figure 4.8: Particles with smaller diameter are better retained on T cells *in vivo*. T cells were conjugated with (A) 1000 nm or (B) 400 nm ICMVs and adoptively transferred. One day later, tissues were isolated, stained for the transferred T cell marker CD45.1 or Thy1.1, and analyzed by flow cytometry for particle fluorescence.

Quantification of drug nanoparticle conjugation efficiency

To quantify the drug cargo on T cells conjugated with particles, we chemically dissolved the cell pellets immediately after conjugation and measured the fluorescence in the supernatant. Maleimide-PEG dox liposomes conjugated to T cells at ~1-5% efficiency, resulting in a net load of 0.01-0.06 μg dox/mil T cells. The μg dox/mil cells load could not be significantly increased by an excess of liposomes during the conjugation reaction. This low conjugation efficiency was consistent with the observation that the majority of dox liposomes remained unbound in the supernatant during conjugation. In contrast, SN-38 ICMVs conjugated to T cells at 30-50% efficiency, equal to 0.1-0.5 μg SN-38/mil T cells. At lower ICMV to T cell ratios, essentially all of the ICMVs will bind and pellet with the cells after incubation.

In order to assess the toxicity exerted by the conjugated nanoparticles on both the T cell carriers and the surrounding Emu-myc Arf^{-/-} cells, we set up co-cultures with 10⁶ Emu-myc Arf^{-/-} cells and doped in T cells at frequencies of 1% to 25%, corresponding to Emu-myc Arf^{-/-}:T ratios of 99:1 to 4:1. Emu-myc Arf^{-/-} viability was measured to assess the potency of T cells (Figure 4.9). T cells alone had insignificant Emu-myc Arf^{-/-} killing ability, as is expected from a mixed CD4 and CD8 α polyclonal population. Similarly, T cells conjugated with blank ICMVs had no activity. However, T cells conjugated with either dox liposomes or SN-38 ICMVs were able to kill Emu-myc Arf^{-/-} cells in a dose-dependent manner. Notably, SN-38 ICMV-conjugated T cells were much more potent than dox liposome-conjugated T cells, e.g. at 1:20 T:Emu-myc Arf^{-/-} cell ratios, dox liposome-conjugate T cells killed approximately 20% of Emu-myc Arf^{-/-} cells, but SN-38 ICMV-conjugated T cells killed approximately 80%. Although this difference in efficacy between the two types of functionalize T cells is predicted from the conjugation efficiency measurements, the co-culture assay confirms this and also provides an estimate of the frequency of T cells required in the tumor to exert significant effects. In co-cultures, T cell viability is unaffected by the presence of conjugated drug-loaded particles. Even though the local concentration of drug is higher around the T cell than the global concentration experienced by the Emu-myc Arf^{-/-} cells, there is preferential killing of the latter.



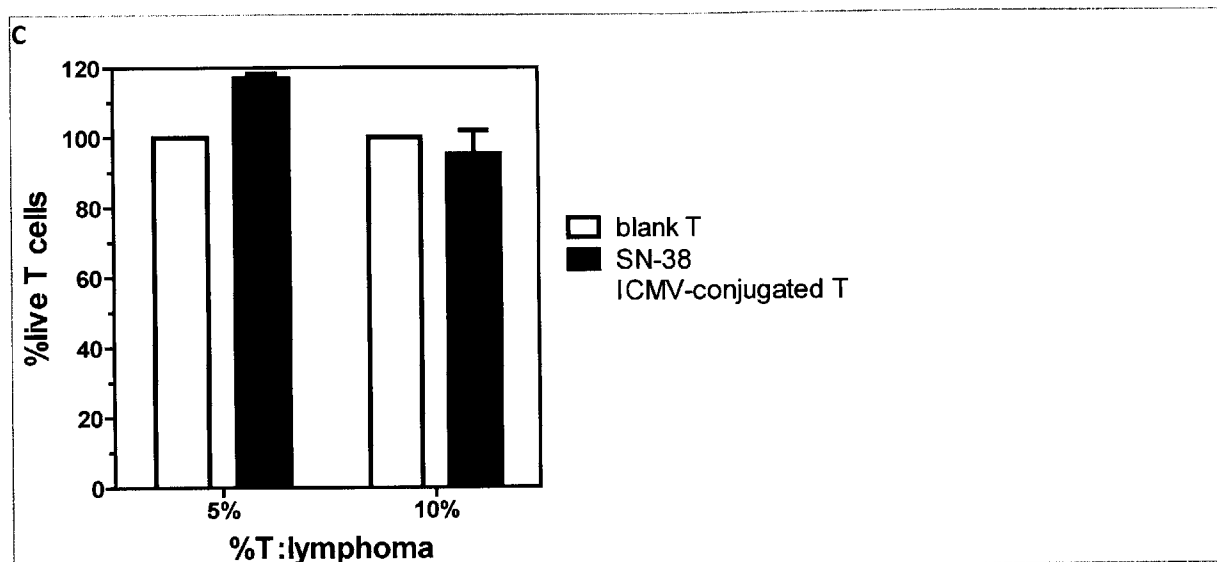


Figure 4.9: T cells carry sufficient doses of drug nanoparticles to kill Emu-myc Arf^{-/-} cells in a co-culture. (Top Left) Emu-myc Arf^{-/-} cells were cultured with increasing numbers of T cells that were either unmodified, conjugated with maleimide-PEG dox liposomes. (Top Right) The analogous experiment with SN-38 ICMV-conjugated T cells. (Bottom) T cell viability in co-cultures was the same regardless of whether they were unconjugated or conjugated with SN-38 ICMVs.

Summary and Conclusion

Given the limited number of T cells that can be adoptively transferred, conjugation efficiency of particles determines the drug loading on the T cells and therefore the potency of the therapy. None of the non-covalent conjugation methods we tried were able to improve the conjugation efficiency of dox liposomes. In the co-culture assay, SN-38 ICMV-functionalized T cells were much more potent than dox liposome-functionalized ones, and the difference is only partially due to the higher potency of SN-38 as a free drug. While dox liposomes have higher drug encapsulation per particle, the conjugation efficiency to T cells was very low. In contrast, SN-38 ICMVs have lower drug encapsulation but conjugate to T cells very efficiently. In almost all cases (oligo-lipid conjugates being the exception), the density of reactive cell surface groups is not limiting. Rather, the conjugation efficiency is much more dependent on the functional group density on the particles.

The co-culture assay is a minimal model that does not recapitulate the tumor stroma or take into account the time required for T cells to traffic into tumors, but it serves as a useful screening tool for whether the T cells carry a therapeutically relevant dose of nanoparticles. In general, the results of the co-culture assay correlated well with the potency of the particular nanoparticle-T cell formulation *in vivo*. The co-culture could be used as a general screening tool for other drug-nanoparticle and cell carrier systems.

5. *In vivo* characterization and therapeutic efficacy of drug nanoparticle-functionalized T cells

Introduction

Based on the promising results from the previous system characterization studies, we moved forward with the evaluation of nanoparticle-conjugated T cells *in vivo*. First, we tracked the migration kinetics of nanoparticle-conjugated T cells after adoptive transfer into tumor-bearing hosts, to verify that nanoparticle functionalization did not disrupt homing to lymphoid organs. We then compared the accumulation of free versus T cell-conjugated nanoparticles in tumor sites. Finally, we tested the efficacy of both dox and SN-38 in free drug, free nanoparticle, and T cell-bound nanoparticle form. Tumor burden was monitored over time by whole animal imaging, and quantified by post-necropsy flow cytometry at the termination of the therapy. Further analysis of the lymphoma response to therapy suggested that Emu-myc Arf^{-/-} cells rely on pro-survival cues from the bone marrow stroma, and that disrupting this tumor-stroma interaction can enhance the efficacy of our targeted delivery method of chemotherapy.

Methods

Flow cytometry

Tissues were isolated and dissociated by grinding through 70 µm cell strainers. Red blood cells in blood and spleen were lysed with ACK buffer for 5 min at room temperature, then washed with PBS. Cells were suspended in PBS + 0.5% BSA) and stained with 1:200 anti-CD16/32 and 1:100 antibodies for 15-30 min at 4°C, then washed and resuspended in PBS + 0.5% BSA with 5 ng/ml DAPI. Analyses were performed on BD Canto or LSR flow cytometers, and data was processed in FlowJo.

Immunofluorescence

All antibodies were purchased from eBioscience or Biolegend, with the exception of anti-GFP Alexa 488, which was purchased from Invitrogen. Tissues were embedded in OCT (Sakura Tech) and snap frozen on dry ice, then sliced into 10 µm sections by the Koch Institute Swanson Biotechnology Center histology facility. Sections were fixed with 10% buffered formalin, stained with antibodies at 1:100 in PBS 0.5% BSA for 4 h at room temperature, and mounted with ProLong Gold Antifade with DAPI (Invitrogen). Brightfield and fluorescent images were obtained on a Zeiss LSM 510 META system.

SN-38 HPLC

HPLC protocols were adapted from (Kuroda et al., 2009). Tissues were isolated, weighed and frozen at -80°C. Immediately before analysis, tissues were rehydrated in glycine-HCl buffer pH 3 at 50% w/v and sonicated for 3 min on ice at power 5 with frequent agitation until homogenized. 100 µl of homogenate was added to 100 µl of methanol, vortexed vigorously, and pelleted at 16,000g for 5 min. 100 µl of the supernatant was acidified with 10 µl 1 M HCl to convert all SN-38 to lactone form, and analyzed on a Shimadzu Prominence HPLC system. 10 µl of each sample was injected into a C₁₈ reverse phase column (Restek) at 35°C, with 55%/45% 0.1 M ammonium

acetate pH 4.2/methanol as the mobile phase at a flow rate of 1 ml/min. Peaks were detected at 380 nm excitation/560 nm emission.

***In vivo* tumor experiments**

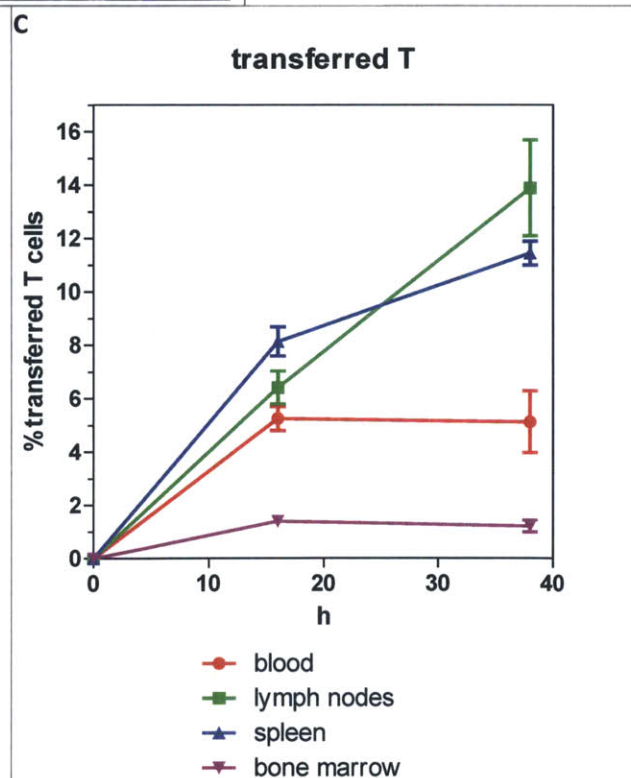
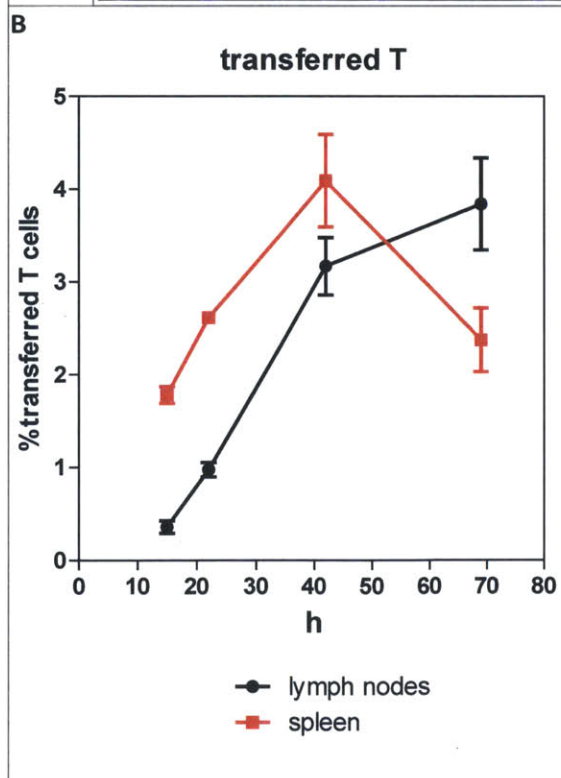
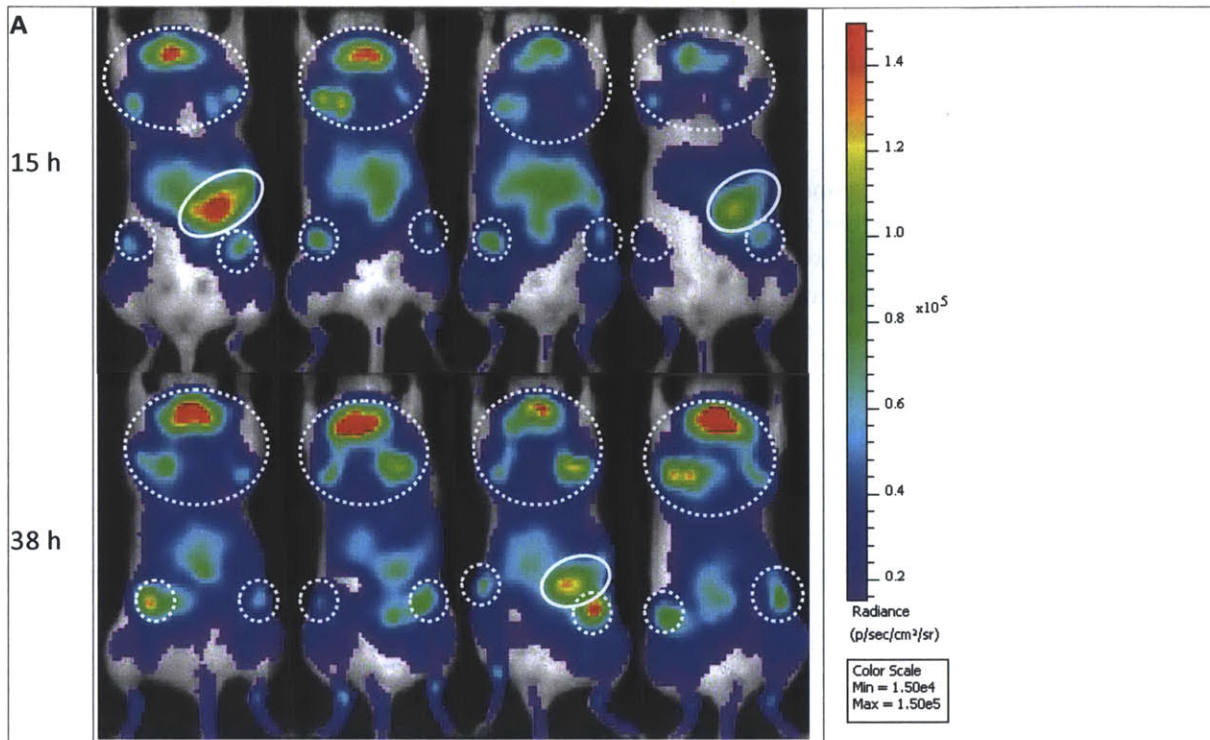
Animal experiments were conducted in accordance with NIH, state, and local guidelines. C57BL/6J wild-type and albino (*Tyr2^{-/-}*) mice were purchased from Jackson Labs. C57BL/6J CD45.1 mice (Jackson Labs) were a gift from Sarah Pfau from Dr. Angelika Amon's lab. To inoculate tumors, 2×10^6 Emu-myc *Arf^{-/-}* cells were injected via the tail vein into wild-type or albino C57BL6/J mice. Some animals received 5 mg/kg AMD3100 (Tocris) by subcutaneous injection.

For luciferase GFP Emu-myc *Arf^{-/-}* cells, tumor burden was assessed by whole animal bioluminescent imaging using a Xenogen Spectrum 200 system. Animals were injected subcutaneously with 150 mg/kg D-luciferin (Xenogen) 10 min prior to imaging. At the terminal timepoint, blood, spleen, lymph nodes (cervical, axillary, brachial, inguinal, mesenteric, iliac), and bone marrow (from femur and tibia) were collected and processed into single cell suspensions. Lymphoma cells were gated on GFP and enumerated using AccuCheck Counting Beads (Invitrogen) by flow cytometry, according to manufacturer instructions.

Results and Discussion

Particle-conjugated T cells home to tumors

As early as 15 h post-adoptive transfer, *in vitro* cultured T cells could be detected in the lymph nodes, spleen and bone marrow by IVIS. At this timepoint, T cell accumulation could also be seen in the liver, due to non-specific trapping of T cells in the fenestrated vasculature, but liver T cell signal fades after another 24 h, while signals in spleen and lymph nodes increase moderately, suggesting that T cell homing had reached equilibrium by 36 h (Figure 5.1). T cell homing kinetics were similar whether the T cells were unmodified, conjugated with unloaded liposomes, or conjugated with dox-loaded liposomes. However, T cell modification with dox liposomes decreased the number of transferred T cells that trafficked into spleen and lymph nodes, suggesting a reduction in T cell viability, probably due to early release of dox from liposomes. Histological sections of tumor-bearing lymph nodes shows the dispersal of transferred T cells in the majority of the lymph node, facilitating drug distribution throughout the tumor.



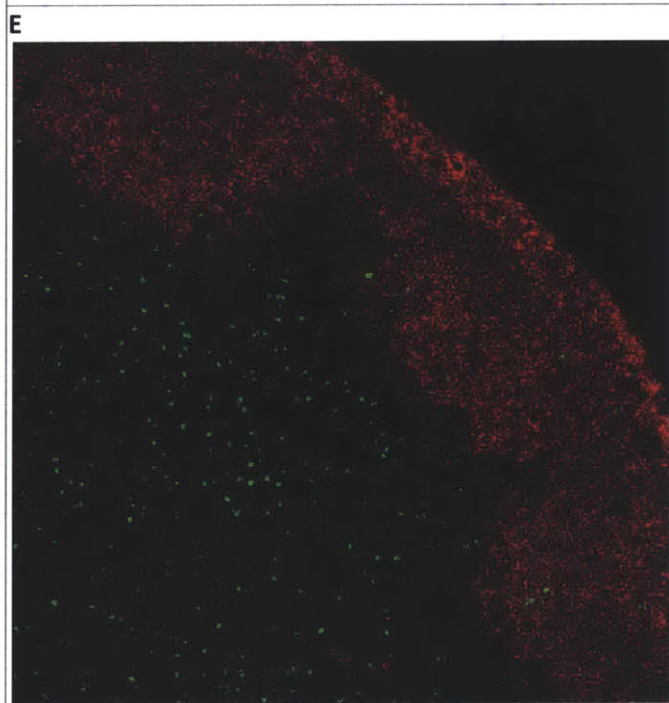
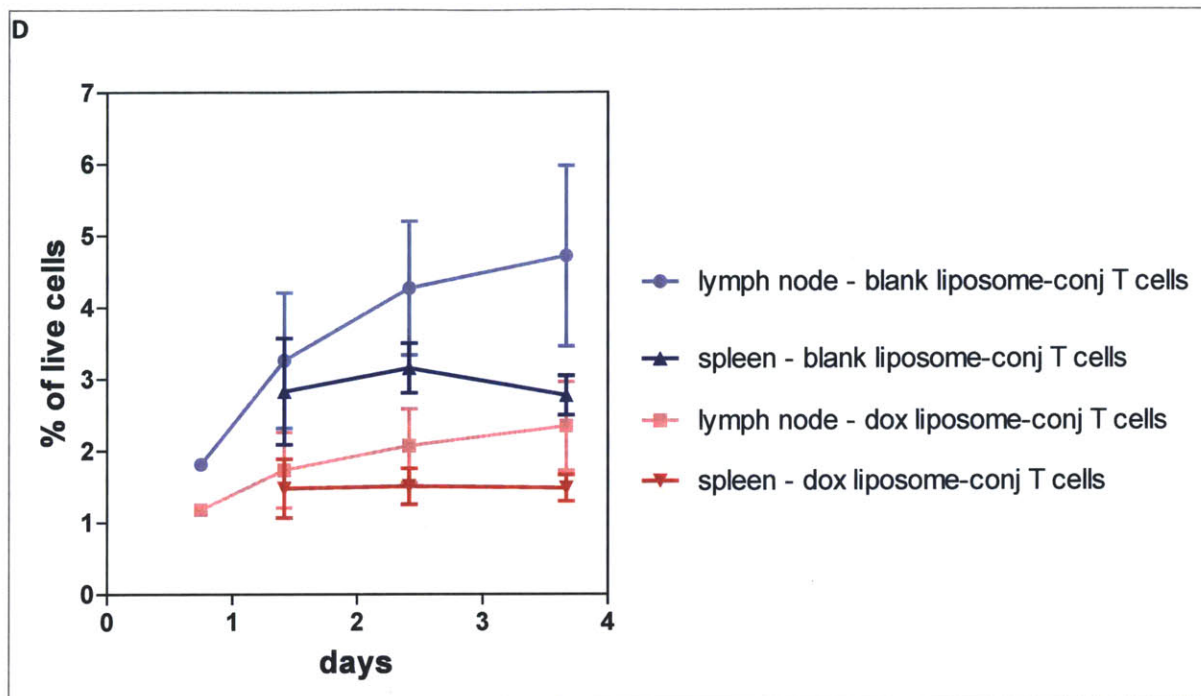
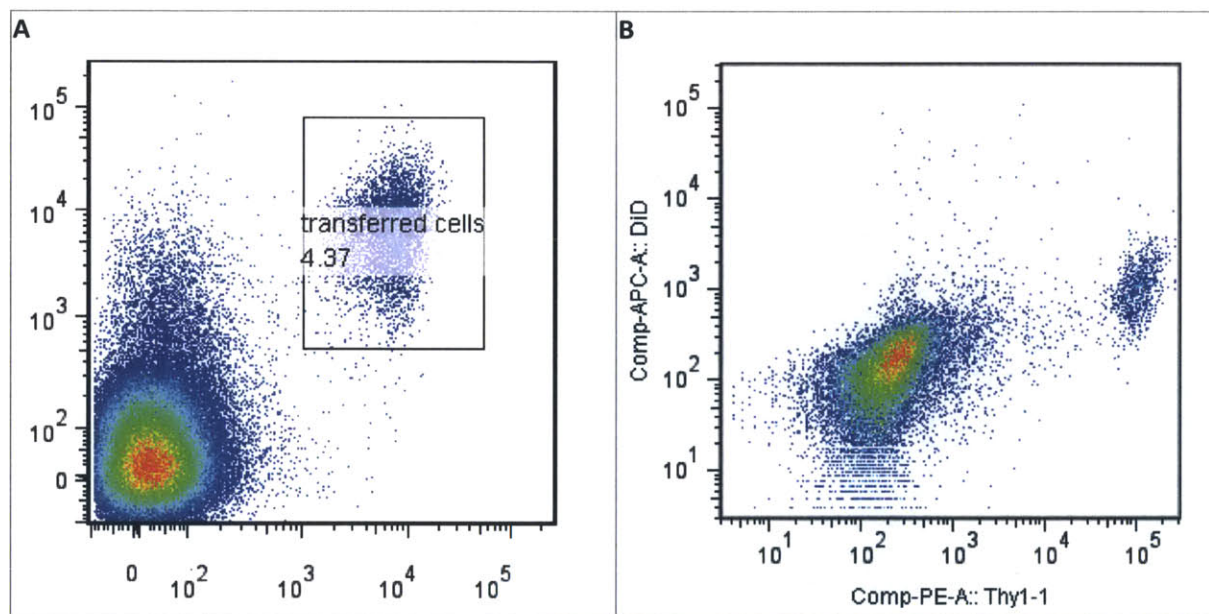


Figure 5.1: Particle-conjugated T cells traffic into spleen, lymph nodes and bone marrow within 15 h. (A) 100×10^6 luc Thy1.1 T cells were conjugated with SN-38 ICMVs and adoptively transferred into mice with Emu-myc *Arf*^{-/-} GFP tumors. T cell biodistribution was imaged by IVIS at 15 and 38 h post-transfer. Lymph nodes are denoted by dashed white circles, spleens by solid white circles. (B) 25×10^6 luc Thy1.1 T cells were adoptively transferred into healthy (non-tumor-bearing) recipients, and the percentage of transferred T cells in spleen and lymph nodes were analyzed by flow cytometry. (C) 100×10^6 luc Thy1.1 T cells were conjugated with SN-38 ICMVs and adoptively transferred into healthy recipients. The

percentages of transferred T cells in tissues were analyzed by flow cytometry. (D) T cells were labeled with CFSE, then conjugated with either blank liposomes or with dox-loaded liposomes. Cells were combined at a 1:1 ratio and 40×10^6 T cells were injected into each blank recipient. (E) Mice with Emu-myc Arf^{-/-} tumors received dox liposome-conjugated T cells and tissues were extracted 3 d later. T cells were stained with CFSE (green) prior to transfer, the lymph node section was stained with anti-B220 PE (red) to visualize B cell follicles.

Dox liposomes and SN-38 ICMVs are carried into Emu-myc Arf^{-/-} tumors by T cells

To confirm that T cells could shuttle their surface-bound particles into lymphoid tumors, we labeled the liposomes and ICMVs with DiD, a fluorescent lipophilic tracer. Flow cytometry analysis of tumor tissues after adoptive transfer of particle-conjugated cells showed populations that were double-positive for the adoptive transferred T cell marker (Thy1.1 or CD45.1) and the fluorescent DiD tracer, suggesting that the transferred T cells retained their particle cargo during trafficking into tumors. This is confirmed by histological sections of lymph nodes show co-localization of T cell and DiD signal (Figure 5.2).



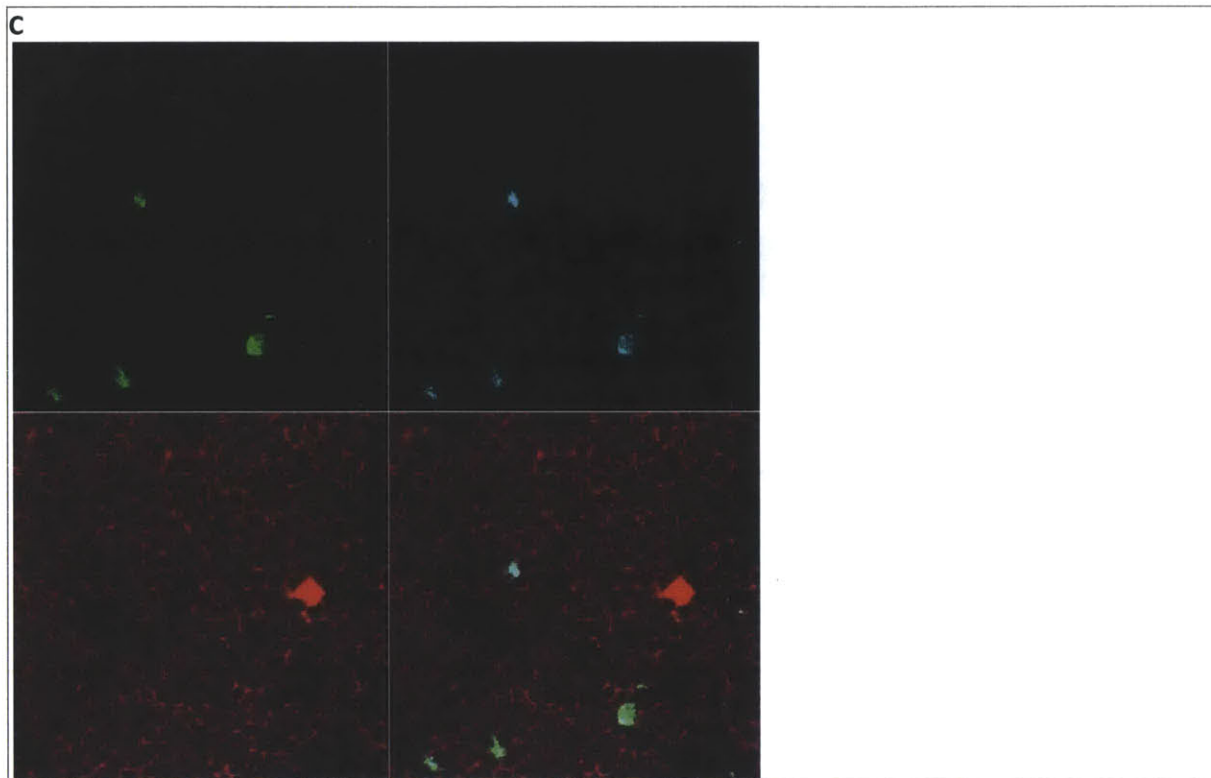


Figure 5.2: T cells transport their conjugated particles into tumor sites.

Mice with Emu-myc *Arf*^{-/-} tumors received luc Thy1.1 T cells conjugated with (A) dox liposomes or (B) SN-38 ICMVs. Tissues were analyzed by flow cytometry 3 d (A) or 15 h (B) post-transfer for presence of transferred T cells and particle fluorescent signal (y-axis). (C) Lymph node histological section from (A), stained with anti-B220 PE to visualize B cell follicles. T cells were stained with CFSE (green) prior to transfer, and ICMVs contained DiD (blue), a lipophilic fluorescent tracer.

To measure biodistribution of free particles versus particles conjugated to T cells, we imaged DiD tracer fluorescence of whole tissues on IVIS. Particle accumulation as measured by DiD fluorescence was significantly enhanced by T cell conjugation in all tumor compartments: blood, spleen, bones and lymph nodes (Figure 5.3). Particle conjugation to T cells may help them to escape phagocytosis by scavenging cells such as Kupffer cells in the liver, and thus prolong their circulation.

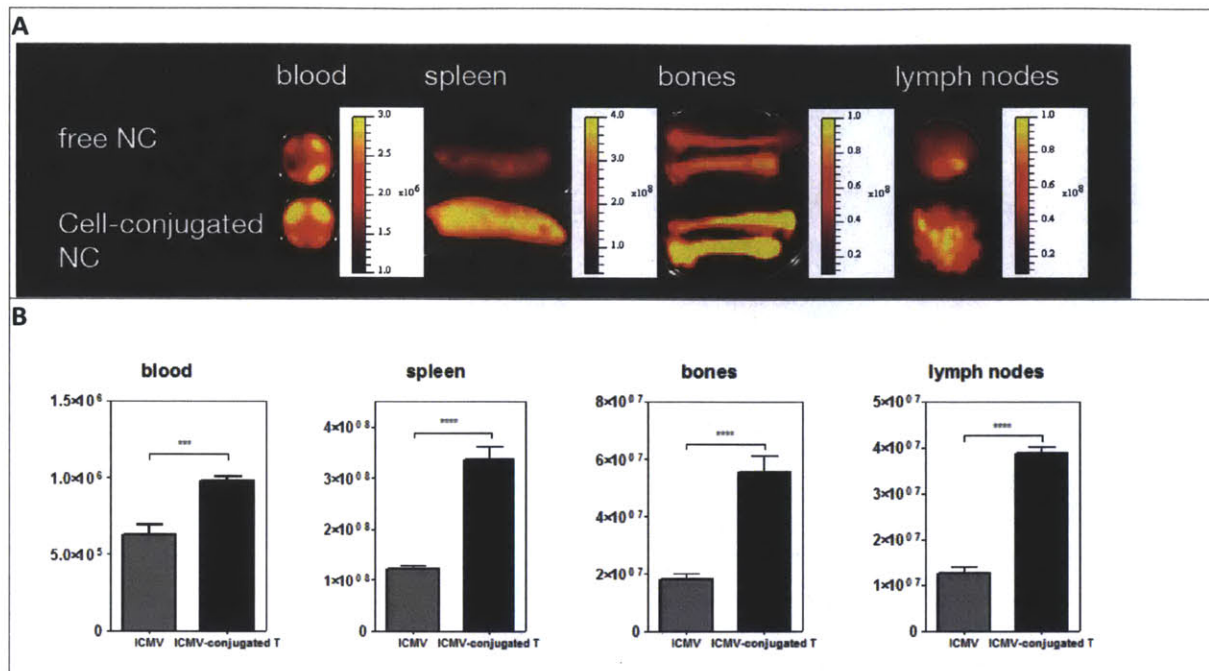


Figure 5.3: T cell conjugation increases SN-38 ICMV accumulation in all tumor tissues. SN-38 ICMVs containing DiD tracer were injected as free particles or conjugated to T cells. (A) Tissues were isolated at 15 h post injection and imaged by IVIS for DiD fluorescence. (B) Quantification of ICMV fluorescent tracer radiant efficiency (background-subtracted against PBS-injected mouse) shows highly significant differences between free ICMVs and T cell-bound ICMVs for all tissues ($p < 0.001$).

SN-38 concentrations in tumors

To confirm that T cell-mediated delivery of SN-38 ICMVs improves therapeutic efficacy by increasing drug accumulation in tumors, we plan to analyze SN-38 concentrations in tumor samples. In the case of free SN-38, the majority of the drug could be observed in the liver, with lower concentrations in the blood, and undetectable amounts in the spleen and lymph nodes (Figure 5.4). Since SN-38 is not water soluble at neutral pH, the injected SN-38 stock had small precipitates that would probably be trapped by the liver immediately upon injection. These results are consistent with pharmacokinetics studies in rats showing rapid clearance from plasma ($t_{1/2}$ is approximately 7 min) and excretion via bile (Atsumi et al., 1995). However, this preliminary experiment used a spectrophotometer to detect SN-38 fluorescence, and was limited by a detection threshold of 100 ng/ml. Recently, we adapted and validated a reverse-phase HPLC protocol from literature, which can detect as low as 1 ng/ml SN-38. We are currently in the process of measuring pharmacokinetics of SN-38 after delivery via free ICMVs and T cell-conjugated ICMVs.

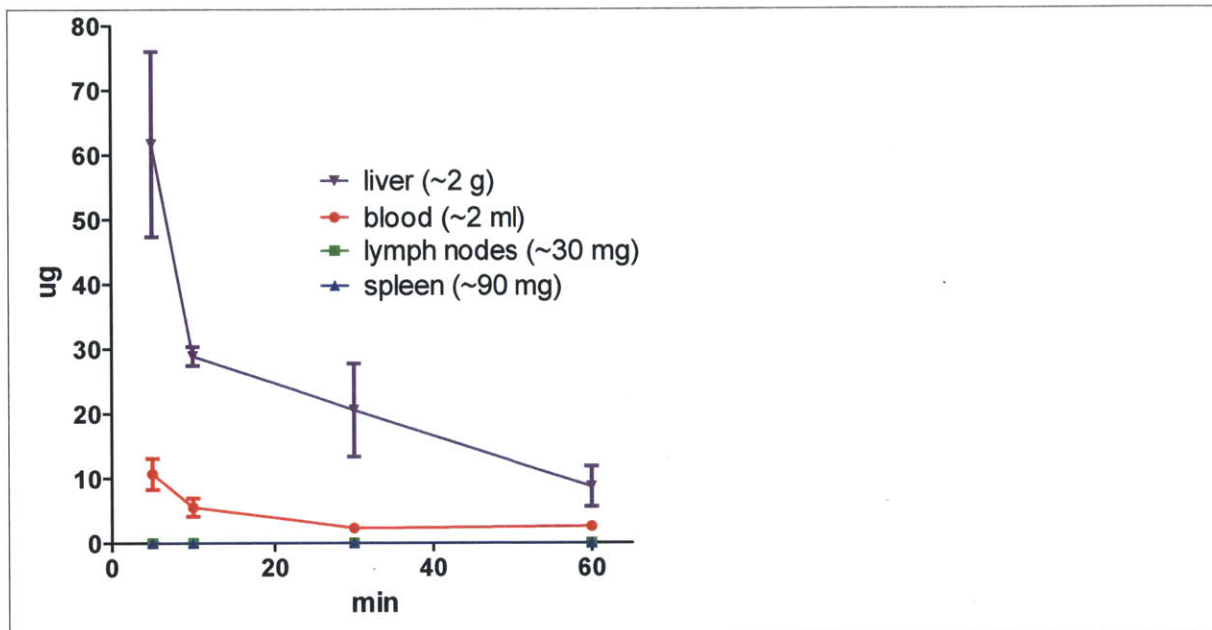


Figure 5.4: Pharmacokinetics of free SN-38 are poor.

500 µg SN-38 was dissolved in 0.1 M NaOH and slowly titrated with 0.1 M HCl to pH 7, then injected intravenously into blank recipients. Tissues were collected, weighed and resuspended at 10% w/v in PBS, homogenized, diluted 1:1 in 0.1 M NaOH + 0.5% Triton X-100, and centrifuged. The supernatant was read on a plate reader and the amount of SN-38 back-calculated from a standard curve.

Having validated the trafficking of particle-conjugated T cells and the delivery of particles to tumors, we proceeded to test the therapeutic efficacy of this strategy in the transplanted Emu-myc Arf^{-/-} model.

Dox liposomes delivered by T cells have modest efficacy *in vivo*

Free dox efficiently clears the majority of Emu-myc Arf^{-/-} tumors *in vivo*, with a maximal tolerated dose of 10 mg/kg (200 µg for a 20 g mouse). Doxil liposomes are also effective at the high dose of 5 mg/kg (100 µg for a 20 g mouse), and significantly extend survival. However, due to the low conjugation efficiency of maleimide-PEG dox liposomes to T cells, and the limit of approximately 100×10^6 T cells that can be injected, only 1-10 µg dox could be delivered by liposome-conjugated T cells. Flow cytometry analysis indicated presence of liposome-conjugated T cells in the tumors, up to 8% of total cells. However, the tumor cell count of untreated versus T cell-treated groups were not significantly different (Figure 5.5). This was not unexpected, since the co-culture experiments suggested that high percentages of maleimide PEG dox liposome-conjugated T cells relative to Emu-myc Arf^{-/-} cells are required to achieve significant Emu-myc Arf^{-/-} killing (see Chapter 4).

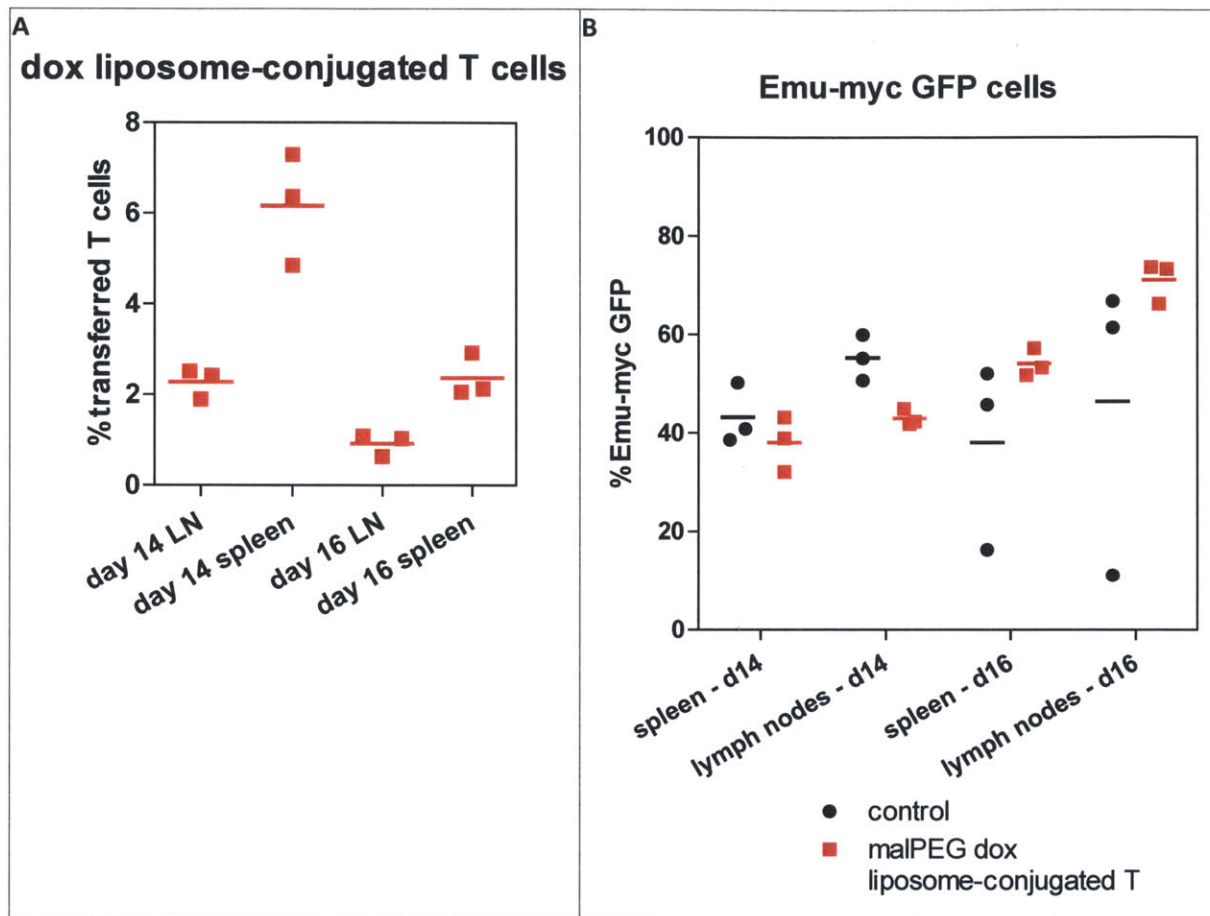


Figure 5.5: Maleimide-PEG dox liposome-conjugated T cells are not therapeutically effective. Emu-myc *Arf*^{-/-} GFP tumor-bearing mice were treated on day 12 post-inoculation with T cells conjugated with maleimide PEG dox liposomes (stable and low conjugation efficiency). At day 14 and 16 post-inoculation, spleen and lymph nodes were analyzed by flow cytometry for the percentages of (A) transferred T cells and (B) Emu-myc *Arf*^{-/-} GFP cells.

Since liposome binding per T cell was already saturated (see Chapter 4), we increased the amount of dox delivered by giving multiple doses of dox liposome-conjugated T cells. While the first two doses did not appear to reduce tumor burden, as measured by IVIS imaging, modest therapeutic efficacy was achieved by the end of this regimen (Figure 5.6). This suggests that the limitation of liposome-conjugated T cells can be the dose of dox that can be delivered.

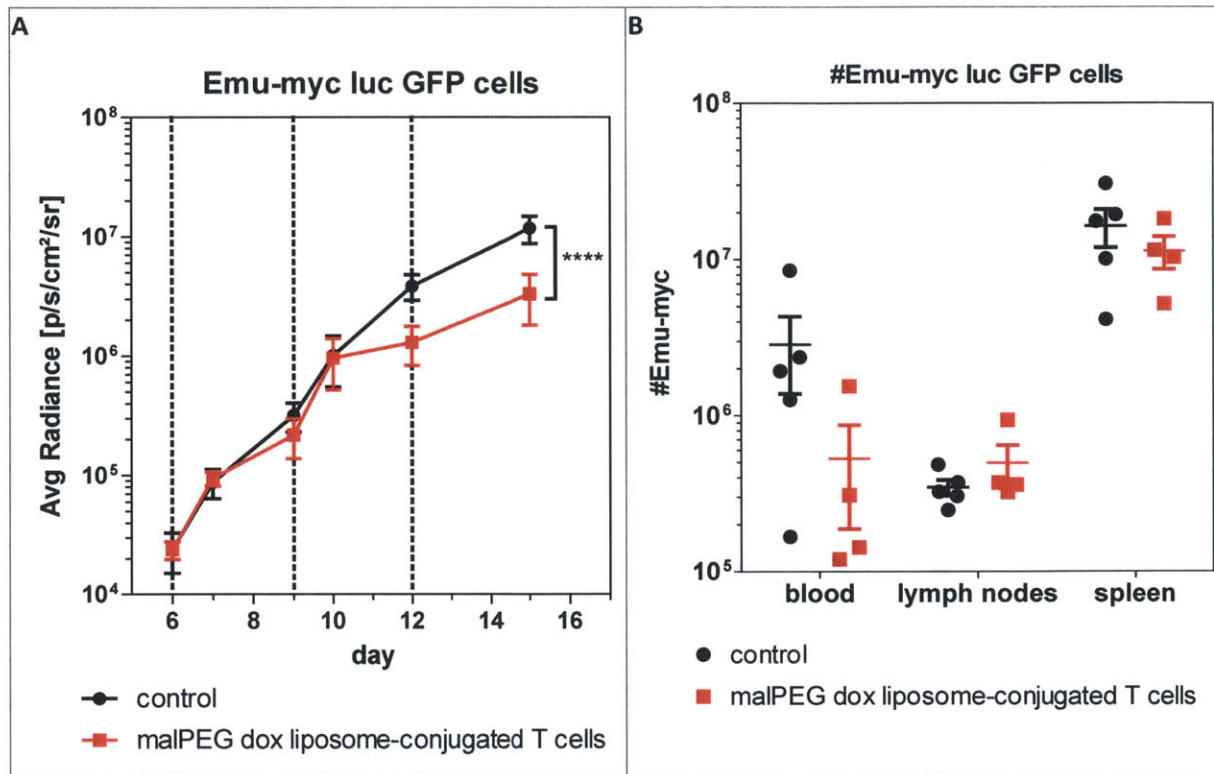


Figure 5.6: Multiple doses of maleimide-PEG dox liposome-conjugated T cells have modest therapeutic efficacy.

Mice were treated on days 6, 9, 12 post-tumor inoculation with malPEG dox liposome-conjugated T cells. (A) Whole body tumor bioluminescence was imaged by IVIS on days 6, 7, 9, 10, 12 and 15. The radiance averages were compared by 2-way ANOVA with Bonferroni post-tests. Only the day 15 averages were significantly different ($p < 0.0001$). (B) Blood, spleen and lymph nodes were isolated on day 15, and the number of Emu-myc *Arf*^{-/-} luc GFP cells measured by flow cytometry using counting beads. There was no statistical significance between the two groups for any tissue.

One parameter that could contribute to the limited therapeutic impact could be because the release kinetics from the maleimide-PEG dox liposomes are too slow. The low sustained release from maleimide-PEG dox liposomes may cause transient tumor death, but may be outweighed by rapid tumor proliferation and development of resistance. Dox liposomes containing MPB-lipid, which are unstable and prone to aggregation (see Chapter 2), have a faster release rate and higher conjugation efficiency. T cells functionalized with MPB dox liposomes were more potent in the co-culture assay. However, MPB dox liposome-bound T cells reached tumors at low frequencies, suggesting the too rapid release that kills the T cell carriers before they have sufficient time to traffic. These functionalized T cell were also therapeutically ineffective (Figure 5.7). An intermediate release rate may be optimal for dox; however, we were not able to develop a liposome system with this release profile to test this hypothesis.

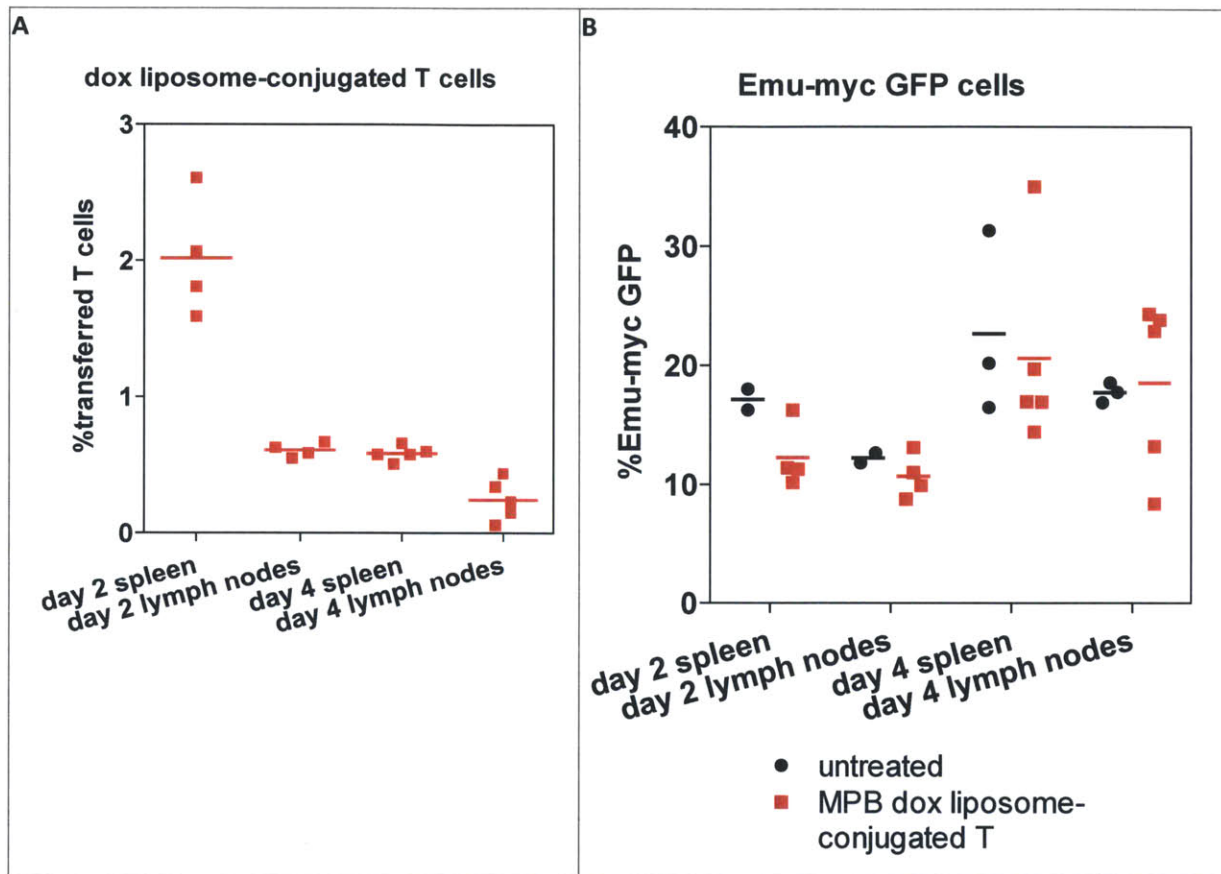


Figure 5.7: MPB dox liposome-conjugated T cells are not therapeutically effective. Emu-myc $Arf^{-/-}$ GFP tumor-bearing mice were treated on day 12 post-inoculation with T cells conjugated with MPB dox liposomes (leaky, unstable and high conjugation efficiency). At days 2 and 4 post-treatment, spleen and lymph nodes were analyzed by flow cytometry for the percentages of (A) transferred T cells and (B) Emu-myc $Arf^{-/-}$ GFP cells. There was no statistical significance between the two groups for either tissue.

SN-38 ICMVs delivered by T cells have potent therapeutic activity

In contrast to dox liposome-conjugated T cells, SN-38 ICMV-conjugated T cells potently suppressed Emu-myc $Arf^{-/-}$ growth *in vivo*. According to our previous studies, T cell trafficking into tumor sites is significant by 16 h and peaks at 2 to 3 d, and similarly, SN-38 release kinetics from ICVMs *in vitro* are on the order of 3 d. Therefore, we expected the tumor suppression to occur steadily over a 2 to 3 d period. However, therapeutic effects were observed by IVIS as early as 16 h post therapy (Figure 5.8). This suggests that the early influx of T cells into tumor sites acts immediately to clear a portion of the tumor, thus reducing the exponentially growing tumor burden. Interestingly, Emu-myc $Arf^{-/-}$ cells were depleted in all organs; we did not observe preferential tumor clearance in lymph nodes versus bone marrow, even though T cells traffic into the former at higher numbers.

CXCR4 antagonism enhances therapeutic efficacy of ICMV-functionalized T cells

Given the significant population of Emu-myc Arf^{-/-} cells in the bone marrow and the limited T cell infiltration into this compartment, we hypothesized that this niche represents a potential source of residual tumor growth. Chemotaxis into and retention in the bone marrow depend on a number of receptors, including integrin VLA-4 and chemokine receptor CXCR4. The majority of non-Hodgkin's lymphoma cell lines and primary patient samples express high levels of CXCR4 mRNA (Bertolini et al., 2002; Trentin et al., 2004). Its ligand, CXCL12, was originally discovered as a pre-B cell growth factor (Nagasawa et al., 1994), but B cells of all maturation stages are highly sensitive to CXCR4-CXCL12 signaling (Burger and Peled, 2008). CXCR4 blockade induced apoptosis and reduced trans-endothelial migration of the human Namalwa lymphoma line *in vitro*, and inhibited tumorigenesis after Namalwa transplantation into SCID recipients (Bertolini et al., 2002).

In vitro, Emu-myc Arf^{-/-} cells express high levels of homing markers for both bone marrow (CXCR4) and lymph nodes (CD62L). Within a few hours after intravenous injection into naïve hosts, Emu-myc Arf^{-/-} cells are found primarily in the bone marrow by flow cytometry (Hemann lab data), suggesting the bone marrow is an important niche for Emu-myc Arf^{-/-} tumorigenesis. Recent work highlights the role of IL-6 in the bone marrow as a factor that fuels lymphomagenesis in this model (Gilbert and Hemann, 2012).

Since IL-2 and rapamycin cultured T cells expressed only moderate levels of CXCR4 and did not infiltrate bone marrow as successfully as other tissues, we attempted to increase their CXCR4 expression. Despite reports that *in vitro* culture with IL-4 can induce CXCR4 upregulation in peripheral and cord blood human T cells (Jourdan et al., 1998), we did not find this effect on our mouse T cells generated from splenocytes (data not shown). Other reports suggest that TGF- β isoforms (Buckley et al., 2000) and glucocorticoids (Okutsu et al., 2005; Wang et al., 1998) also upregulate CXCR4 on human T cells *in vitro*; we are currently testing these agents on our mouse T cell cultures. In parallel, we considered the converse strategy of luring the Emu-myc Arf^{-/-} cells out of the bone marrow.

AMD3100 is a small molecule CXCR4 antagonist that potently mobilizes hematopoietic stem cells from the bone marrow within 1 h of administration (Broxmeyer et al., 2005). AMD3100 and its analogs have also been shown to mobilize leukemia and lymphoma cells into circulation on a similar timescale (Zeng et al., 2009). This strategy has been used to increase leukemia and lymphoma exposure to systemic chemotherapy, and improves the efficacy of drugs such as cytarabine and doxorubicin (Nervi et al., 2006; Nervi et al., 2009). When we supplemented our therapy regime with AMD3100, we saw significant improvement only for SN-38 ICMV-conjugated T cells, not for SN-38 ICMV alone (Figure 5.9). We hypothesize this may be due to Emu-myc Arf^{-/-} egress from the bone marrow into other sites where T cells are more enriched, such as the lymph nodes. Since free SN-38 ICMVs would primarily be trapped in the liver, altered biodistribution of Emu-myc Arf^{-/-} cells would not improve its efficacy. Again, for all therapy conditions, we saw a uniform reduction of tumor burden throughout the mouse, suggesting that Emu-myc Arf^{-/-} cells are able to actively circulate throughout the body and rapidly repopulate depleted sites. The ability of Emu-myc Arf^{-/-} cells to traffic between organs was confirmed by a recent imaging study, which showed that the lymphoma cells primarily seed the spleen and bone marrow immediately after tumor inoculation, but after a period of growth,

waves of lymphoma cells leave these organs to colonize lymph nodes via circulation (Ito et al., 2012). In light of this study, the potency of our therapeutic strategy can perhaps be attributed to the prevention of lymphoma cell spread to the lymph nodes.

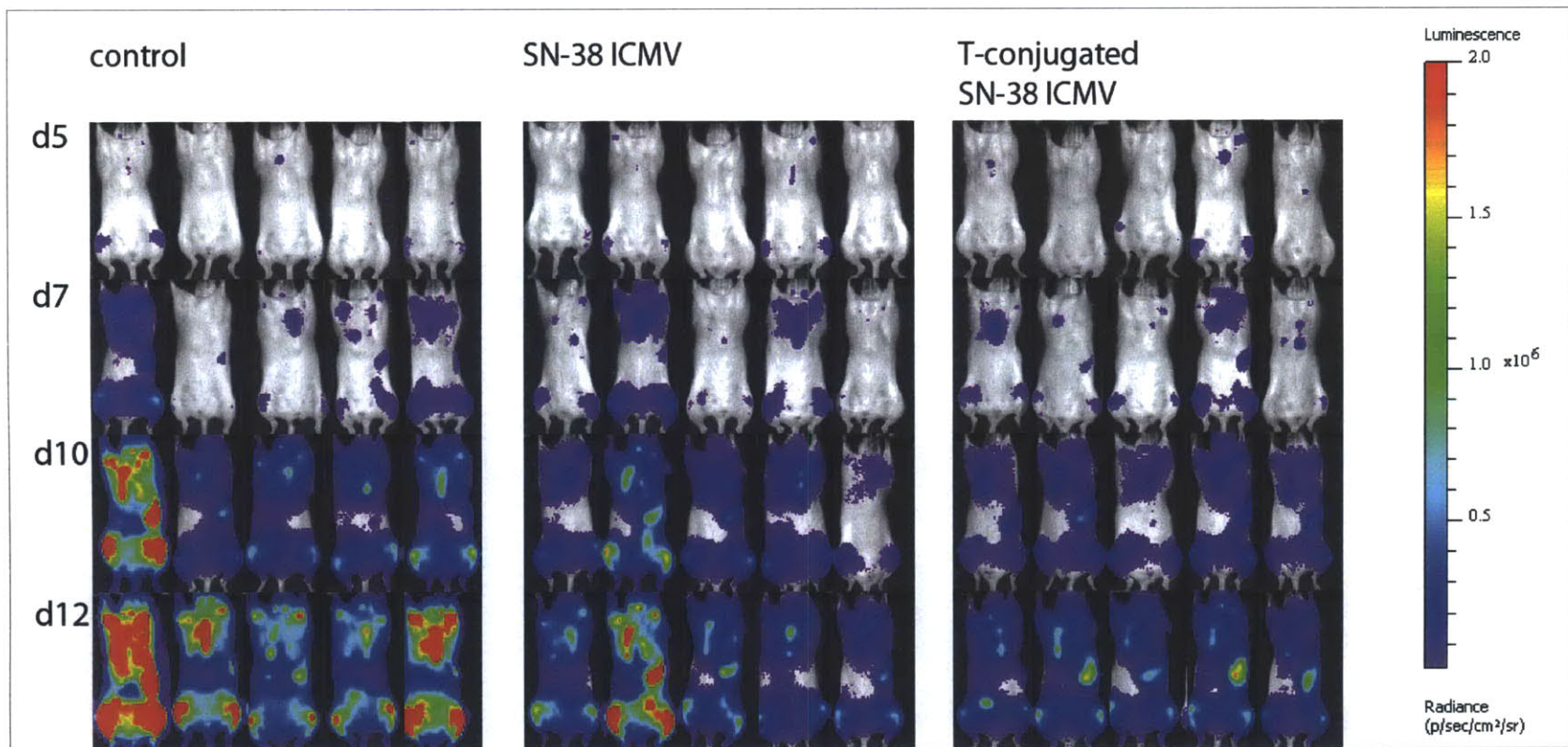


Figure 5.8: SN-38 ICMV have superior therapeutic effect when delivered via T cell conjugation. Albino mice were inoculated with Emu-myc *Arf*^{-/-} luc GFP cells. On days 5, 8 and 10, mice were treated with 10 μg doses of SN-38 as free ICMVs or as ICMVs conjugated to T cells.

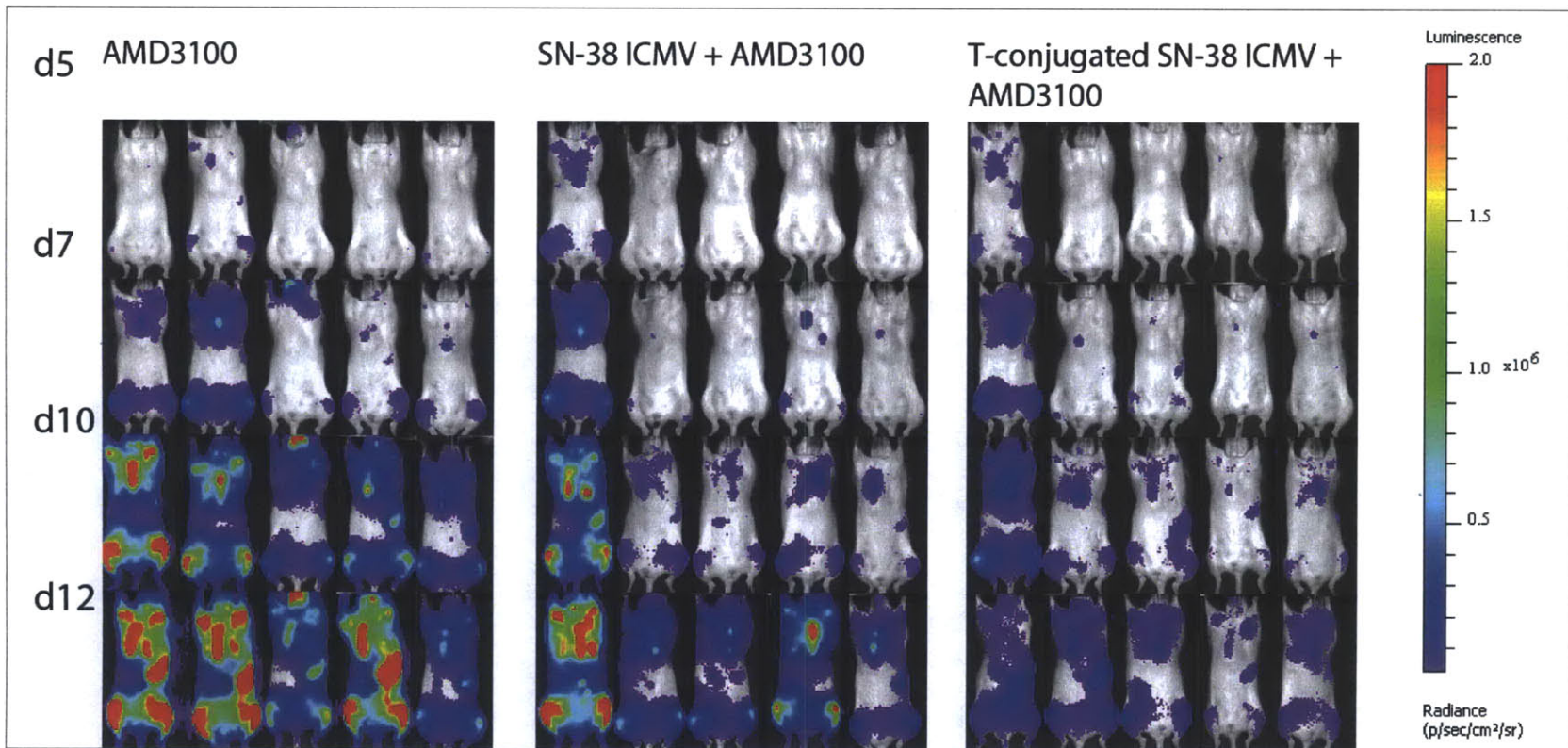


Figure 5.9: CXCR4 inhibition enhances the therapeutic efficacy of SN-38 ICMV-conjugated T cells. Mice were treated with SN-38 formulations as described in Figure 5.8. In addition, on days 5, 6, 8, 9, 10 and 11, the above groups received 5 mg/kg AMD3100 by subcutaneous injection.

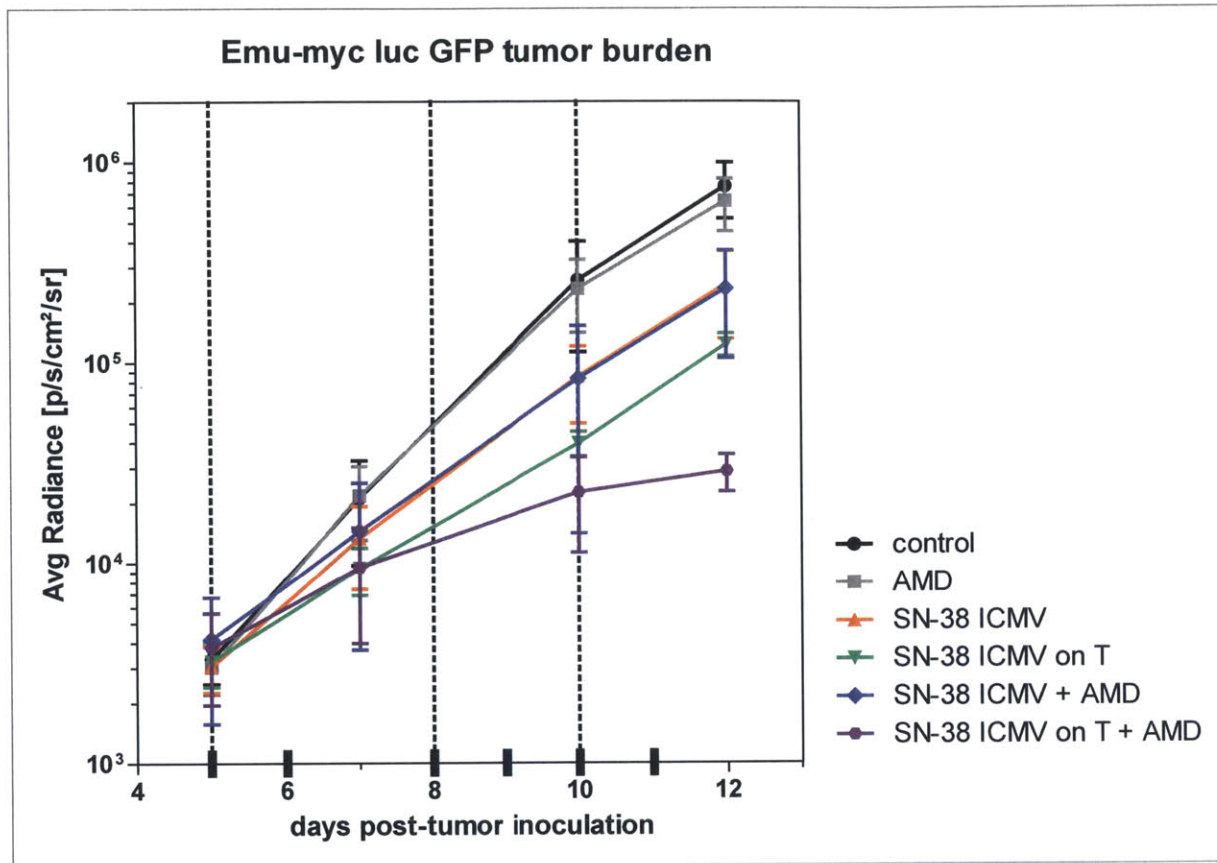


Figure 5.10: Tumor burdens over the course of SN-38 therapy, as measured by IVIS bioluminescence. Group averages of tumor burden from the therapy experiment described in Figure 5.8 and Figure 5.9.

Putative mechanisms for AMD3100-mediated therapeutic enhancement

CXCL12 did not increase Emu-myc Arf^{-/-} proliferation; neither did it promote Emu-myc Arf^{-/-} resistance to SN-38 (Figure 5.11). Consistent with this, AMD3100 did not have a direct cytotoxic effect on Emu-myc Arf^{-/-} cells, and it also did not sensitize Emu-myc Arf^{-/-} cells to SN-38 killing *in vitro* (Figure 5.11).

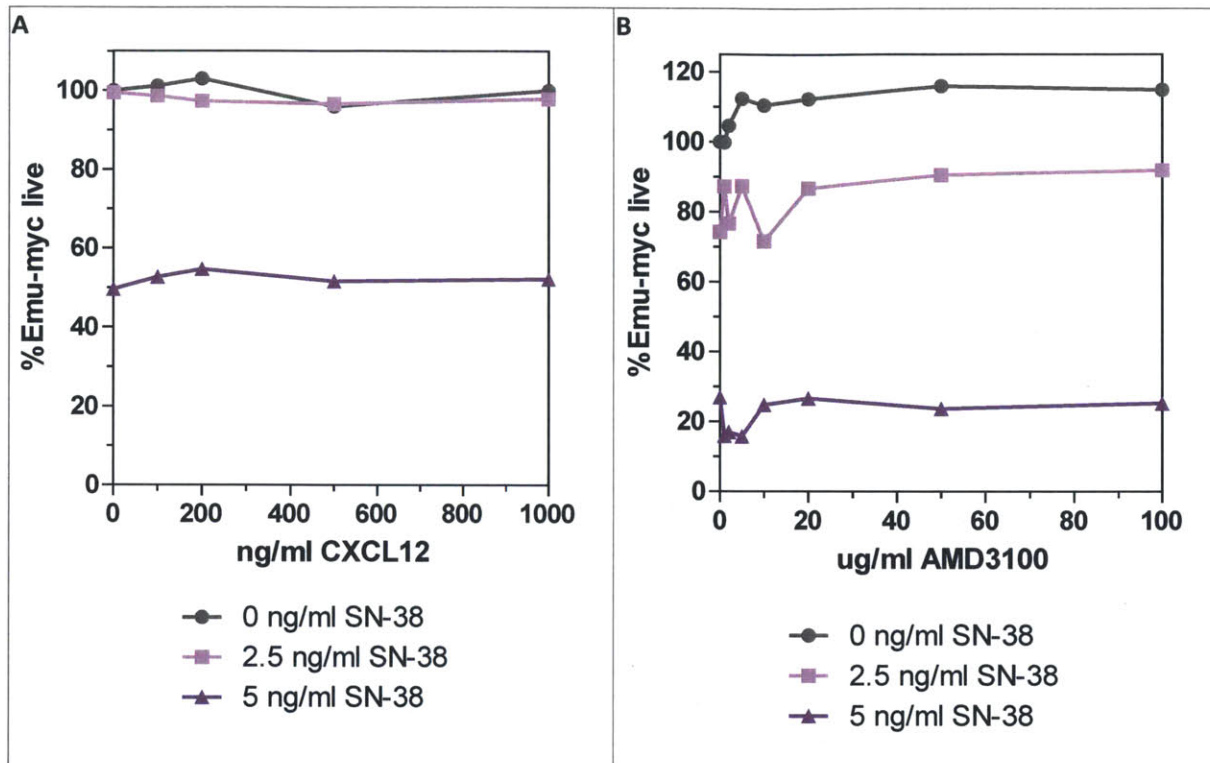


Figure 5.11: CXCL12 and AMD3100 have no direct effect on Emu-myc $Arf^{-/-}$ cell proliferation or survival *in vitro*.

Emu-myc $Arf^{-/-}$ cells were cultured with (A) CXCL12 (100-1000 ng/ml) or (B) AMD3100 (1-100 μ g/ml), and viability was measured by flow cytometry 1 d later.

We investigated the effect of AMD3100 on Emu-myc $Arf^{-/-}$ cell trafficking *in vivo*. AMD3100 did not cause significant redistribution of Emu-myc $Arf^{-/-}$ cells *in vivo*, as imaged by IVIS. When tissues were analyzed by flow cytometry, the percentage of Emu-myc $Arf^{-/-}$ cells was found to be different only in the blood. These results suggest that AMD3100-mediated mobilization of Emu-myc $Arf^{-/-}$ cells into systemic circulation is modest, and populations in the bone marrow, spleen and lymph nodes remain stable.

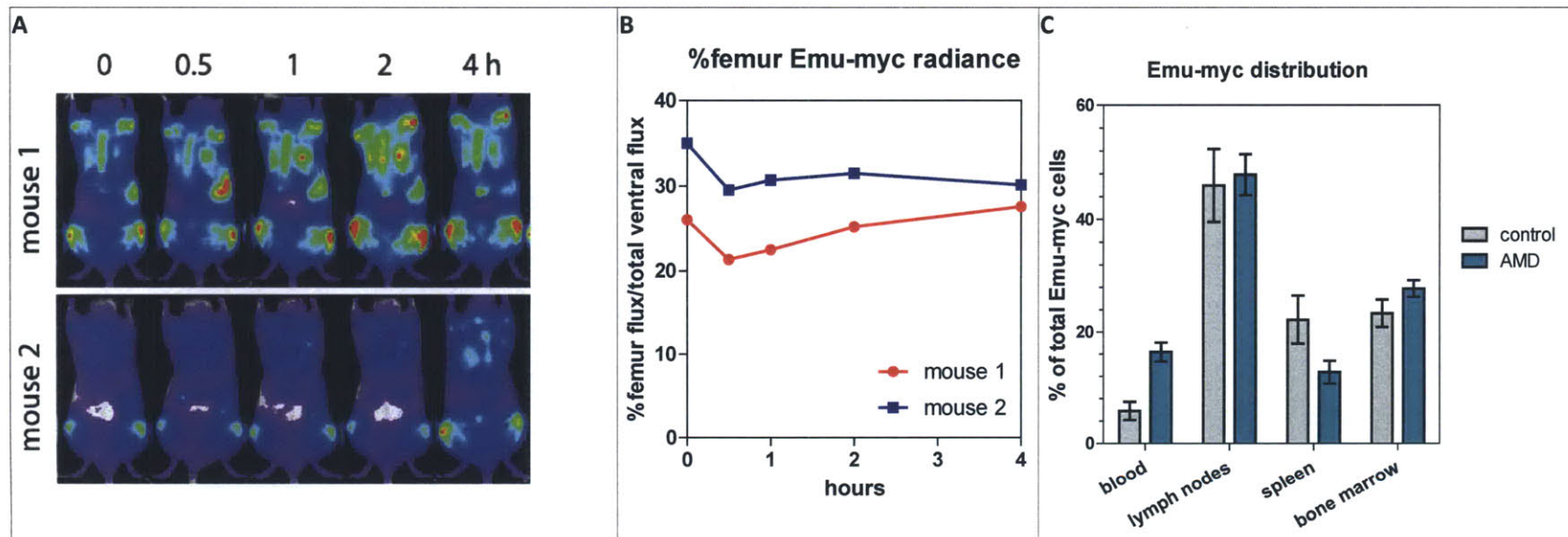


Figure 5.12: AMD3100 increases Emu-myc Arf^{-/-} redistribution into the blood, but does not significantly change Emu-myc Arf^{-/-} tumor burden in lymph nodes, bone marrow or spleen.

(A) Two Emu-myc Arf^{-/-} luc GFP tumor-bearing mice were given 5 mg/kg AMD3100, then imaged by IVIS over the course of 4 h. (B) The radiance in the femurs was used to represent bone marrow Emu-myc Arf^{-/-} concentrations, and is plotted as a percentage of the total body radiance. (C) Five Emu-myc Arf^{-/-} luc GFP tumor-bearing mice were given 5 mg/kg AMD3100 and four were given PBS. Tissues were collected at 2 h post-injection and the number of Emu-myc Arf^{-/-} cells in each organ was measured by flow cytometry using counting beads. The total Emu-myc Arf^{-/-} cells in each mouse and the percentage in each tissue was calculated. Only the percentages in the blood showed statistical significance ($p = 0.03$).

These results suggested that AMD3100 exerts its effects on CXCR4 signaling only when Emu-myc Arf^{-/-} cells are in the presence of stromal cells. A previous study has shown that mantle cell lymphoma is significantly more resistant to cytarabine *in vitro* when they are co-cultured with a bone marrow stromal cell line (Kurtova et al., 2009). We are currently evaluating whether this phenomenon also occurs in co-cultures of Emu-myc Arf^{-/-} cells and bone marrow stromal cells *in vitro*. If so, we would expect AMD3100 to counteract the protective effect of the stromal cells and restore lymphoma cell sensitivity to SN-38.

Summary and Conclusion

We confirmed that nanoparticle-conjugated T cells trafficked into multiple lymphoma tumor sites and successfully carried their nanoparticle cargo into the tumors. While dox liposome-conjugated T cells had limited therapeutic effect, SN-38 ICMV-conjugated T cells effectively suppressed tumor growth. Comparing the therapeutic efficacy of one versus three doses of dox liposome-conjugated T cells, it is clear that one crucial factor is sufficient drug dose. In mice treated with SN-38 ICMV-conjugated T cells, tumor growth suppression can be observed by imaging as early as one day post-treatment. Although we attempted to detect *in vivo* lymphoma cell apoptosis by tissue staining with Annexin V, γ -H2AX and activated Caspase 3, we failed to detect significant differences between control and treated groups. This may be due to the high basal rate of apoptosis in Emu-myc cells due to c-myc activation (Gilbert and Hemann, 2012), as well as rapid scavenging of dead lymphoma cells by macrophages (Jacobsen et al., 1994). Alternatively, SN-38 treatment could be acting therapeutically through induction of senescence. Previous *in vivo* studies have shown that Emu-myc Arf^{-/-} cells become senescent after systemic cyclophosphamide treatment (Schmitt et al., 2002b), and that the thymic stroma was senescent after dox treatment (Gilbert and Hemann, 2010).

The AMD3100 experiments highlight the importance of studying tumor progression and therapeutic response in the context of the *in vivo* microenvironment, which provides a plethora of factors that can either suppress or promote tumor growth. A previous study shows that transplanted Emu-myc cell survival and growth are dependent on Hedgehog ligands secreted by stromal cells in the lymph nodes, spleen and bone marrow (Dierks et al., 2007). IL-6 secreted by the bone marrow stroma normally regulate hematopoietic stem cell survival and B cell differentiation, but also influence the rate of Emu-myc Arf^{-/-} tumorigenesis, depending on the maturation stage of the lymphoma cells (Gilbert and Hemann, 2012). Transplanted Emu-myc Arf^{-/-} cells also respond to chemotherapy in a tissue-specific manner. In particular, the thymic stroma can modulate the growth and survival of Emu-myc Arf^{-/-} cells in opposing ways. The signaling of transplanted Emu-myc Arf^{-/-} cells was directly affected by the stromal cells in the thymus as compared to in the lymph nodes, as shown by the importance of Bid-dependent apoptotic signaling in the former organ but not the latter (Pritchard et al., 2011). IL-6, an inflammatory cytokine that is normally secreted by thymic endothelial cells in response to tissue damage, can be co-opted by Emu-myc Arf^{-/-} cells to survive systemic dox therapy and eventually cause tumor relapse (Gilbert and Hemann, 2010). The therapy-enhancing effects of AMD3100 in our studies may very well be due to the blockade of pro-survival stromal interactions with Emu-myc Arf^{-/-} cells.

6. Conclusion and Future Directions

Summary of T cell-mediated delivery of drug nanoparticles

A major challenge in cancer therapy is the targeted delivery of drugs to the appropriate disease sites. The concentration of drugs at the tumors is one way to compensate for the lack of drug target specificity with tissue specificity. Traditional work in the drug delivery field has focused on designing fully synthetic particle systems that can bypass anatomical barriers to the target tissue. In this work, we have incorporated an element of “active” delivery in the form of cellular chaperones that carry nanoparticles to the desired tissue compartments. This resulted in enhancement of drug nanoparticle accumulation in lymphoma tumors and therapeutic benefit.

Our studies highlight two important parameters for the therapeutic success of cell-mediated nanoparticle delivery to tumors. First, in addition to the traditional attributes of stability and high drug encapsulation, the nanoparticle must also conjugate efficiently to the cell carrier, in order to load the cells with therapeutically relevant doses of drug. In part, this can be compensated for by a more potent drug cargo. Second, the cell carriers themselves must be relatively resistant to the drug cargo, and be able to traffic into the tumor sites on a timescale that is comparable with the timescale of drug release from the nanoparticle, such that the drug cargo will not be depleted by the time the cells arrive in the tumor. Each component of SN-38 ICMV-conjugated T cells was optimized to fulfill these criteria, and therefore the compounded formulation was therapeutically effective. In comparison, dox liposome-conjugated T cells suffered from very low conjugation efficiency, and this single deficiency could not be rescued by the high dox loading in liposomes. In principle, if dox could be encapsulated in a particle system that can overcome the conjugation efficiency limits of Doxil liposomes, it could also be therapeutically effective in this tumor model.

Therapeutic efficacy in the context of the Emu-myc Arf^{-/-} model

The Emu-myc Arf^{-/-} model is extremely aggressive and plastic in its phenotype, so it is unlikely that any single therapeutic modality will be able to achieve a cure. Although this model has been well studied from the angle of classic tumor cell-intrinsic processes such as evasion of apoptosis, it is clear that other emerging hallmarks of cancer must also contribute to its progression and its response to chemotherapy. Transplantation studies suggest that this tumor model may not have a rare cancer stem cell population, since just a few Emu-myc cells can seed fully-developed tumors (Kelly et al., 2007). This perhaps is unsurprising, given that c-myc is known to play a crucial role in the maintenance of stem cells (Meyer and Penn, 2008), and if every Emu-myc cell has the activated c-myc oncogene, each one also has the potential to be self-renewing and therefore a cancer stem cell. Additionally, Emu-myc Arf^{-/-} cells can reduce their sensitivity to dox by down-regulating the drug target Topoisomerase II and relying on Topoisomerase I for replication (Burgess et al., 2008). Analogously, sensitivity to camptothecin (an SN-38-related drug) is reduced by Topoisomerase I downregulation and increased usage of Topoisomerase II. A potential therapy to reduce drug resistance may be to use the combination or sequence of dox and camptothecin/SN-38, such that the Emu-myc Arf^{-/-} cells cannot escape the simultaneous poisoning of both topoisomerases.

Future directions for cell-mediated drug delivery

Our strategy of delivering particles via cell carriers can be modified for a variety of other applications, not limited to just cancer. The drug can be easily changed, since the ICMV platform self-assembles robustly and can incorporate a variety of cargos: proteins, lipids, nucleic acids, as well as small molecule drugs such as the one described in this thesis. A major focus of current pharmaceutical research is on antagonists of aberrant signaling pathways that are specific to cancer cells (Younes, 2011). Compared to first-generation cytotoxic chemotherapies, these molecularly-targeted drugs can distinguish between healthy tissues and tumors with much greater sensitivity, but in some cases, toxicity is still a concern (Keefe and Bateman, 2012). Additionally, systemic administration of targeted drugs may be cost-prohibitive, or be limited by drug solubility in pharmaceutically-acceptable carriers. Cell-mediated nanoparticle delivery could be applied to these next-generation drugs as a way to reduce the dose required, or to stabilize them for sustained release, as we did for SN-38.

Other particle systems can also be adapted to cell conjugation, given an appropriate size range ($<1 \mu\text{m}$) and high surface density of functionalization with maleimide. Finally, the cell carrier itself can be engineered to express the appropriate homing markers for the targeted tissue of interest. Extensive studies of leukocyte trafficking in both homeostasis and disease has elucidated many of the homing receptor patterns associated with particular tissues, such as the skin, gut (Sigmundsdottir and Butcher, 2008), lungs (Luster and Tager, 2004), and central nervous system (Ransohoff and Engelhardt, 2012). Optimized cytokine and small molecule drug cocktails may be able to skew *in vitro* cell carrier cultures to express the correct homing markers for the desired target organ.

We have developed a simple protocol for generation of cellular carriers and attachment of drug nanoparticles, but the cell culture and particle-cell conjugation protocol may be too complex for scale-up standardization or clinical translation. One follow-up project in the lab is focused on designing nanoparticles with high reactivity and specificity that can attach to T cells in circulation, which will then act as carriers in the same way that *ex vivo* primed and particle-functionalized T cells would. This “*in vivo* conjugation” strategy would allow direct injection of off-the-shelf particles for a cell-mediated delivery of drug nanoparticles. Current efforts are focused on screening for an appropriate targeting ligand for T cell conjugation; candidates include an IL-2-Fc fusion protein developed by the Wittrup lab, as well as several antibodies tested in Figure 4.4. The antibody target determines to a great extent the kinetics of particle retention on the cell surface. For example, anti-CD3 ϵ -conjugated dox particles are rapidly endocytosed by T cell leukemia cells (Dinauer et al., 2005). Endocytosis is not desirable for the case of drug delivery to tumors, where the antibody-targeted T cell is the carrier and must hand off the cargo. However, for particles containing cargo that is intended for consumption by the targeted cell, such as a Shp-1 inhibitor for cytotoxic T cells that enhances their activation (Stephan et al., 2012), endocytosis of the particle may actually be favorable.

I. Appendix: Dox nanoparticle formulations

Select dox liposome formulations

All formulations loaded via ammonium sulfate gradient unless otherwise specified.

Composition (mol%)	Stability	Feed, $\mu\text{g dox}$	Loading, $\mu\text{g dox}/\mu\text{mol lipids}$	Release
Doxil (gold standard)	Stable		250	~1 week
56.2/38.3/5.3/0.2 HSPC/cholesterol/PEG2000-DSPE/ vitamin E				
80/20 DOPC/DOPG, passive encapsulation	Stable	46.4 – 185.6	21	50-100% in 1d
80/20 DOPC/DOPG	Stable	46.4	31	
		92.8	63	
		185.6	114	60% in 2d
50/40/10 MCC-DOPE/DOPC/DOPG, passive encapsulation	Stable	46.4	7	
50/40/10 MCC-DOPE/DOPC/DOPG	Stable	46.5	9	
	Stable	92.8	15	
	Aggregates	185.6	7	
56.2/38.3/5.3/0.2 DOPC/cholesterol/PEG2000-DOPE/ vitamin E, passive encapsulation	Stable	185.6	56	55% in 2d
56.2/38.3/5.3/0.2 DOPC/cholesterol/PEG2000-DOPE/ vitamin E	Stable	185.6	80	50% in 2d
50/11.5/38.3/0.2 MPB-DOPE/HSPC/cholesterol/vitamin E	Aggregates	92.8-371.2	41	
50/11.5/38.3/0.2 Mal-PEG2000-DSPE/ HSPC/cholesterol/vitamin E	Stable	371.2	59	
50/11.5/38.3/0.2 MPB-DPPE/HSPC/cholesterol/vitamin E	Aggregates	185.6	5.5	
10/51.5/38.3/0.2 MPB-DOPE/HSPC/cholesterol/vitamin E	Aggregates	92.8	33	

5/56.5/38.3/0.2 MPB-DOPE/HSPC/cholesterol/vitamin E	Aggregates	92.8	30	
1/60.5/38.3/0.2 MPB-DOPE/HSPC/cholesterol/vitamin E	Aggregates	92.8	33	
5/56.5/38.3/0.2 MPB-DOPE/HSPC/cholesterol/vitamin E, MPB-DOPE post-inserted	Stable (poor post-insertion)	92.8	25	
10/51.5/38.3/0.2 MPB-DPPE/HSPC/cholesterol/vitamin E	Aggregates	92.8	84	
5/56.5/38.3/0.2 MPB-DPPE/HSPC/cholesterol/vitamin E	Aggregates	92.8	42	
1/60.5/38.3/0.2 MPB-DPPE/HSPC/cholesterol/vitamin E	Aggregates	92.8	49	

Dox ICMVs

We attempted to encapsulate dox in ICMVs by a number of methods. Passive encapsulation by rehydrating lipids with dox solution gave low encapsulation and burst release within 1 day. We then attempted to use gradient loading to increase the dox encapsulation. We first synthesized liposomes that were gradient-loaded with a high amount of dox, then added the stapling reagents. However, the calcium-driven fusion probably disrupted the dox-encapsulating liposomes and released the loaded dox, again resulting in low encapsulation. When we took ICMVs formed through the usual synthesis procedure and buffer-exchanged them into ammonium sulfate, the gradient loading of dox was very inefficient, suggesting that diffusion of both ammonium sulfate and dox through the multilamellar structure of ICMVs is significantly slower than through the single bilayer of unilamellar liposomes.

Dox PLGA particles

We synthesized dox-encapsulating PLGA nanoparticles using the double-emulsion method described in (Bershteyn et al., 2008). Dox was either in the first water phase and emulsified into the PLGA solution in the oil phase, or co-dissolved with the PLGA in the oil phase. In both cases, particle formation proceeded as expected, but dox encapsulation was poor (~2 µg per 30 mg batch of PLGA), and particles were very prone to aggregation during the solvent evaporation step.

II. Appendix: SN-38 particle formulations

SN-38 ICMVs

Composition (mol%)	Stability	Feed, μg SN-38	Loading, μg SN-38/ μmol lipids
50/50 MPB-DOPE/DOPG	Stable	150	14

SN-38 liposomes

SN-38 containing liposomes were synthesized by co-dissolving lipids and SN-38 in organic solvent, followed by either 1) rehydration in a small volume of aqueous buffer and sonication, or 2) solvent displacement by drop-wise addition into a large aqueous buffer reservoir.

Lipid	Synthesis	Liposome yield
5.8 μmol 90/10 DOPC/MPB-DOPE dried with 125 μg SN-38	Resuspend in 200 μl 100 mM citrate pH 4, sonicate 2 min 4/1 on ice, run through GE MiniTrap to remove unencapsulated SN-38	Good yield, very little precipitation

SN-38 dehydration rehydration vesicles

The synthesis protocol for SN-38 DRVs was adapted from (Zhang et al., 2004). This protocol includes a resuspension step in pH 10 buffer to solubilize SN-38, but alkaline conditions drive irreversible hydrolyzation and inactivation of maleimides, which is probably responsible for the low conjugation efficiency of the final DRVs.

Lipid	Synthesis	Yield
5.8 μmol 5/55/40 malPEG-DSPE/ DOPC/cholesterol dried with 125 μg SN-38	Resuspend in 250 μl 10% sucrose + 24 mM NaOH, sonicate 2 min 4/1 on ice, add 60 μl 10% sucrose, lyophilize overnight, resuspend in 500 μl 100 mM citrate pH 4 w/vortexing, run through GE MiniTrap to remove unencapsulated SN-38	Good yield
5.8 μmol 5/55/40 malPEG-DSPE or MPB-DOPE/DOPC/ cholesterol	Dissolve 125 μg SN-38 in 250 μl 10% sucrose + 24 mM NaOH, resuspend lipids in solution, sonicate 2 min 4/1 on ice, add 60 μl 10% sucrose, lyophilize overnight, resuspend in 500 μl 100 mM citrate pH 4 w/vortexing, run through GE MiniTrap to remove unencapsulated SN-38	Good yield, some drug precipitates

SN-38 PLGA nanoparticles

Due to its low solubility in dichloromethane and chloroform (Figure II.1), SN-38 could not be incorporated into the oil phase of single or double emulsion PLGA particle synthesis (Bershteyn et al., 2008). However, because SN-38 does partially dissolve in water-miscible solvents such as THF, we could encapsulate it in PLGA particles using a nanoprecipitation protocol based on one developed in our lab for poly- β -aminoester particles (Su et al., 2011) and another one for PLGA nanoparticles from the Langer lab (Cheng et al., 2007). We consistently observed that PLGA particles were very prone to aggregation during synthesis, and their stability required PEG-lipids

that masked surface maleimide groups, similar to how heavily-PEGylated dox liposomes are stable but unreactive.

Solvent	Solubility
Ethanol	Insoluble
Methanol	Insoluble
Acetone	Fully dissolved
Acetonitrile	Fully dissolved, but slower than acetone
Dimethylformamide	Fully dissolved, but slower than acetone
Tetrahydrofuran	Fully dissolved
Ethyl acetate	Partial/very slow
Dichloromethane	Soluble
Chloroform	Soluble

Figure II.1: PLGA (Lakeshore 5050 4A) solubility, 10 mg in 1 ml solvent.

Lipid	Synthesis	Yield
5-10 umol 50/50 DOPC/MPB-DOPE 50/50 DPPC/MPB-DPPE	40 mg PLGA +/- 50 µg SN-38 + lipids in 4 ml 60C acetone, into 40 ml water at room temp	Partial aggregation when pelleted
6 mg 80/20 HSPC/PEG2000-DSPE	40 mg PLGA +/- 500 µg SN-38 in 3-4 ml acetone, lipids in 40 ml water + 4% ethanol at 50-60C	No particle formation
5 umol 90/10 or 95/5 DOPC/MPB-DOPE DOPC/malPEG-DSPE DOPC/PEG2000-DSPE	40 mg PLGA +/- 500 µg SN-38 in + lipids in 40 ml water at room temp	Low yield of aggregated particles
2 mg 80/20 HSPC/PEG350-DSPE 80/20 HSPC/PEG1000-DSPE 80/20 HSPC/PEG2000-DSPE	10 mg PLGA in 1 ml acetone or DMSO, lipids in 5 ml water+ 4% ethanol at 65C	Particles formed for acetone + PEG1000/2000-DSPE conditions, no particles for DMSO condition, particle aggregation for PEG350-DSPE condition
2 mg 95/5 DOPC/PEG2000-DSPE	10 mg PLGA + lipids + 500 µg SN-38 in 1 ml dioxane/THF/DMF, 5 ml water at room temp	Particles formed in THF, no particles in DMF, particle aggregation in dioxane
5.8 umol 90/10 DOPC/MPB-DOPE	40 mg PLGA + 125 µg SN-38 + lipids in 4 ml THF, in 40 ml water at room temp	Most particles aggregated
5.8 umol 90/10 DOPC/MPB-DOPE	40 mg PLGA + 125 µg SN-38 + lipids in 4 ml dioxane, in 40 ml water +/- 0.58 umol PEG350-DPPE at room temp	Better yield without PEG350-DPPE post-insertion

SN-38 lipid conjugate

Dox's pendant amine group is reactive and allows chemical conjugation to lipids, polymers, and other moieties, which can then be delivered alone or further assembled into more complex structures such as micelles. SN-38's most reactive group is the 20 hydroxyl, which can be functionalized into a carboxylate, but amide bonds formed with this group is highly unstable and is cleaved within 24 h. More stable functionalization requires activation of the 10 hydroxyl, however, this is still low-efficiency and requires protection and de-protection of the 20 hydroxyl.

Dr. Haipeng Liu conjugated SN-38 to PGPC (structure shown below) by a condensation reaction between the 20 hydroxyl of SN-38 and the terminal carboxyl of PGPC to form an ester bond. The reaction was conducted in tetrahydrofuran at room temperature overnight, similar to the scheme described in (Koizumi et al., 2006). The reactants and products were separated by preparative thin layer chromatography. The yield was low (approximately 20%) and the product was unstable, with spontaneous dissociation into the reactants even when stored in organic solvent at -20C.

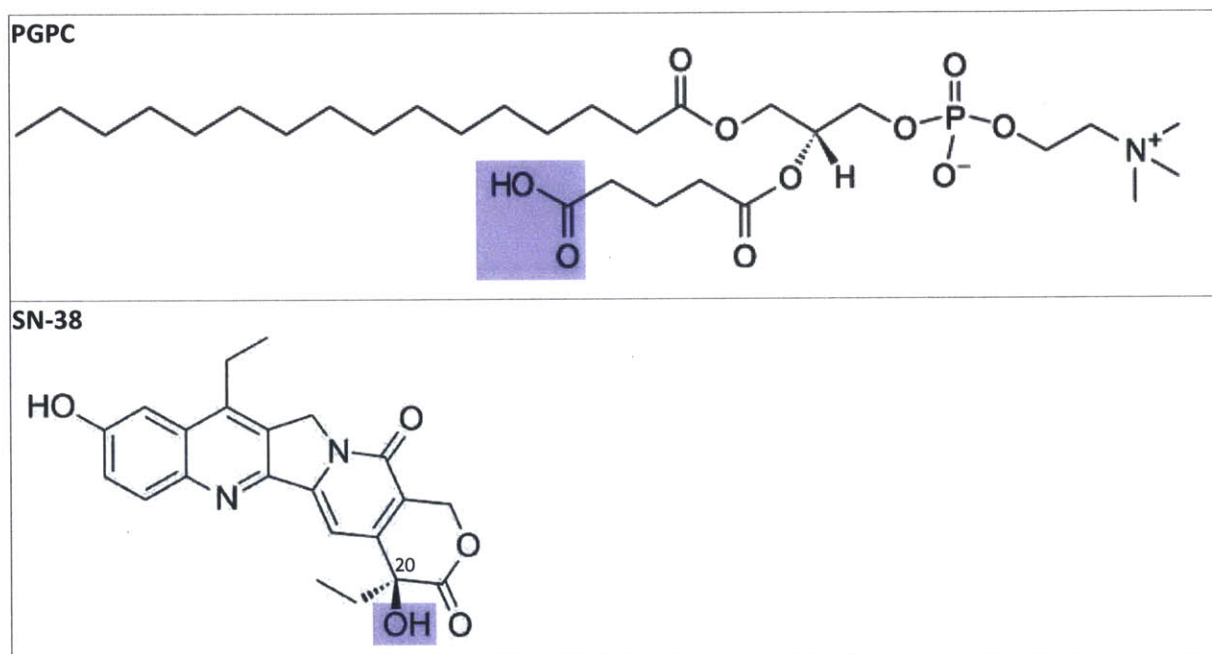


Figure II.2: Structures of PGPC and SN-38.

The reactive carboxylate of PGPC and the reactive hydroxyl of SN-38 are highlighted in blue.

III. Appendix: ICMV encapsulation of anti-CD40 antibody

Anti-CD40 is a potent immunotherapy agent against lymphoma (French et al., 1999) and melanoma (Kwong et al., 2011). In particular, French et al. demonstrated that anti-CD40 can achieve impressive cure rates of mice with high tumor burdens of disseminated A20 lymphoma. However, systemic administration of anti-CD40 causes severe side effects including cytokine storm and liver damage. Therefore, we were motivated to deliver anti-CD40 in a T cell-mediated manner similar to chemotherapy targeted delivery.

We chose the lipid-based ICMV particle system (Moon et al., 2011) due to its high encapsulation of proteins and its high conjugation efficiency to T cells. As a model antibody cargo, we first used FITC-labeled human IgG (Sigma). Fluorescence readings indicated encapsulation of FITC huIgG in ICMVs in the range of 25-40 μg antibody/batch, and release over about a week (Figure III.1).

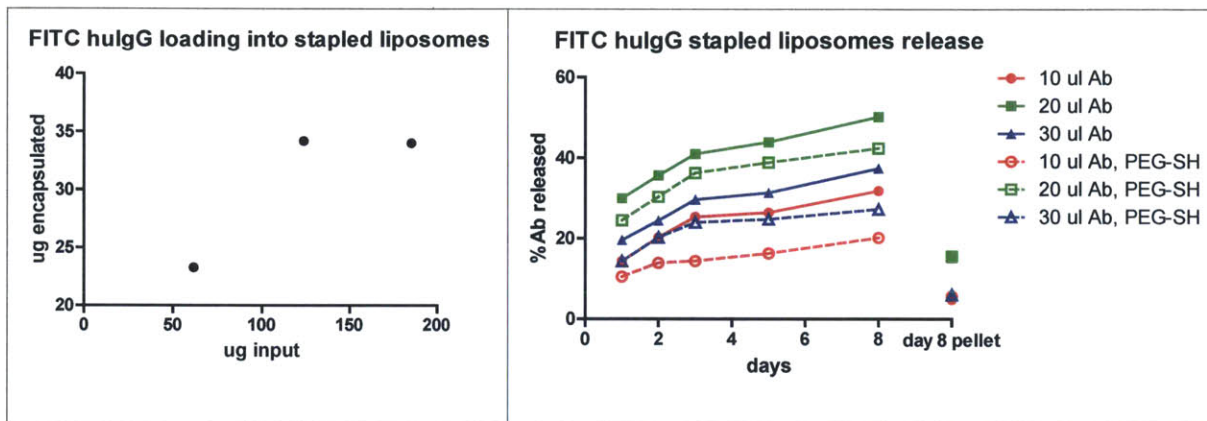


Figure III.1: FITC-labeled human IgG can be encapsulated into ICMVs.

We followed the synthesis protocol described in the work of (Moon et al., 2011). PEGylated ICMVs were then placed in 1 ml PBS 10% FCS and incubated at 37C; at each timepoint, the fluorescence in the supernatant was measured to calculate the amount released. HuIgG release kinetics are similar to those published for ova, despite the former's larger size (150 versus 53 kDa, respectively).

We repeated the ICMV synthesis with anti-CD40 (clone FGK4.5, BioExpress), and silver staining of SDS-PAGE gels showed the presence of encapsulated anti-CD40. However, functional ELISA measurements (Kwong et al., 2011) for anti-CD40 antibody did not detect encapsulation (data not shown). This suggested the anti-CD40 binding epitope was disrupted by the ICMV synthesis process.

Experiments were performed with the assistance of Temesgen Woldeyesus (HHMI EXROP, summer 2010).

IV. Appendix: Generation of the Emu-myc Arf^{-/-} Luciferase GFP line

Emu-myc Arf^{-/-} cells can be stably transduced with MLS constructs containing reporters such as GFP. However, GFP (excitation 475 nm, emission 505 nm) is not ideal for *in vivo* imaging due to high tissue autofluorescence and tissue absorption of light at short wavelengths, and the Emu-myc Arf^{-/-} GFP cells from the Hemann lab were not visible by IVIS imaging of the intact mouse (data not shown, consistent with discussions with Hemann lab members). Thus, we were motivated to use a luciferase reporter for increased imaging signal, however, we also wanted to keep GFP as a reporter for flow cytometry analysis. Therefore, we generated a vector containing both firefly luciferase and GFP.

MLS luc4 GFP was constructed by inserting the BglII – Sall fragment of pGL4.10 (Promega) into the corresponding backbone fragment of MLS (Gilbert and Hemann, 2010). The FseI – BamHI fragment was then excised and the vector backbone ends blunted with Klenow and religated to form the final construct (with assistance from Luke Gilbert of Hemann lab). Retrovirus was produced by Phoenix-Eco packaging cell transfection and the viral supernatant was used to transduce Emu-myc Arf^{-/-} cells with 8 µg/ml polybrene for 2 days. GFP positive cells were sorted on a BD FACS Aria.

References

- Adams, J.M., Harris, A.W., Pinkert, C.A., Corcoran, L.M., Alexander, W.S., Cory, S., Palmiter, R.D., and Brinster, R.L. (1985). The c-myc oncogene driven by immunoglobulin enhancers induces lymphoid malignancy in transgenic mice. *Nature* *318*, 533-538.
- Allen, T.M., and Cleland, L.G. (1980). Serum-induced leakage of liposome contents. *Biochimica et Biophysica Acta (BBA) - Biomembranes* *597*, 418-426.
- Allen, T.M., Hansen, C., Martin, F., Redemann, C., and Yau-Young, A. (1991). Liposomes containing synthetic lipid derivatives of poly(ethylene glycol) show prolonged circulation half-lives in vivo. *Biochimica et Biophysica Acta (BBA) - Biomembranes* *1066*, 29-36.
- Allen, T.M., Hong, K., and Papahadjopoulos, D. (1990). Membrane contact, fusion, and hexagonal (HII) transitions in phosphatidylethanolamine liposomes. *Biochemistry* *29*, 2976-2985.
- Allen, T.M., Mumbengegwi, D.R., and Charrois, G.J.R. (2005). Anti-CD19-targeted liposomal doxorubicin improves the therapeutic efficacy in murine B-cell lymphoma and ameliorates the toxicity of liposomes with varying drug release rates. *Clinical Cancer Research* *11*, 3567-3573.
- Atsumi, R., Okazaki, O., and Hokusui, H. (1995). Pharmacokinetics of SN-38 [(+)-(4S)-4, 11-diethyl-4, 9-dihydroxy-1H-pyrano [3', 4': 6, 7]-indolizino [1, 2-b] quinoline-3, 14 (4H, 12H)-dione], an active metabolite of irinotecan, after a single intravenous dosing of ¹⁴C-SN-38 to rats. *Biol Pharmacol Bull* *18*, 1114-1119.
- Bershteyn, A., Chaparro, J., Yau, R., Kim, M., Reinherz, E., Ferreira-Moita, L., and Irvine, D.J. (2008). Polymer-supported lipid shells, onions, and flowers. *Soft matter* *4*, 1787-1791.
- Bertolini, F., Dell'Agnola, C., Mancuso, P., Rabascio, C., Burlini, A., Monestiroli, S., Gobbi, A., Pruneri, G., and Martinelli, G. (2002). CXCR4 Neutralization, a Novel Therapeutic Approach for Non-Hodgkin's Lymphoma. *Cancer Research* *62*, 3106-3112.
- Biragyn, A., Tani, K., Grimm, M.C., Weeks, S., and Kwak, L.W. (1999). Genetic fusion of chemokines to a self tumor antigen induces protective, T-cell dependent antitumor immunity. *Nature biotechnology* *17*, 253-258.
- Brody, J., Kohrt, H., Marabelle, A., and Levy, R. (2011). Active and passive immunotherapy for lymphoma: proving principles and improving results. *Journal of clinical oncology : official journal of the American Society of Clinical Oncology* *29*, 1864-1875.
- Broxmeyer, H.E., Orschell, C.M., Clapp, D.W., Hangoc, G., Cooper, S., Plett, P.A., Liles, W.C., Li, X., Graham-Evans, B., Campbell, T.B., *et al.* (2005). Rapid mobilization of murine and human hematopoietic stem and progenitor cells with AMD3100, a CXCR4 antagonist. *The Journal of Experimental Medicine* *201*, 1307-1318.
- Buckley, C.D., Amft, N., Bradfield, P.F., Pilling, D., Ross, E., Arenzana-Seisdedos, F., Amara, A., Curnow, S.J., Lord, J.M., Scheel-Toellner, D., *et al.* (2000). Persistent Induction of the Chemokine Receptor CXCR4 by TGF- β 1 on Synovial T Cells Contributes to Their Accumulation Within the Rheumatoid Synovium. *The Journal of Immunology* *165*, 3423-3429.
- Burger, J.A., and Peled, A. (2008). CXCR4 antagonists: targeting the microenvironment in leukemia and other cancers. *Leukemia* *23*, 43-52.
- Burgess, D.J., Doles, J., Zender, L., Xue, W., Ma, B., McCombie, W.R., Hannon, G.J., Lowe, S.W., and Hemann, M.T. (2008). Topoisomerase levels determine chemotherapy response in vitro and in vivo. *Proc Natl Acad Sci U S A* *105*, 9053-9058.
- Burke, T.G., and Mi, Z. (1994). The structural basis of camptothecin interactions with human serum albumin: impact on drug stability. *Journal of Medicinal Chemistry* *37*, 40-46.
- Burke, T.G., Mishra, A.K., Wani, M.C., and Wall, M.E. (1993). Lipid bilayer partitioning and stability of camptothecin drugs. *Biochemistry* *32*, 5352-5364.
- Chabner, B.A., and Roberts, T.G. (2005). Chemotherapy and the war on cancer. *Nature Reviews Cancer* *5*, 65-72.

- Charo, J., Finkelstein, S.E., Grewal, N., Restifo, N.P., Robbins, P.F., and Rosenberg, S.A. (2005). Bcl-2 overexpression enhances tumor-specific T-cell survival. *Cancer Res* 65, 2001-2008.
- Charrois, G.J., and Allen, T.M. (2004). Drug release rate influences the pharmacokinetics, biodistribution, therapeutic activity, and toxicity of pegylated liposomal doxorubicin formulations in murine breast cancer. *Biochim Biophys Acta* 1663, 167-177.
- Cheng, H., Kastrup, C.J., Ramanathan, R., Siegwart, D.J., Ma, M., Bogatyrev, S.R., Xu, Q., Whitehead, K.A., Langer, R., and Anderson, D.G. (2010). Nanoparticulate Cellular Patches for Cell-Mediated Tumorotropic Delivery. *ACS Nano* 4, 625-631.
- Cheng, J., Teply, B.A., Sherifi, I., Sung, J., Luther, G., Gu, F.X., Levy-Nissenbaum, E., Radovic-Moreno, A.F., Langer, R., and Farokhzad, O.C. (2007). Formulation of functionalized PLGA-PEG nanoparticles for in vivo targeted drug delivery. *Biomaterials* 28, 869-876.
- Choi, J., Kim, H.-Y., Ju, E.J., Jung, J., Park, J., Chung, H.-K., Lee, J.S., Lee, J.S., Park, H.J., Song, S.Y., *et al.* (2012a). Use of macrophages to deliver therapeutic and imaging contrast agents to tumors. *Biomaterials* 33, 4195-4203.
- Choi, J., Woo, H.-N., Ju, E.J., Jung, J., Chung, H.-K., Park, J., Park, S.S., Shin, S.H., Park, H.J., Lee, J.S., *et al.* (2012b). Immunocytes as a Biocarrier to Delivery Therapeutic and Imaging Contrast Agents to Tumors. *Journal of Nanomaterials* 2012, 8.
- Choi, M.-R., Stanton-Maxey, K.J., Stanley, J.K., Levin, C.S., Bardhan, R., Akin, D., Badve, S., Sturgis, J., Robinson, J.P., Bashir, R., *et al.* (2007). A Cellular Trojan Horse for Delivery of Therapeutic Nanoparticles into Tumors. *Nano Letters* 7, 3759-3765.
- Chung, Y., Qin, H., Kang, C.-Y., Kim, S., Kwak, L.W., and Dong, C. (2007). An NKT-mediated autologous vaccine generates CD4 T-cell-dependent potent antilymphoma immunity. *Blood* 110, 2013-2019.
- Combes, O., Barré, J., Duché, J.-C., Vernillet, L., Archimbaud, Y., Marietta, M.P., Tillement, J.-P., and Urien, S. (2000). In Vitro Binding and Partitioning of Irinotecan (CPT-11) and its Metabolite, SN-38, in Human Blood. *Investigational New Drugs* 18, 1-5.
- Davis, M.E., Chen, Z., and Shin, D.M. (2008). Nanoparticle therapeutics: an emerging treatment modality for cancer. *Nat Rev Drug Discov* 7, 771-782.
- Dierks, C., Grbic, J., Zirlik, K., Beigi, R., Englund, N.P., Guo, G.R., Veelken, H., Engelhardt, M., Mertelsmann, R., Kelleher, J.F., *et al.* (2007). Essential role of stromally induced hedgehog signaling in B-cell malignancies. *Nat Med* 13, 944-951.
- Dinauer, N., Balthasar, S., Weber, C., Kreuter, J., Langer, K., and von Briesen, H. (2005). Selective targeting of antibody-conjugated nanoparticles to leukemic cells and primary T-lymphocytes. *Biomaterials* 26, 5898-5906.
- Dos Santos, N., Allen, C., Doppen, A.-M., Anantha, M., Cox, K.A.K., Gallagher, R.C., Karlsson, G., Edwards, K., Kenner, G., Samuels, L., *et al.* (2007). Influence of poly(ethylene glycol) grafting density and polymer length on liposomes: Relating plasma circulation lifetimes to protein binding. *Biochimica et Biophysica Acta (BBA) - Biomembranes* 1768, 1367-1377.
- Doshi, N., Swiston, A.J., Gilbert, J.B., Alcaraz, M.L., Cohen, R.E., Rubner, M.F., and Mitragotri, S. (2011). Cell-Based Drug Delivery Devices Using Phagocytosis-Resistant Backpacks. *Advanced Materials* 23, H105-H109.
- Eischen, C.M., Weber, J.D., Roussel, M.F., Sherr, C.J., and Cleveland, J.L. (1999). Disruption of the ARF-Mdm2-p53 tumor suppressor pathway in Myc-induced lymphomagenesis. *Genes & Development* 13, 2658-2669.
- French, R.R., Chan, H.T.C., Tutt, A.L., and Glennie, M.J. (1999). CD40 antibody evokes a cytotoxic T-cell response that eradicates lymphoma and bypasses T-cell help. *Nat Med* 5, 548-553.
- Fritze, A., Hens, F., Kimpfler, A., Schubert, R., and Peschka-Süss, R. (2006). Remote loading of doxorubicin into liposomes driven by a transmembrane phosphate gradient. *Biochimica et Biophysica Acta (BBA) - Biomembranes* 1758, 1633-1640.
- Gabizon, A., Catane, R., Uziely, B., Kaufman, B., Safra, T., Cohen, R., Martin, F., Huang, A., and Barenholz, Y. (1994). Prolonged circulation time and enhanced accumulation in malignant

- exudates of doxorubicin encapsulated in polyethylene-glycol coated liposomes. *Cancer Research* 54, 987-992.
- Gilbert, L.A., and Hemann, M.T. (2010). DNA Damage-Mediated Induction of a Chemoresistant Niche. *Cell* 143, 355-366.
- Gilbert, L.A., and Hemann, M.T. (2012). Context-specific roles for paracrine IL-6 in lymphomagenesis. *Genes Dev* 26, 1758-1768.
- Goldstein, M.J., Varghese, B., Brody, J.D., Rajapaksa, R., Kohrt, H., Czerwinski, D.K., Levy, S., and Levy, R. (2011). A CpG-loaded tumor cell vaccine induces antitumor CD4⁺ T cells that are effective in adoptive therapy for large and established tumors. *Blood* 117, 118-127.
- Gooden, M.J., de Bock, G.H., Leffers, N., Daemen, T., and Nijman, H.W. (2011). The prognostic influence of tumour-infiltrating lymphocytes in cancer: a systematic review with meta-analysis. *British journal of cancer* 105, 93-103.
- Hamaguchi, T., Doi, T., Eguchi-Nakajima, T., Kato, K., Yamada, Y., Shimada, Y., Fuse, N., Ohtsu, A., Matsumoto, S., Takanashi, M., *et al.* (2010). Phase I study of NK012, a novel SN-38-incorporating micellar nanoparticle, in adult patients with solid tumors. *Clinical cancer research : an official journal of the American Association for Cancer Research* 16, 5058-5066.
- Hanahan, D., Wagner, E.F., and Palmiter, R.D. (2007). The origins of oncomice: a history of the first transgenic mice genetically engineered to develop cancer. *Genes & Development* 21, 2258-2270.
- Hanahan, D., and Weinberg, Robert A. (2011). *Hallmarks of Cancer: The Next Generation*. *Cell* 144, 646-674.
- Hansen, C.B., Kao, G.Y., Moase, E.H., Zalipsky, S., and Allen, T.M. (1995). Attachment of antibodies to sterically stabilized liposomes: evaluation, comparison and optimization of coupling procedures. *Biochimica et Biophysica Acta (BBA)-Biomembranes* 1239, 133-144.
- Haran, G., Cohen, R., Bar, L.K., and Barenholz, Y. (1993). Transmembrane ammonium sulfate gradients in liposomes produce efficient and stable entrapment of amphipathic weak bases. *Biochimica et Biophysica Acta (BBA)-Biomembranes* 1151, 201-215.
- Harris, A.W., Pinkert, C.A., Crawford, M., Langdon, W.Y., Brinster, R.L., and Adams, J.M. (1988). The E mu-myc transgenic mouse. A model for high-incidence spontaneous lymphoma and leukemia of early B cells. *J Exp Med* 167, 353-371.
- Hemann, M.T., Fridman, J.S., Zilfou, J.T., Hernando, E., Paddison, P.J., Cordon-Cardo, C., Hannon, G.J., and Lowe, S.W. (2003). An epi-allelic series of p53 hypomorphs created by stable RNAi produces distinct tumor phenotypes in vivo. *Nat Genet* 33, 396-400.
- Hinrichs, C.S., Borman, Z.A., Cassard, L., Gattinoni, L., Spolski, R., Yu, Z., Sanchez-Perez, L., Muranski, P., Kern, S.J., Logun, C., *et al.* (2009). Adoptively transferred effector cells derived from naive rather than central memory CD8⁺ T cells mediate superior antitumor immunity. *Proc Natl Acad Sci U S A* 106, 17469-17474.
- Huang, X., Jain, P., El-Sayed, I., and El-Sayed, M. (2008). Plasmonic photothermal therapy (PPTT) using gold nanoparticles. *Lasers in Medical Science* 23, 217-228.
- Hurley, L.H. (2002). DNA and its associated processes as targets for cancer therapy. *Nature Reviews Cancer* 2, 188-200.
- Iden, D.L., and Allen, T.M. (2001). In vitro and in vivo comparison of immunoliposomes made by conventional coupling techniques with those made by a new post-insertion approach. *Bba-Biomembranes* 1513, 207-216.
- Ishida, T., Iden, D.L., and Allen, T.M. (1999). A combinatorial approach to producing sterically stabilized (Stealth) immunoliposomal drugs. *FEBS Lett* 460, 129-133.
- Ito, K., Smith, B.R., Parashurama, N., Yoon, J.-K., Song, S.Y., Miething, C., Mallick, P., Lowe, S., and Gambhir, S.S. (2012). Unexpected Dissemination Patterns in Lymphoma Progression Revealed by Serial Imaging within a Murine Lymph Node. *Cancer Research* 72, 6111-6118.
- Jacobs, J.J.L., Scheijen, B., Voncken, J.-W., Kieboom, K., Berns, A., and van Lohuizen, M. (1999). Bmi-1 collaborates with c-Myc in tumorigenesis by inhibiting c-Myc-induced apoptosis via INK4a/ARF. *Genes & Development* 13, 2678-2690.

- Jacobsen, K., Prasad, V., Sidman, C., and Osmond, D. (1994). Apoptosis and macrophage-mediated deletion of precursor B cells in the bone marrow of E mu-myc transgenic mice. *Blood* *84*, 2784-2794.
- Jain, R.K., and Stylianopoulos, T. (2010). Delivering nanomedicine to solid tumors. *Nat Rev Clin Oncol* *7*, 653-664.
- Jain, S., Hirst, D.G., and O'Sullivan, J.M. (2012). Gold nanoparticles as novel agents for cancer therapy. *British Journal of Radiology* *85*, 101-113.
- Jourdan, P., Abbal, C., Nora, N., Hori, T., Uchiyama, T., Vendrell, J.-P., Bousquet, J., Taylor, N., PÃ"ne, J.r.m., and Yssel, H. (1998). Cutting Edge: IL-4 Induces Functional Cell-Surface Expression of CXCR4 on Human T Cells. *The Journal of Immunology* *160*, 4153-4157.
- Joyce, J.A., and Pollard, J.W. (2009). Microenvironmental regulation of metastasis. *Nat Rev Cancer* *9*, 239-252.
- June, C.H., Blazar, B.R., and Riley, J.L. (2009). Engineering lymphocyte subsets: tools, trials and tribulations. *Nat Rev Immunol* *9*, 704-716.
- Kaneda, N., Nagata, H., Furuta, T., and Yokokura, T. (1990). Metabolism and Pharmacokinetics of the Camptothecin Analogue CPT-11 in the Mouse. *Cancer Research* *50*, 1715-1720.
- Kawato, Y., Aonuma, M., Hirota, Y., Kuga, H., and Sato, K. (1991). Intracellular roles of SN-38, a metabolite of the camptothecin derivative CPT-11, in the antitumor effect of CPT-11. *Cancer Res* *51*, 4187-4191.
- Keefe, D.M., and Bateman, E.H. (2012). Tumor control versus adverse events with targeted anticancer therapies. *Nat Rev Clin Oncol* *9*, 98-109.
- Kelly, P.N., Dakic, A., Adams, J.M., Nutt, S.L., and Strasser, A. (2007). Tumor Growth Need Not Be Driven by Rare Cancer Stem Cells. *Science* *317*, 337.
- Kennedy, L.C., Bear, A.S., Young, J.K., Lewinski, N.A., Kim, J., Foster, A.E., and Drezek, R.A. (2011). T cells enhance gold nanoparticle delivery to tumors in vivo. *Nanoscale Res Lett* *6*, 283.
- Klebanoff, C.A., Finkelstein, S.E., Surman, D.R., Lichtman, M.K., Gattinoni, L., Theoret, M.R., Grewal, N., Spiess, P.J., Antony, P.A., Palmer, D.C., *et al.* (2004). IL-15 enhances the in vivo antitumor activity of tumor-reactive CD8+ T cells. *Proc Natl Acad Sci U S A* *101*, 1969-1974.
- Kochenderfer, J.N., Dudley, M.E., Feldman, S.A., Wilson, W.H., Spaner, D.E., Maric, I., Stetler-Stevenson, M., Phan, G.Q., Hughes, M.S., Sherry, R.M., *et al.* (2012). B-cell depletion and remissions of malignancy along with cytokine-associated toxicity in a clinical trial of anti-CD19 chimeric-antigen-receptor-transduced T cells. *Blood* *119*, 2709-2720.
- Koizumi, F., Kitagawa, M., Negishi, T., Onda, T., Matsumoto, S., Hamaguchi, T., and Matsumura, Y. (2006). Novel SN-38-incorporating polymeric micelles, NK012, eradicate vascular endothelial growth factor-secreting bulky tumors. *Cancer Res* *66*, 10048-10056.
- Koster, A., and Raemaekers, J.M.M. (2005). Angiogenesis in malignant lymphoma. *Current Opinion in Oncology* *17*, 611-616.
- Kotani, A., Kakazu, N., Tsuruyama, T., Okazaki, I.-m., Muramatsu, M., Kinoshita, K., Nagaoka, H., Yabe, D., and Honjo, T. (2007). Activation-induced cytidine deaminase (AID) promotes B cell lymphomagenesis in Emu-cmyc transgenic mice. *Proceedings of the National Academy of Sciences* *104*, 1616-1620.
- Kuroda, J.-i., Kuratsu, J.-i., Yasunaga, M., Koga, Y., Saito, Y., and Matsumura, Y. (2009). Potent antitumor effect of SN-38-incorporating polymeric micelle, NK012, against malignant glioma. *International journal of cancer* *124*, 2505-2511.
- Kurtova, A.V., Tamayo, A.T., Ford, R.J., and Burger, J.A. (2009). Mantle cell lymphoma cells express high levels of CXCR4, CXCR5, and VLA-4 (CD49d): importance for interactions with the stromal microenvironment and specific targeting. *Blood* *113*, 4604-4613.
- Kwong, B., Liu, H., and Irvine, D.J. (2011). Induction of potent anti-tumor responses while eliminating systemic side effects via liposome-anchored combinatorial immunotherapy. *Biomaterials* *32*, 5134-5147.

- Laginha, K.M., Verwoert, S., Charrois, G.J.R., and Allen, T.M. (2005). Determination of Doxorubicin Levels in Whole Tumor and Tumor Nuclei in Murine Breast Cancer Tumors. *Clinical Cancer Research* *11*, 6944-6949.
- Langdon, W.Y., Harris, A.W., Cory, S., and Adams, J.M. (1986). The c-myc oncogene perturbs B lymphocyte development in E-mu-myc transgenic mice. *Cell* *47*, 11-18.
- Li, L., Guan, Y., Liu, H., Hao, N., Liu, T., Meng, X., Fu, C., Li, Y., Qu, Q., Zhang, Y., *et al.* (2011). Silica Nanorattle–Doxorubicin-Anchored Mesenchymal Stem Cells for Tumor-Tropic Therapy. In *ACS Nano* (American Chemical Society), pp. 7462-7470.
- Liddy, N., Bossi, G., Adams, K.J., Lissina, A., Mahon, T.M., Hassan, N.J., Gavarret, J., Bianchi, F.C., Pumphrey, N.J., Ladell, K., *et al.* (2012). Monoclonal TCR-redirected tumor cell killing. *Nat Med* *18*, 980-987.
- Liu, H., Kwong, B., and Irvine, D.J. (2011). Membrane Anchored Immunostimulatory Oligonucleotides for In Vivo Cell Modification and Localized Immunotherapy. *Angewandte Chemie International Edition* *50*, 7052-7055.
- Luster, A.D., and Tager, A.M. (2004). T-cell trafficking in asthma: lipid mediators grease the way. *Nat Rev Immunol* *4*, 711-724.
- Madsen, S.J., Baek, S.K., Makkouk, A.R., Krasieva, T., and Hirschberg, H. (2012). Macrophages as cell-based delivery systems for nanoshells in photothermal therapy. *Ann Biomed Eng* *40*, 507-515.
- Mattarollo, S.R., West, A.C., Steegh, K., Duret, H., Paget, C., Martin, B., Matthews, G.M., Shortt, J., Chesi, M., Bergsagel, P.L., *et al.* (2012). NKT cell adjuvant-based tumor vaccine for treatment of myc oncogene-driven mouse B-cell lymphoma. *Blood* *120*, 3019-3029.
- Mayer, L.D., Tai, L.C.L., Ko, D.S.C., Masin, D., Ginsberg, R.S., Cullis, P.R., and Bally, M.B. (1989). Influence of vesicle size, lipid composition, and drug-to-lipid ratio on the biological activity of liposomal doxorubicin in mice. *Cancer Research* *49*, 5922-5930.
- Meyer, N., and Penn, L.Z. (2008). Reflecting on 25 years with MYC. *Nat Rev Cancer* *8*, 976-990.
- Minchinton, A.I., and Tannock, I.F. (2006). Drug penetration in solid tumours. *Nat Rev Cancer* *6*, 583-592.
- Moon, J.J., Huang, B., and Irvine, D.J. (2012). Engineering nano- and microparticles to tune immunity. *Adv Mater* *24*, 3724-3746.
- Moon, J.J., Suh, H., Bershteyn, A., Stephan, M.T., Liu, H.P., Huang, B., Sohail, M., Luo, S., Um, S.H., Khant, H., *et al.* (2011). Interbilayer-crosslinked multilamellar vesicles as synthetic vaccines for potent humoral and cellular immune responses. *Nature materials* *10*, 243-251.
- Moon, S.J., Govindan, S.V., Cardillo, T.M., D'Souza, C.A., Hansen, H.J., and Goldenberg, D.M. (2008). Antibody conjugates of 7-ethyl-10-hydroxycamptothecin (SN-38) for targeted cancer chemotherapy. *J Med Chem* *51*, 6916-6926.
- Nagasawa, T., Kikutani, H., and Kishimoto, T. (1994). Molecular cloning and structure of a pre-B-cell growth-stimulating factor. *Proceedings of the National Academy of Sciences* *91*, 2305-2309.
- Nervi, B., Holt, M., Rettig, M.P., Bridger, G., Ley, T.J., and DiPersio, J.F. (2006). In vivo bioluminescence imaging of acute promyelocytic leukemia cell trafficking and mobilization by AMD3100. *Biology of blood and marrow transplantation : journal of the American Society for Blood and Marrow Transplantation* *12*, 18.
- Nervi, B., Ramirez, P., Rettig, M.P., Uy, G.L., Holt, M.S., Ritchey, J.K., Prior, J.L., Piwnica-Worms, D., Bridger, G., Ley, T.J., *et al.* (2009). Chemosensitization of acute myeloid leukemia (AML) following mobilization by the CXCR4 antagonist AMD3100. *Blood* *113*, 6206-6214.
- Ogino, S., Galon, J., Fuchs, C.S., and Dranoff, G. (2011). Cancer immunology--analysis of host and tumor factors for personalized medicine. *Nat Rev Clin Oncol* *8*, 711-719.
- Okutsu, M., Ishii, K., Niu, K.J., and Nagatomi, R. (2005). Cortisol-induced CXCR4 augmentation mobilizes T lymphocytes after acute physical stress. *American Journal of Physiology - Regulatory, Integrative and Comparative Physiology* *288*, R591-R599.
- Olive, K.P., Jacobetz, M.A., Davidson, C.J., Gopinathan, A., McIntyre, D., Honess, D., Madhu, B., Goldgraben, M.A., Caldwell, M.E., Allard, D., *et al.* (2009). Inhibition of Hedgehog Signaling

- Enhances Delivery of Chemotherapy in a Mouse Model of Pancreatic Cancer. *Science* 324, 1457-1461.
- Pals, S.T., de Gorter, D.J., and Spaargaren, M. (2007). Lymphoma dissemination: the other face of lymphocyte homing. *Blood* 110, 3102-3111.
- Peer, D., Karp, J.M., Hong, S., Farokhzad, O.C., Margalit, R., and Langer, R. (2007). Nanocarriers as an emerging platform for cancer therapy. *Nature nanotechnology* 2, 751-760.
- Porter, D.L., Levine, B.L., Kalos, M., Bagg, A., and June, C.H. (2011). Chimeric antigen receptor-modified T cells in chronic lymphoid leukemia. *The New England journal of medicine* 365, 725-733.
- Pritchard, J.R., Gilbert, L.A., Meacham, C.E., Ricks, J.L., Jiang, H., Lauffenburger, D.A., and Hemann, M.T. (2011). Bcl-2 Family Genetic Profiling Reveals Microenvironment-Specific Determinants of Chemotherapeutic Response. *Cancer Research* 71, 5850-5858.
- Qian, B.-Z., and Pollard, J.W. (2010). Macrophage Diversity Enhances Tumor Progression and Metastasis. *Cell* 141, 39-51.
- Ransohoff, R.M., and Engelhardt, B. (2012). The anatomical and cellular basis of immune surveillance in the central nervous system. *Nat Rev Immunol* 12, 623-635.
- Ravizzini, G., Turkbey, B., Barrett, T., Kobayashi, H., and Choyke, P.L. (2009). Nanoparticles in sentinel lymph node mapping. *Wiley Interdisciplinary Reviews: Nanomedicine and Nanobiotechnology* 1, 610-623.
- Reddy, S.T., van der Vlies, A.J., Simeoni, E., Angeli, V., Randolph, G.J., O'Neil, C.P., Lee, L.K., Swartz, M.A., and Hubbell, J.A. (2007). Exploiting lymphatic transport and complement activation in nanoparticle vaccines. *Nature biotechnology* 25, 1159-1164.
- Relling, M.V., and Dervieux, T. (2001). Pharmacogenetics and cancer therapy. *Nat Rev Cancer* 1, 99-108.
- Rosenberg, S.A., Restifo, N.P., Yang, J.C., Morgan, R.A., and Dudley, M.E. (2008). Adoptive cell transfer: a clinical path to effective cancer immunotherapy. *Nature Reviews Cancer* 8, 299-308.
- Roth, J.C., Curiel, D.T., and Pereboeva, L. (2008). Cell vehicle targeting strategies. *Gene Ther* 15, 716-729.
- Ruan, J., Hajjar, K., Rafii, S., and Leonard, J.P. (2009). Angiogenesis and antiangiogenic therapy in non-Hodgkin's lymphoma. *Annals of Oncology* 20, 413-424.
- Sahaf, B., Heydari, K., Herzenberg, L.A., and Herzenberg, L.A. (2003). Lymphocyte surface thiol levels. *Proc Natl Acad Sci U S A* 100, 4001-4005.
- Schmitt, C.A., Fridman, J.S., Yang, M., Baranov, E., Hoffman, R.M., and Lowe, S.W. (2002a). Dissecting p53 tumor suppressor functions in vivo. *Cancer Cell* 1, 289-298.
- Schmitt, C.A., Fridman, J.S., Yang, M., Lee, S., Baranov, E., Hoffman, R.M., and Lowe, S.W. (2002b). A Senescence Program Controlled by p53 and p16INK4a Contributes to the Outcome of Cancer Therapy. *Cell* 109, 335-346.
- Schmitt, C.A., McCurrach, M.E., de Stanchina, E., Wallace-Brodeur, R.R., and Lowe, S.W. (1999). INK4a/ARF mutations accelerate lymphomagenesis and promote chemoresistance by disabling p53. *Genes & Development* 13, 2670-2677.
- Schmitt, C.A., Rosenthal, C.T., and Lowe, S.W. (2000). Genetic analysis of chemoresistance in primary murine lymphomas. *Nat Med* 6, 1029-1035.
- Schultze, J.L. (1999). Why do B cell lymphoma fail to elicit clinically sufficient T cell immune responses? *Leuk Lymphoma* 32, 223-236.
- Sigmundsdottir, H., and Butcher, E.C. (2008). Environmental cues, dendritic cells and the programming of tissue-selective lymphocyte trafficking. *Nat Immunol* 9, 981-987.
- Sinclair, L.V., Finlay, D., Feijoo, C., Cornish, G.H., Gray, A., Ager, A., Okkenhaug, K., Hagenbeek, T.J., Spits, H., and Cantrell, D.A. (2008). Phosphatidylinositol-3-OH kinase and nutrient-sensing mTOR pathways control T lymphocyte trafficking. *Nat Immunol* 9, 513-521.
- Stephan, M.T., and Irvine, D.J. (2011). Enhancing Cell therapies from the Outside In: Cell Surface Engineering Using Synthetic Nanomaterials. *Nano today* 6, 309-325.

- Stephan, M.T., Moon, J.J., Um, S.H., Bershteyn, A., and Irvine, D.J. (2010). Therapeutic cell engineering with surface-conjugated synthetic nanoparticles. *Nat Med* *16*, 1035-1041.
- Stephan, M.T., Ponomarev, V., Brentjens, R.J., Chang, A.H., Dobrenkov, K.V., Heller, G., and Sadelain, M. (2007). T cell-encoded CD80 and 4-1BBL induce auto- and transcostimulation, resulting in potent tumor rejection. *Nat Med* *13*, 1440-1449.
- Stephan, M.T., Stephan, S.B., Bak, P., Chen, J., and Irvine, D.J. (2012). Synapse-directed delivery of immunomodulators using T-cell-conjugated nanoparticles. *Biomaterials* *33*, 5776-5787.
- Su, X., Fricke, J., Kavanagh, D.G., and Irvine, D.J. (2011). In vitro and in vivo mRNA delivery using lipid-enveloped pH-responsive polymer nanoparticles. *Mol Pharm* *8*, 774-787.
- Taurin, S., Nehoff, H., and Greish, K. (2012). Anticancer nanomedicine and tumor vascular permeability; Where is the missing link? *Journal of controlled release : official journal of the Controlled Release Society* *164*, 265-275.
- Trentin, L., Cabrelle, A., Facco, M., Carollo, D., Miorin, M., Tosoni, A., Pizzo, P., Binotto, G., Nicolardi, L., Zambello, R., *et al.* (2004). Homeostatic chemokines drive migration of malignant B cells in patients with non-Hodgkin lymphomas. *Blood* *104*, 502-508.
- Tutt, A.L., O'Brien, L., Hussain, A., Crowther, G.R., French, R.R., and Glennie, M.J. (2002). T cell immunity to lymphoma following treatment with anti-CD40 monoclonal antibody. *Journal of immunology* *168*, 2720-2728.
- Undevia, S.D., Gomez-Abuin, G., and Ratain, M.J. (2005). Pharmacokinetic variability of anticancer agents. *Nat Rev Cancer* *5*, 447-458.
- Uster, P.S., Allen, T.M., Daniel, B.E., Mendez, C.J., Newman, M.S., and Zhu, G.Z. (1996). Insertion of poly(ethylene glycol) derivatized phospholipid into pre-formed liposomes results in prolonged in vivo circulation time. *FEBS letters* *386*, 243-246.
- Vaux, D.L., Adams, J.M., Alexander, W.S., and Pike, B.L. (1987). Immunologic competence of B cells subjected to constitutive c-myc oncogene expression in immunoglobulin heavy chain enhancer myc transgenic mice. *The Journal of Immunology* *139*, 3854-3860.
- Wang, A.Z., Langer, R., and Farokhzad, O.C. (2012). Nanoparticle delivery of cancer drugs. *Annual review of medicine* *63*, 185-198.
- Wang, J., Harada, A., Matsushita, S., Matsumi, S., Zhang, Y., Shioda, T., Nagai, Y., and Matsushima, K. (1998). IL-4 and a glucocorticoid up-regulate CXCR4 expression on human CD4+ T lymphocytes and enhance HIV-1 replication. *Journal of Leukocyte Biology* *64*, 642-649.
- Weninger, W., Crowley, M.A., Manjunath, N., and Von Andrian, U.H. (2001). Migratory properties of naive, effector, and memory CD8+ T cells. *The Journal of Experimental Medicine* *194*, 953-966.
- Wilson, J.T., Cui, W., Kozlovskaya, V., Kharlampieva, E., Pan, D., Qu, Z., Krishnamurthy, V.R., Mets, J., Kumar, V., Wen, J., *et al.* (2011). Cell surface engineering with polyelectrolyte multilayer thin films. *J Am Chem Soc* *133*, 7054-7064.
- Younes, A. (2011). Beyond chemotherapy: new agents for targeted treatment of lymphoma. *Nat Rev Clin Oncol* *8*, 85-96.
- Yu, P., and Fu, Y.X. (2006). Tumor-infiltrating T lymphocytes: friends or foes? *Laboratory investigation; a journal of technical methods and pathology* *86*, 231-245.
- Zeng, Z., Xi Shi, Y., Samudio, I.J., Wang, R.-Y., Ling, X., Frolova, O., Levis, M., Rubin, J.B., Negrin, R.R., Estey, E.H., *et al.* (2009). Targeting the leukemia microenvironment by CXCR4 inhibition overcomes resistance to kinase inhibitors and chemotherapy in AML. *Blood* *113*, 6215-6224.
- Zhang, J.A., Xuan, T., Parmar, M., Ma, L., Ugwu, S., Ali, S., and Ahmad, I. (2004). Development and characterization of a novel liposome-based formulation of SN-38. *Int J Pharm* *270*, 93-107.
- Zou, W. (2005). Immunosuppressive networks in the tumour environment and their therapeutic relevance. *Nat Rev Cancer* *5*, 263-274.